Load Sensitivity Studies and Contingency Analysis in Power Systems

by

Parag Mitra

A Dissertation Presented in Partial Fulfillment
of the Requirements for the Degree
Doctor of Philosophy

Approved August 2016 by the
Graduate Supervisory Committee:

Vijay Vittal, Chair
Gerald Heydt
Raja Ayyanar
Jiangchao Qin

ARIZONA STATE UNIVERSITY

December 2016

ABSTRACT

The past decades have seen a significant shift in the expectations and requirements related to power system analysis tools. Investigations into major power grid disturbances have suggested the need for more comprehensive assessment methods. Accordingly, significant research in recent years has focused on the development of better power system models and efficient techniques for analyzing power system operability. The work done in this report focusses on two such topics

1. Analysis of load model parameter uncertainty and sensitivity based parameter estimation for power system studies

2. A systematic approach to *n*-1-1 analysis for power system security assessment

To assess the effect of load model parameter uncertainty, a trajectory sensitivity based approach is proposed in this work. Trajectory sensitivity analysis provides a systematic approach to study the impact of parameter uncertainty on power system response to disturbances. Furthermore, the non-smooth nature of the composite load model presents some additional challenges to sensitivity analysis in a realistic power system. Accordingly, the impact of the non-smooth nature of load models on the sensitivity analysis is addressed in this work. The study was performed using the Western Electricity Coordinating Council (WECC) system model. To address the issue of load model parameter estimation, a sensitivity based load model parameter estimation technique is presented in this work. A detailed discussion on utilizing sensitivities to improve the accuracy and efficiency of the parameter estimation process is also presented in this work.

Cascading outages can have a catastrophic impact on power systems. As such, the NERC transmission planning (TPL) standards requires utilities to plan for *n*-1-1 outages. However, such analyses can be computationally burdensome for any realistic power system owing to the staggering number of possible *n*-1-1 contingencies. To address this problem, the report proposes a systematic approach to analyze *n*-1-1 contingencies in a computationally tractable manner for power system security assessment. The proposed approach addresses both static and dynamic security assessment. The proposed methods have been tested on the WECC system.

DEDICATION

Dedicated to my mom Krishna Mitra and my dad Late Ratan Lal Mitra. Without their encouragement and selflessness none of this could have been achieved.

ACKNOWLEDGMENTS

I would like to offer my deepest gratitude to Dr. Vijay Vittal for providing me with the opportunity to work on this project. It has truly been an enriching experience for me. Dr. Vittal has been a continuous source of encouragement and guidance. Without his efforts and insightful feedback, this work would not have been possible.

I would like to thank Dr. Gerald Heydt, Dr. Raja Ayyanar and Dr. Jiangchao Qin, for taking out time to review this work and for being on my graduate supervisory committee.

I would also like to thank Dr. Daniel Tylavsky and Dr. Jennie Si, for taking out time to review this work and for being on my comprehensive examination committee.

I would like to thank Pouyan Pourbiek and Anish Gaikwad from EPRI for providing constant guidance and valuable comments during my research. I would also like to thank Brian Keel and Jeni Mistry from SRP for providing important data and evaluating this research work at different stages. Special thanks to Dr. John Undrill for his invaluable insights, ideas and encouragement.

I would like to thank EPRI and SRP for providing financial assistance during the course of this work.

I am deeply indebted to my parents Late Mr. Ratan Lal Mitra and Dr (Mrs.) Krishna Mitra for their love and support. I am also indebted to my elder brother Anurag Mitra and sister-in-law Priyanka Mitra for their constant encouragement and help. Last but not the least; I am thankful to all my friends for supporting me all this while.

TABLE OF CONTENTS

Page

APPENDIX Page

LIST OF TABLES

Table Page

LIST OF FIGURES

Figure Page

Figure Page

Figure Page

Figure Page

NOMENCLATURE

A	Product of normalized maximum sensitivity and perturbation
ac	Alternating current
ACLODF	Line outage distribution factors based on MVA flows
ACMTBLU1	Composite load model in Siemens PSSE
A/C	Air-conditioner
BVP	Boundary value problem
cmpldw	Composite load model in GE-PSLF
CR	The group of critical contingencies for dynamic security assessment
DAE	Differential algebraic equation
DAIS	Differential algebraic impulse system
dc	Direct current
DSA	Dynamic security assessment
f	frequency
F	Set of differential equations
F_{new}	The state variable sensitivity equations
F_x	Partial derivative of F with respect to x
F_y	Partial derivative of F with respect to y
$F_{\lambda i}$	Partial derivative of F with respect to λ_i
Fma	Percentage of motor A in composite load
Fmb	Percentage of motor B in composite load
Fmd	Percentage of motor D in composite load
FERC	Federal Energy Regulatory Commission
FIDVR	Fault induced delayed voltage recovery
Fmd	Percentage of A/C load in the composite load model
G	Set of algebraic equations
G_{new}	Algebraic variable sensitivity equations
G_x	Partial derivative of G with respect to x
G_y	Partial derivative of G with respect to y

$G_{\lambda i}$	Partial derivative of G with respect to λ_i
GE	General Electric
HS	High summer
IEEE	Institute of Electrical and Electronic Engineers
IROL	Interconnection reliability operating limits
Kp1	The active power coefficient in region 1
Kq1	The reactive power coefficient in region 1
Kp2	The active power coefficient in region 2
Kq2	The reactive power coefficient in region 2
K_{pf}	Active power frequency sensitivity
K_{qf}	Reactive power frequency sensitivity
l	Number of equations describing the switching conditions
LCR	The group of contingencies that are of least concern for dynamic security assessment
ld1pac	Performance model of an air-conditioner driven by a single phase induction motor in GE-PSLF
m	Number of algebraic variables in the expression $\mathbb{R}^m$
motorw	Model of single/double cage induction motor in GE-PSLF
MVWG	Model validation working group
MWLODF	Line outage distribution factor based on MW flows
n	Number of power system elements in the expression *n*-1-1
n	Number of state variables in the expression $\mathbb{R}^n$
Np1	The active power exponent in region 1
Nq1	The reactive power exponent in region 1
Np2	The active power exponent in region 2
Nq2	The reactive power exponent in region 2
nl	Number of monitored branches in the system
nb	Number of monitored buses in the system
NCR	The group of contingencies that are not critical for dynamic security assessment

NERC	North American Electric Reliability Corporation
O	Big-O notation
p	Number of parameters in the expression $\mathbb{R}^p$
P_{run}	Active power consumed by the single phase induction motor in the run-
P_{stall}	Active power consumed by the single phase induction motor in the stalled
P_0	A component of active power in the single phase induction motor model
pf	Power factor
PCR	The group of contingencies that are possibly critical for dynamic security assessment
PI	Performance index
PI_V	Voltage-based index
PI_{MVA}	Flow-based index
PSAT	Power system analysis toolbox based in MATLAB
PSLF	Positive sequence power system analysis tool developed by General
Q_0	A component of reactive power in the single phase induction motor
Q_{run}	Reactive power consumed by the single phase induction motor in the run-
Q_{stall}	Reactive power consumed by the single phase induction motor in the
$\mathbb{R}$	The real number space
$Rstall$	Stall resistance of the single phase induction motor
S	A set of functions describing the switching conditions
S_i	Post-contingency flow in branch i
S_i^{lim}	Short term emergency rating of branch i
$S_{\max}$	Normalized maximum sensitivity
S_λ	Partial derivative of S with respect to λ
SPIM	Single phase induction motor
SSA	Static security assessment
SSTools	Contingency analysis module in GE-PSLF
t	Time
TDS	Time domain simulation

TPL	Transmission planning
TS	Trajectory sensitivity
Tstall	Parameter representing the time after which a single phase induction motor stalls if the voltage is below a set threshold
U_i	vector of the partial derivatives of the variables *x* with respect to param-
ULTC	Under load tap changer
V_{brk}	Breakdown voltage of an air-conditioner
V_t	Terminal voltage
V_{stall}	Stall voltage of the air-conditioner
V_i	Post-contingency voltage at a bus *i*
V_i^{sp}	Nominal voltage at a bus *i*
ΔV_i^{lim}	Maximum voltage change limit bus *i*
w_{bi}	Weighting factor in the voltage-based index
Vstall	Parameter representing voltage threshold below which a single phase induction motor stalls
W_i	Vector of the partial derivatives of the variables *y* with respect to param-
w_{li}	Weighting factor in the flow-based index
WECC	Western electricity coordinating council
WSCC	Western system coordinating council
x	Power system state variables
$x(t)_{old}$	Trajectory of power system state variables in the base case
$x(t)_{est}$	Estimated trajectory of power system state variables
xra	Rotor reactance of motor A
xrb	Rotor reactance of motor B
xsa	Stator reactance of motor A
xsb	Stator reactance of motor B
Xstall	Stall reactance of the single phase induction motor
y	Power system algebraic variables
$y(t)_{old}$	Trajectory of power system algebraic variables in the base case

$y(t)_{est}$	Estimated trajectory of power system algebraic variables
Z_{th}	Thévenin's impedance
α	Exponent term in the voltage-based and flow-based index
λ	Power system parameters
ε	Small change in parameter
ϕ	A function that maps the initial conditions, parameter values and time to the current value of x
τ	Time duration to trigger the time difference switching action
Δf	Change in frequency
ΔFmd	Percentage change in Fmd
Δt	Change in time
$\lvert\Delta Z_{thmax}\rvert$	Magnitude of maximum change in Thévenin's impedance

CHAPTER 1: INTRODUCTION

The past decades have seen a significant shift in the expectations and requirements related to power system analysis tools. Investigations into major power grid disturbances have suggested the need for more comprehensive assessment methods. Accordingly, significant research in recent years has focused on the development of better power system models and efficient techniques for analyzing power system operability. The work done in this report focuses on two such topics

1. The analysis of uncertainty in load model parameters and sensitivity based parameter estimation, and

2. A systematic approach to *n*-1-1 analysis for power system security assessment

Although, these topics are separate and not linked to each other, both these topics are important in terms of understanding the behavior of power systems and guaranteeing reliable operation. The research work presented on the first topic aids the development of accurate load models, which benefits power system simulation studies and more accurate evaluation of operating limits. The second topic explores systematic methods to perform contingency studies, which otherwise are computationally burdensome. A brief overview of both the topics and the primary goals of the research conducted in these two areas are provided in this chapter.

1.1 Load model parameter uncertainty and parameter estimation

Dynamic simulations play a crucial role in understanding the behavior of power systems under a variety of operating scenarios. Planners and operators rely on simulation

studies to determine whether operating scenarios are safe and take corrective measures if needed [1], [2], [3]. As such, the simulation studies are expected to replicate the actual behavior of the system closely. Since the simulations are only as good as the models used, developing accurate power systems models has been pivotal in the power systems research sphere. Presently, well-established mathematical models of conventional generation and transmission equipment exist for computer simulations [4], [5], [6]. The development of accurate load models is still an ongoing process, although much has been done in this field [7], [8], [9], [10], [11].

The postmortem analyses of the 1996 western system coordinating council (WSCC) outage have shown that inaccurate load models can cause substantial discrepancies in the simulated and actual system response [7]. The increased penetration of load components with complex characteristics and dynamics has further necessitated the development of accurate load models for power system studies. A large volume of work already done in this field has led to the issue of two IEEE load modeling recommendations [8], [9]. The recommendations require load models to represent air conditioners (A/C), power electronic drives and loads, heat pumps and energy efficient lighting [9], [10], [11]. Presently, the NERC transmission planning (TPL) standard -001-4 recommends that at system peak load levels the load models should be able to reproduce the expected dynamic behavior of loads that could affect the study area [12]. In recent years, for a better representation of the loads, the WECC model validation and working group (MVWG) developed the composite load model [13], [14]. The composite load model has been implemented in several commercial power system simulators. The composite load model represents the aggregation of

different types of loads at the distribution substation level [14]. A detailed description of this model is provided in a later chapter of this report.

Although detail load models exist, the major challenge remains in determining the exact composition of the various components. This is required to establish a reasonable aggregated load model [15], [16]. Presently, the compositions of aggregate load models and load parameters are determined mostly by surveys conducted by utilities to assess the level of loads in various categories such as residential, commercial and industrial load [15], [16]. The survey results are also augmented with measurement based parameter estimation in some cases [15], [16]. Nevertheless, the load on the system is constantly changing not only in terms of the consumption level but also in terms of the composition. Moreover, parameter estimation for aggregated load models is challenging due to the distributed nature and the diversity of the consumer loads. Therefore, there are always significant uncertainties and approximations in the load models. The inherent variability in load levels and composition makes load modeling for power system studies uniquely different from generation or transmission component modeling. It is not only important to assess the effect of such uncertainties on the dynamic behavior of the system, but also to investigate techniques to develop better load models that can represent the aggregated load response accurately. Sensitivity studies provide a systematic approach to tackle these problems efficiently. The work done in this report addresses both these challenges related to load modeling in power system analysis. To analyze the effect of load model parameter uncertainty and to efficiently estimate load model parameters, the report

1. describes a trajectory sensitivity analysis based method to study the effect of load model uncertainty in a computationally efficient manner, and

2. documents the development of a sensitivity-based parameter estimation tool and highlights the insight that parameter sensitivities provide in the parameter estimation process.

A detailed introduction to these topics and a relevant literature survey is provided in the later chapters.

1.2 *n*-1-1 contingency analysis in power system operation

Cascading outages can have a catastrophic impact on power system operation. One such incident in recent times was the September 8, 2011 blackout that affected San Diego and large parts of the southwestern United States. The findings of the FERC/NERC report on the 2011 blackout suggested that the cascading nature of the events resulted in violation of interconnection reliability operating limits (IROLs) that were not recognized previously [17]. This event highlighted the need to examine the impact of *n*-1-1 contingencies, where the second outage is not related or dependent on the initiating outage [18]. Accordingly, the NERC transmission planning (TPL) standards require utilities to plan for *n*-1-1 outages [19]. To comply with the NERC TPL standards, utilities must ensure that the system is able to maintain stability and operate within acceptable limits following such outages. Ensuring the safe and reliable operation of a power system requires assessing both the static and the dynamic security for every *n*-1-1 contingency [20], [21].

Although such assessments improve the overall reliability of a system, it comes with an additional burden of evaluating a vast number of outages. The number of *n*-1-1 contingencies can be overwhelming, even for a small power system. For a system with *n* elements, the number of possible *n*-1-1 contingencies is given by;

$$number\ of\ n\text{-}1\text{-}1\ contingencies = \frac{n(n-1)}{2}. \quad (1.1)$$

Due to the large number of possible *n*-1-1 outages, a systematic approach to screen *n*-1-1 contingencies is needed. It is important to identify the contingencies that are critical from a system security viewpoint in a computationally efficient manner. The critical contingencies can be consequential, and need to be identified and analyzed prior to the non-critical cases. To achieve the stated objective, this report proposes

1. a method to screen and rank *n*-1-1 contingencies for static security assessment (SSA), and
2. a method to screen and classify *n*-1-1 contingencies for dynamic security assessment (DSA).

Contingency screening methods have been proposed in the past for both static and dynamic security assessment. However, most of these methods are applicable for screening *n*-1 contingencies and cannot be extended reliably for screening *n*-1-1 contingencies. This issue has been discussed in detail in a later chapter. The work done in this report aims to develop screening methods, which are convenient to implement in practice while being highly accurate in detecting critical contingencies. Both the proposed contingency analysis techniques are intended to be used by operators/planners in the planning phase.

1.3 Organization of the report

The report is organized in two parts. The first part comprises of chapter 2 to chapter 7. This part of the report presents the research on load modeling and analysis of uncertainty in the load model parameters. The second part of the report consists of chapter 8 to chapter 13. This part of the report describes the development of a systematic approach to *n*-1-1

contingency analysis. The conclusions of the first part and the second part are presented separately at in chapters 7 and chapter 13 respectively.

Chapter 2 provides a mathematical background of trajectory sensitivity analysis and its application in power systems. This chapter further illustrates the application of trajectory sensitivity to study the impact of parameter uncertainty. Chapter 3 presents the application of trajectory sensitivity to analyze load parameter uncertainty in the WECC system. Chapter 3 also presents a detailed description of the composite load model and discusses the parameter sensitivities of a few selected composite load parameters. Chapter 4 presents a discussion on the parameter sensitivity studies in power systems with non-smooth models like the composite load model. A detailed discussion on the associated estimation error is presented here. Chapter 5 discusses the implementation of the trajectory sensitivity analysis module in commercial power system simulators. In Chapter 5, the trajectory sensitivity analysis is formulated such that it is conducive to implementation in the presently available commercial power system simulators. Chapter 6 presents the development of a sensitivity based parameter estimation tool in MATLAB. A theoretical background for parameter estimation using least squares estimation is presented here. Furthermore, an example of parameter estimation is presented here. Chapter 7 summarizes the main conclusions of the research work done on parameter uncertainty in load modeling and load model parameter estimation. Furthermore, this chapter discusses some of the future research avenues that can be explored.

Chapter 8 presents an introduction to power system security assessment. The chapter introduces some key concepts of power system security assessment and a review of the

work already done in this field. Chapter 9 presents the proposed *n*-1-1 contingency screening and ranking method for static security assessment. Chapter 10 presents the results of the application of the proposed contingency screening and ranking method on a real power system. A comparison of the proposed screening and ranking method with an exhaustive *n*-1-1 analysis is also presented here. Chapter 11 presents the proposed *n*-1-1 contingency screening and classification for dynamic security assessment. Chapter 12 presents the results of the application of the proposed contingency screening and classification method on a real power system. Chapter 13 summarizes the main conclusions of the research done on the development of a systematic approach to *n*-1-1 power system security assessment. In addition, this chapter discusses some of the future work that needs to be done for advancement of the proposed contingency analysis tools.

In addition, the report has an appendix; Appendix A. Table A.1 of appendix A provides a description of the 2012 WECC high summer case. Table A.2 lists the composition of the load model at the different types of load buses in the WECC system. Table A.3 lists the default composite load model parameters that have been used in this work.

CHAPTER 2: TRAJECTORY SENSITIVITY ANALYSIS IN POWER SYSTEMS

The concepts of trajectory sensitivity (TS) analysis are well known and have been introduced in [24-27]. TS based analysis has been used for a wide variety of applications in power systems. TS based analysis has been used for validating system models from disturbance measurements [28]. TS based methods have been proposed to solve power system inverse problems [29]. Applications of TS in studying the effect of parameter uncertainty on power system response have been presented in [30]. Utilization of TS for dynamic security assessment and computation of stability constrained active power flow limits have been in investigated in [31], [32], [33]. Application of TS has also been explored for tuning non-linear controllers of power system equipment [34]. This chapter provides a brief mathematical background on TS computation. The application of TS to estimate the effect of parameter uncertainty is also described here.

2.1 System description

A detailed description of the analytical basis for TS analysis of hybrid systems can be found in [27]. A brief introduction to TS analysis for power systems is presented in this section. A power system is a hybrid dynamical system, which has both continuous-time as well as discrete-time dynamics. A power system can be represented by a set of non-linear differential algebraic equations (DAE) [27] given by

$$\dot{x} = F(x, y, \lambda) \text{, and} \tag{2.1}$$

$$\left.\begin{aligned} G^{-}(x,y,\lambda) = 0 \ for \ S(x,y,\lambda) < 0 \\ G^{+}(x,y,\lambda) = 0 \ for \ S(x,y,\lambda) \geq 0 \end{aligned}\right\}, \tag{2.2}$$

where,

$x \in \mathbb{R}^n$ is a vector of state variables

$y \in \mathbb{R}^m$ is a vector of algebraic variables

$\lambda \in \mathbb{R}^p$ is a vector of parameters that may be subject to change

$F: \mathbb{R}^{n+n+p} \rightarrow \mathbb{R}^n$ is the set of differential equations describing the evolution of the power system state variables

$G: \mathbb{R}^{n+n+p} \rightarrow \mathbb{R}^m$ is the set of algebraic equations. The + and – superscripts denote the pre and post switching conditions

$S: \mathbb{R}^{n+n+p} \rightarrow \mathbb{R}^l$ is the set of algebraic equations that define the switching conditions in power systems

In the context of power systems, x includes the machine state variables like rotor angles, angular speed, flux linkages and all associated controller state variables. y includes the network algebraic variables like bus voltage magnitudes and angles. λ includes the various parameters that are used while representing the power system elements at a certain operating condition. The parameters in a power system problem can be the machine impedances, line and transformer impedances, load parameters, generator outputs, shunt reactance, and controller set points, to name a few. These parameters can greatly influence the response of a power system to an event like a fault or a large load or generation change. S defines the conditions when switching actions occur in models. Examples of switching events would be the switching of a contactor, tripping of a component by a relay or the

transition of an induction motor from a running state to a stall state. It should be noted that the model described by (2.1) and (2.2) does not adequately capture events where discrete jumps occur in the state variables. A differential algebraic impulse system (DAIS) representation has been suggested in [29] to account for such jumps. Nevertheless, the model described by (2.1) and (2.2) is adequate for the purpose of this study since the events leading to discrete jumps in state variables are not pursued in this research work.

2.2 Numerical evaluation of trajectory sensitivities

The trajectory sensitivities can be evaluated either numerically or analytically. In the numerical approach to sensitivity evaluation, the finite differencing method is used [35]. The finite differencing method is based on the Taylor's theorem [35]. The partial derivatives can be computed by using a forward difference or a central difference method. In the forward difference method [35], the partial derivatives are computed by

$$\frac{\partial x(t,\lambda)}{\partial \lambda} \approx \frac{x(t,\lambda+\varepsilon)-x(t,\lambda)}{\varepsilon}. \tag{2.3}$$

In the central difference method [35], the partial derivatives are computed by

$$\frac{\partial x(t,\lambda)}{\partial \lambda} \approx \frac{x(t,\lambda+\varepsilon)-x(t,\lambda-\varepsilon)}{2\varepsilon}, \tag{2.4}$$

where, ε is a small perturbation and t is the time. A detailed discussion on the different finite difference methods can be found in [35]. For an infinitesimal small perturbation ε, the finite differencing methods provide a reasonably accurate estimate of the partial derivatives. Between the two finite difference methods described, the central difference method

provides a better estimate of the partial derivatives. The order of error in the central difference method is $O(\varepsilon^2)$ as compared to $O(\varepsilon)$ in the forward difference method [35]. However, for small values of the perturbation size, the accuracy achieved by both methods is comparable [35]. For evaluating of the trajectory sensitivities, the DAEs described by (2.1) and (2.2) are solved twice to obtain the values of the variables x and y at two different values of the uncertain parameter λ and $\lambda+\varepsilon$. The trajectory sensitivities are then computed by using either (2.3) or (2.4).

The numerical method for sensitivity evaluation, although easier to implement is computationally more expensive than the analytical method. This is because in (2.3) or (2.4), two time domain simulations (TDS) need to be performed to compute the sensitivities by differencing. The analytical method of sensitivity evaluation requires less computational effort compared to the numerical method. To evaluate the sensitivities analytically, the sensitivity dynamic equations given by [24-27]

$$\frac{d\dot{x}}{d\lambda_i} = \frac{dF}{d\lambda_i} = \frac{dU_i}{dt} = F_x U_i + F_y W_i + F_{\lambda_i}, \text{ and} \tag{2.5}$$

$$0 = \frac{dG}{d\lambda_i} = G_x U_i + G_y W_i + G_{\lambda_i}, \tag{2.6}$$

where,

$U_i = \partial x/\partial \lambda_i$ is the $n \times 1$ vector of the partial derivatives of the states x with respect to the parameter λ_i

$W_i = \partial y/\partial \lambda_i$ is the $m \times 1$ vector of the partial derivatives of the variables y with respect to

the parameter λ_i

F_x is the $n \times n$ matrix of the partial derivatives of F with respect to the state variables x

F_y is the $n \times m$ matrix of the partial derivatives of F with respect to the algebraic variables y

$F_{\lambda i}$ is the $n \times 1$ vector of partial derivative of F with respect to the i^{th} parameter λ_i

G_x is the $m \times n$ matrix of the partial derivatives of G with respect to the state variables x

G_y is the $m \times m$ matrix of the partial derivatives of G with respect to the algebraic variables y

$G_{\lambda i}$ is the $m \times 1$ vector of the partial derivatives of G with respect to the i^{th} parameter λ_i

The sensitivity dynamic equations (2.5) and (2.6) are solved simultaneously with the system equations (2.1) and (2.2) to evaluate the sensitivities U_i and V_i for a change in the i^{th} parameter λ_i. While evaluating the DAEs given by (2.1) and (2.2) using an implicit integration routine like the trapezoidal method [36], the updated variables for the next time step is found by solving

$$x(t+\Delta t) - x(t) - \frac{\Delta t}{2}(F(x(t+\Delta t), y(t+\Delta t), \lambda) + F(x(t), y(t), \lambda)) = 0 \text{, and} \qquad (2.7)$$

$$G(x(t+\Delta t), y(t+\Delta t), \lambda) = 0 \text{,} \qquad (2.8)$$

where, t is the time and Δt is the time step of integration. Since (2.7) and (2.8) are a set of non-linear equations, an iterative technique like the Newton-Raphson method is used to solve for $x(t+\Delta t)$ and $y(t+\Delta t)$ at each time step of the integration. The Jacobian required for solving (2.7) and (2.8) is given by

$$\begin{bmatrix} I - F_x \frac{\Delta t}{2} & F_y \frac{\Delta t}{2} \\ G_x & G_y \end{bmatrix}. \tag{2.9}$$

To augment the computation of trajectory sensitivities with the TDS routine, (2.5) and (2.6) can are rewritten as

$$\frac{d\dot{x}}{d\lambda_i} = \frac{dU_i}{dt} = F_{new}(U_i(t), W_i(t)) = 0 \text{, and} \tag{2.10}$$

$$G_{new}(U_i(t), W_i(t)) = 0, \tag{2.11}$$

where, F_{new} and G_{new} are the right hand sides of (2.5) and (2.6) respectively. Using the trapezoidal rule (2.10) and (2.11) are rewritten as

$$U_i(t+\Delta t) = U_i(t) + \frac{\Delta t}{2}(F_{new}(U_i(t+\Delta t), W_i(t+\Delta t)) + F_{new}(U_i(t), W_i(t))) \text{, and} \tag{2.12}$$

$$G(U_i(t+\Delta t), W_i(t+\Delta t)) = 0. \tag{2.13}$$

(2.12) and (2.13) can be expanded and written as a linear matrix equation given by

$$\begin{bmatrix} I - \frac{\Delta t}{2} F_x(t+\Delta t) & -\frac{\Delta t}{2} F_y(t+\Delta t) \\ G_x(t+\Delta t) & G_y(t+\Delta t) \end{bmatrix} \begin{bmatrix} U_i(t+\Delta t) \\ W_i(t+\Delta t) \end{bmatrix} = \begin{bmatrix} U_i(t) + \frac{\Delta t}{2}(F_x(t)U_i(t) + F_y(t)W_i(t) + F_{\lambda_i}(t) + F_{\lambda_i}(t+\Delta t)) \\ -G_{\lambda_i}(t+\Delta t) \end{bmatrix}. \tag{2.14}$$

The generic form of (2.14) for hybrid dynamical systems can also be found in [27]. It can be seen that F_x, F_y, G_x and G_y required to solve the linear matrix equation (2.29) are already computed during the TDS. All the terms in (2.14) except $U_i(t+\Delta t)$, and $W_i(t+\Delta t)$

are known and the unknown terms can be found by factorizing the right hand side of (2.14) and solving the linear matrix equation. Furthermore, the matrix in the right hand side of (2.14) is same as the Jacobian (2.9). Therefore, the factors of the Jacobian given by (2.9) that are computed in the TDS routine can be used directly. The only additional computational effort required in this method is to evaluate the vectors F_λ and G_λ in (2.14), which are sparse. Therefore, the evaluation of the trajectory sensitivities by the analytical method does not require any major additional computational effort. The implementation of the TS routine in PSAT has been described in [37].

The sensitivities U_i and W_i are discontinuous at the switching events described by S in (2.2). Reference [27] provides details on the calculation of the switching conditions and the sensitivities at these switching events. The sensitivity dynamic equations for different parameter changes are independent of each other and hence amenable to parallel computation. The use of parallel computation results in additional savings in computation time. References [37] and [38] describe the implementation of TS analysis in power systems using cluster computing.

2.3 Estimating the effect of parameter uncertainty

Once the trajectory sensitivities are evaluated, the impact of the change in a parameter value on the system trajectories can be studied without the need for multiple TDSs. For a change in the magnitude of a parameter λ_i the perturbed trajectories can be estimated by a linear approximation as

$$x(t)_{est} = x(t)_{old} + \frac{\partial x(t)}{\partial \lambda_i} \Delta \lambda_i \text{, and} \tag{2.15}$$

$$y(t)_{est} = y(t)_{old} + \frac{\partial y(t)}{\partial \lambda_i} \Delta \lambda_i \text{,} \tag{2.16}$$

where, $x(t)_{old}$, and $y(t)_{old}$ are the base case trajectories, $x(t)_{est}$, and $y(t)_{est}$ are the estimated trajectories and $\Delta\lambda_i$ the change in λ_i for which the trajectories are being estimated

The linear approximation of trajectories is reasonably accurate when the parameter perturbation sizes are small. If the perturbation sizes are large, truncation error associated with the omission higher order terms of the Taylor series arises. It is therefore important to evaluate the limit of perturbation size for which linear approximations hold. The evaluation of perturbation size is a topic in itself and has been discussed in a later chapter.

2.4 Summary

This chapter presented an introduction to TS analysis and its applications in power system. A discussion of both the numerical method and the analytical method of evaluating the sensitivities is presented here. The implementation of the analytical approach along with an implicit integration based TDS is presented here. In addition, it is shown that the analytical method of TS evaluation is computationally less burdensome as compared to the numerical method.

CHAPTER 3: APPLICATION OF TRAJECTORY SENSITIVITY TO ANALYZE LOAD PARAMETER UNCERTAINTY

In power system studies, loads are modeled as an aggregation of different types of consumer loads at the distribution substation [11], [13-16]. The WECC composite load model developed by the WECC MVWG [13], [14] is one such load model that has been widely incorporated in several commercial power system simulators [22], [23]. Since the WECC composite load is an aggregated load model, one of the main challenges is in determining the exact composition of the load. Furthermore, the load parameter estimation process, which primarily relies on surveys and measurements, introduces additional variability [15], [16]. It is therefore important to assess the impact of load composition and parameter uncertainty on the dynamic response of the system. TS analysis provides a suitable avenue to perform such assessments. In addition to estimating the change in the system response, TS analysis serves to identify the most important load parameters, which are consequential from a system performance viewpoint.

This chapter describes the composite load model and the application of TS analysis for studying load parameter uncertainty. In the following sections, the composite load model is described in details and the sensitivities of some of the important composite load model parameters are studied. Furthermore, the application of TS to estimate the system response to a change in a load parameter is demonstrated here.

3.1 The WECC composite load model

The WECC composite load model represents an aggregation of consumer loads at the substation level. Figure 3.1 shows the implementation of the WECC composite load

model in GE-PSLF a commercially available power system simulator [22]. The WECC composite load model is referred to as '*cmpldw*' in the GE-PSLF model library [22]. A detailed description of the '*cmpldw*' model and the associated parameters can be found in [22].

To ensure flexibility in terms of the implementation of various models and algorithms, PSAT a MATLAB based open source power system simulator was used for this research [39], [40]. PSAT is a positive sequence power flow and electromechanical transient simulator like GE-PSLF. A composite load model based on the GE-PSLF '*cmpldw*' was created in PSAT. Figure 3.2 shows the composite load model developed for the study in PSAT. The motors are labeled as A, B, C and D since the same nomenclature is adopted by most commercial power system simulators [22], [23]. The description of the various components shown in Figure 3.2 is as follows:

1. Motor A is the cumulative representation of the motors with high inertia connected to the distribution bus.

2. Motor B is the cumulative representation of the motors with low inertia connected to the distribution bus.

3. Motor C is the cumulative representation of the motors connected to the distribution bus with low inertia, which trip under low voltage condition with a pre-specified time delay.

4. Motor D is the cumulative representation of the single-phase induction motor (SPIM) driven A/C connected to the distribution bus.

5. Electronic load: The electronic load is a constant PQ load operating at a constant power factor. The load disconnects and reconnects linearly when the terminal voltage drops or rises above set thresholds respectively [22].

6. Static load: The static load is represented by the standard ZIP load model [22].

Motor A, motor B and motor C are modeled as three-phase double cage induction motors with a quadratic load torque versus speed characteristics [6], [40]. The dynamics of the three-phase induction motors are represented by differential equations and can be found in [40]. Motor A, motor B and motor C are represented by the 'Order V' induction motor model in PSAT [40]. The 'Order V' induction motor model in PSAT is similar the '*motorw*' model in the PSLF model library [22].

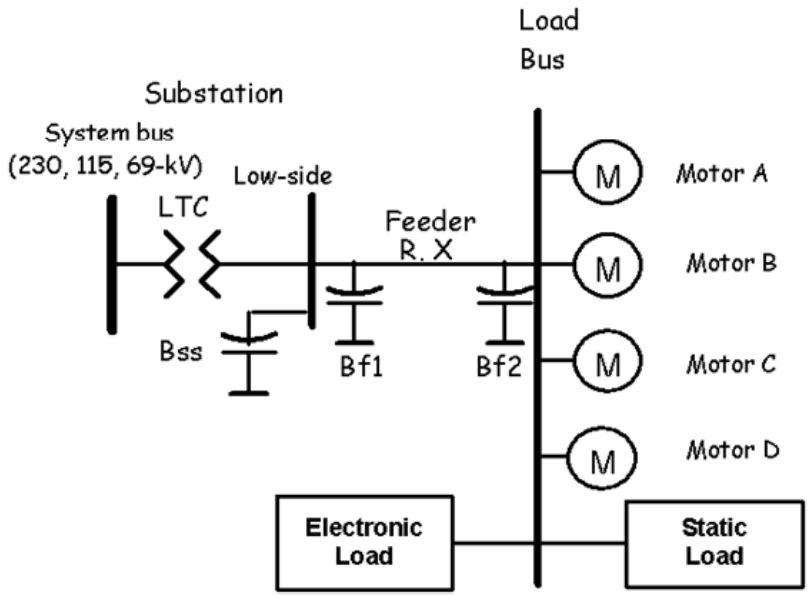

Figure 3.1 The composite load model '*cmpldw*' in GE-PSLF [22]

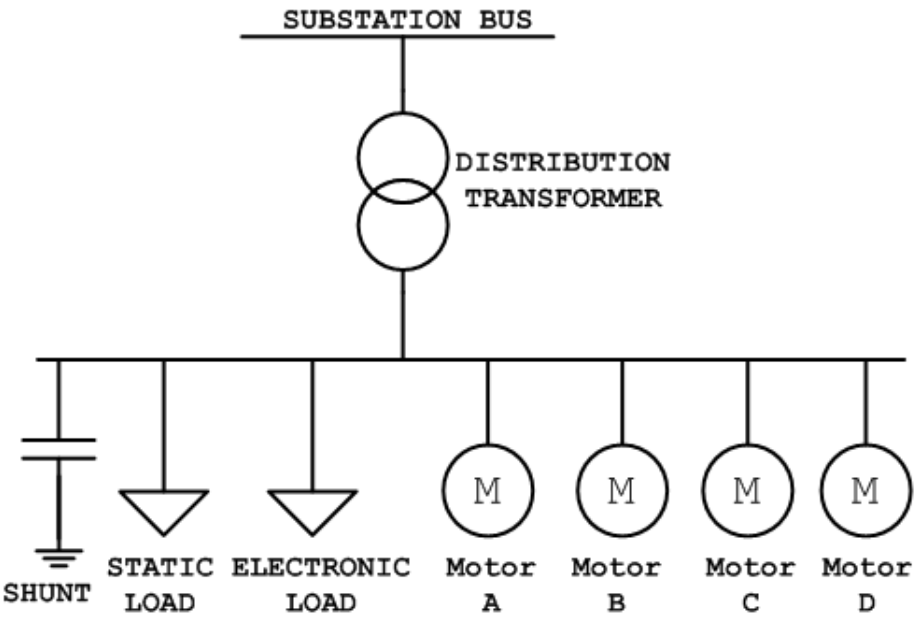

Figure 3.2 The composite load model created in PSAT

Motor D is a performance based SPIM driven A/C model. PSAT does not have an existing model for a SPIM driven A/C and hence, this model was added to the PSAT model library. Motor D is based on the '*ld1pac*' model in the PSLF model library [22]. A similar model is available in the Siemens PSS/E model library under the name '*ACMTBLU1*' [23]. The schematic diagram of motor D is shown in Figure 3.3. The dynamics of motor D is described by algebraic equations. Reference [41] provides a detailed test report of the '*ld1pac*' model in PSLF, which is the basis for developing the motor D model in PSAT. Motor D has three distinct operating states [41]. The three distinct regions are as follows:

1. Region 1: Terminal voltage (V_t) > Compressor break down voltage (V_{brk}).

2. Region 2: Stall voltage (V_{stall}) < Terminal voltage (V_t) ≤ Compressor break down voltage (V_{brk}).

3. Region 3:Terminal voltage (V_t) ≤ Stall voltage (V_{stall})

Region 1 and region 2 are running states, while region 3 represents the stalled condition of the SPIM driven A/C. The active and the reactive power consumed by the SPIM driven A/C in the different operating states are as follows [41]:

Region 1: Terminal voltage (V_t) > Compressor break down voltage (V_{brk})

The active and reactive power consumed by the SPIM in region 1 is given by

$$P_{run} = Kp1\left(V_t - V_{brk}\right)^{Np1} + P_0, \text{ and} \tag{3.1}$$

$$Q_{run} = Kq1\left(V_t - V_{brk}\right)^{Nq1} + Q_0, \tag{3.2}$$

where,

P_{run} is the active power consumed by motor D in the running state
Q_{run} is the reactive power consumed by motor D in the running state
$Kp1$ is the active power coefficient in region 1
$Kq1$ is the reactive power coefficient region 1
$Np1$ is the active power exponent in region 1
$Nq1$ is the reactive power exponent in region 1
V_t is the terminal voltage of the machine
V_{brk} is the breakdown voltage of the A/C

P_0 and Q_0 are given by

$$P_0 = 1 - Kp1\left(1 - V_{brk}\right)^{Np1}, \text{ and} \tag{3.3}$$

$$Q_0 = \frac{\sqrt{1 - pf^2}}{pf} - Kq1\left(1 - V_{brk}\right)^{Nq1}, \tag{3.4}$$

where, pf is the power factor

Region 2: Stall voltage (V_{stall}) < Terminal voltage (V_t) ≤ Compressor break down voltage (V_{brk})

The active and reactive power consumed by the SPIM in region 2 is given by

$$P_{run} = Kp2\left(V_{brk} - V_t\right)^{Np2} + P_0 \text{, and} \tag{3.5}$$

$$Q_{run} = Kq2\left(V_{brk} - V_t\right)^{Nq2} + Q_0 , \tag{3.6}$$

where,

$Kq2$	is the reactive power coefficient region 2
$Np2$	is the active power exponent in region 2
$Nq2$	is the reactive power exponent in region 2
V_t	is the terminal voltage of the machine
V_{brk}	is the breakdown voltage of the A/C

P_0 and Q_0 are given by (3.3) and (3.4) respectively.

Region 3: Terminal voltage (V_t) ≤ Stall voltage (V_{stall})

The active and reactive power consumed by the SPIM in region 3 is given by

$$P_{stall} = V_t^2 G_{stall}, \text{ and} \tag{3.7}$$

$$Q_{stall} = V_t^2 B_{stall}, \tag{3.8}$$

where,

P_{stall}	is the active power consumed by motor D in the stalled state
Q_{stall}	is the reactive power consumed by motor D in the stalled stalled
B_{stall}	is the stall susceptance of the SPIM
G_{stall}	is the stall conductance of the SPIM

The frequency dependency of the single-phase air conditioner load is modeled by including the active power and the reactive power frequency sensitivity factors. The frequency dependent characteristics for the running and the stall condition are given by

$$P_{run}(f) = P_{run}\left(1 + K_{pf}\Delta f\right), \tag{3.9}$$

$$P_{stall}(f) = P_{stall}\left(1 + K_{pf}\Delta f\right), \tag{3.10}$$

$$Q_{run}(f) = Q_{run}\left(1 + K_{qf}\frac{\Delta f}{\sqrt{1 - pf^2}}\right), \text{ and} \tag{3.11}$$

$$Q_{stall}(f) = Q_{stall}\left(1 + K_{qf}\frac{\Delta f}{\sqrt{1 - pf^2}}\right), \tag{3.12}$$

where,

$P_{run}(f)$	is the active power consumed by motor D in the running state with frequency sensitivity
$P_{stall}(f)$	is the active power consumed by motor D in the stall state with frequency sensitivity
$Q_{run}(f)$	is the reactive power consumed by motor D in the running state with frequency sensitivity
$Q_{stall}(f)$	is the reactive power consumed by motor D in the stall state with frequency sensitivity
Δf	is the frequency deviation
K_{pf}	is the active power frequency sensitivity
K_{qf}	is the reactive power frequency sensitivity

As shown in Figure 3.3, the total load represented by motor D is further divided internally into a restartable part and a non-restarable part. The restartable part of motor D represents the SPIM driven A/C, which are capable of restarting when the terminal voltage at the SPIM recovers. The non-restartable part of motor D does not restart after the SPIM

has stalled, even if the voltage recovers above the restarting threshold. Both the restartable and non-restatable part of motor D is equipped with a thermal relay. The thermal relay implemented in motor D is shown in Figure 3.4. When the simulated winding temperature rises beyond the lower set point T_{th1}, the load represented by motor D is disconnected linearly and the entire load is disconnected when the simulated winding temperature rises beyond T_{th2}. In addition to the thermal relay, motor D is equipped with an undervoltage contactor and an undervoltage trip relay.

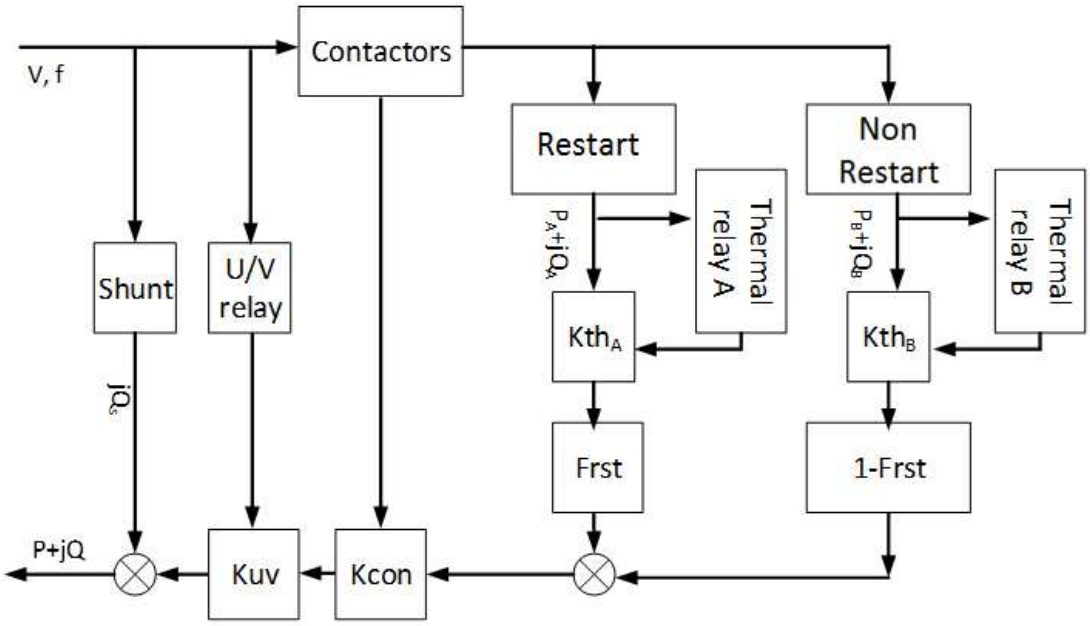

Figure 3.3 The performance based SPIM driven A/C model [22],[23]

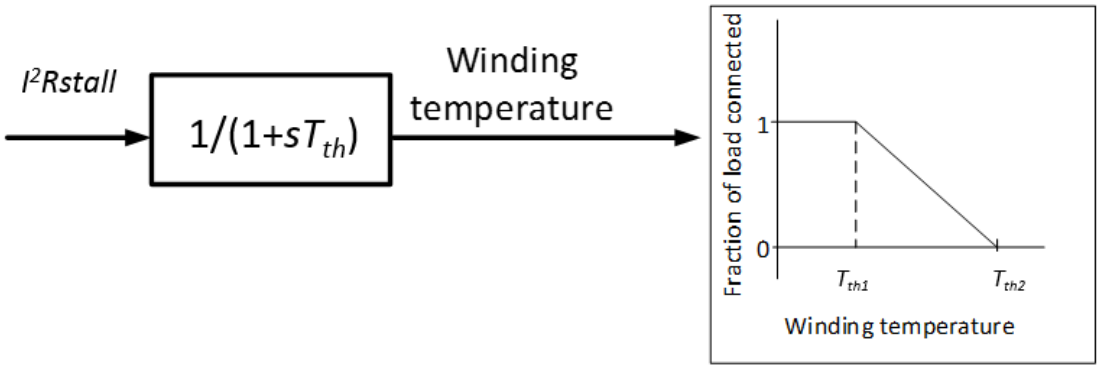

Figure 3.4 The thermal relay model in motor D [22], [23]

3.2 Case description

The WECC 2012 high summer (HS) case has been used in this research to perform the load parameter sensitivity study. Accordingly, the power flow file for the WECC system was converted appropriately for use in PSAT. Details of the WECC 2012 HS case can be found in APPENDIX A. The loads in the system were represented by the composite load model developed for PSAT. It should be noted that the original WECC 2012 HS case, available through the WECC website, does not use a composite load model to represent the loads. The composite load model was later added to the WECC 2012 HS case separately. The composition of the composite load model connected at a load bus was determined based on the season, hour of the day and the region where the load bus is located. The region where the load bus is located can be ascertained by the long identifier associated with every load bus provided in the WECC power flow data. APPENDIX A lists the composition of the load at different buses based on the long identifier, which is used for the work presented in this dissertation. In addition, the load buses have been renamed arbitrarily to mask the identity of the actual buses in the system.

3.3 Parameter sensitivities during a large disturbance

The work done in this research particularly focuses on the parameters of the motor D part of the WECC composite load described in chapter 2 [42]. Motor D, which represents a SPIM driven A/C primarily responsible for the fault induced delayed voltage recovery (FIDVR) phenomenon [43]. FIDVR is the unexpected delay in the recovery of the voltage after the normal clearing of a fault [43]. Larger motors have higher inertia and hence do not stall immediately after a transient voltage dip or a transient fault. Since the larger motors do not stall immediately, they have less effect on the system voltage recovery. In addition, the motor D part of the composite load model is interesting from a sensitivity analysis viewpoint because of its non-smooth nature. Although only the parameters of motor D are examined here, the same analysis could be extended without loss of generality to any uncertain parameter of the composite load model. The motor D component of the composite load model will be referred to as SPIM in the remainder of the dissertation.

The complete list of parameters of the composite load model is provided in APPENDIX A. The default values for the composite load model parameters as suggested by GE-PSLF can be found in [22]. Table 3.1 lists some of the parameters of the SPIM used for this research. As indicated in Table 3.1, *Vstall* and *Tstall* are used to define the conditions, when the SPIM transitions from a running state to a stall state.

To simulate the FIDVR event, a three-phase 5-cycle fault was applied on one of the major 500 kV lines in the southwestern WECC system. The fault was applied at $t = 0.2$ s. The simulation was conducted with the values for the load parameters listed in Table 3.1.

The sensitivities of the power system state and algebraic variables to the parameters considered in Table 3.1, were computed. Two load buses, LB1 and LB2, were chosen to study the parameter sensitivities. Figure 3.5 and Figure 3.6 show the bus voltages and the sensitivities of the bus voltages to the load parameters at buses LB1 and LB2 respectively. Bus LB1 is closer to the fault and the SPIM connected at this bus stalls immediately after the fault is applied. This is shown in Figure 3.5(a). Bus LB2 is farther away from the fault and the SPIM connected at this bus stalls approximately 0.6s after the fault is cleared due to the depressed voltage. This is shown in Figure 3.6(a). The stalling of the SPIM can be seen as a sharp dip in the voltage in both Figure 3.5(a) and Figure 3.6(a). The sharp dip in the voltage is due to the transition of the SPIM from the running state to the stall state. Once stalled, the active and the reactive power consumption of SPIM increases abruptly depending on the *Rstall* and the *Xstall* respectively [41], [42]. The stalling of the SPIM at the load buses results in a delayed voltage recovery in the area of interest.

A few important observations can be made from Figure 3.5 and Figure 3.6 [42]. The negative value of the voltage sensitivity to *Fmd* in Figure 3.5(b) and Figure 3.6(b) indicates that that an increase in the percentage of SPIM (*Fmd*) in the load composition at the buses will result in a poorer voltage recovery due to the fault. This is expected since a larger number of stalled SPIMs exacerbate the FIDVR phenomenon. Conversely, increasing the stall resistance and reactance (*Rstall* and *Xstall*) causes the SPIM to consume less power in the stalled state. Therefore increasing *Rstall* and *Xstall* aids the voltage recovery process. This can be interpreted from the positive values of the voltage sensitivities to *Rstall* and *Xstall* [42].

The sensitivity of bus voltages to *Tstall* and *Vstall* are different from the sensitivity behavior to *Rstall* and *Xstall*. Figure 3.5(c) and Figure 3.6(c) show the sensitivity of bus voltages to *Tstall* and *Vstall*. From Figure 3.6(c) it can be seen that a change in *Tstall* and *Vstall* affects the voltage at bus LB2 only at the time of stall. As time progresses, the sensitivity of bus voltage to these parameters diminish to zero. From Figure 3.5(c) a similar conclusion can be drawn about the sensitivity of the voltage at bus LB1 to *Tstall*. However, unlike in Figure 3.6(c), the voltage at bus LB1 is not sensitive to *Vstall* in Figure 3.5(c). The bus LB1 being electrically closer to the fault location experiences a larger dip in voltage due to the fault. As shown in Figure 3.5(a), the voltage drops sharply below 0.5 pu at the instant of the fault and remains close to 0.5 pu till the fault is cleared. The fault causes the voltage at the bus to drop below the SPIM voltage threshold *Vstall* instantaneously. Small changes in *Vstall* do not appreciably change the time instant when the SPIM stalls. Therefore, the voltage at bus LB1 is not sensitive to *Vstall*. However, at bus LB2, which is farther away from the fault, the voltage drops gradually below the SPIM stall conditions (around 0.8s in Figure 3.6(c)). Due to the gradual descent of the voltage into the stall condition, a change in *Vstall* significantly changes the time instant when the SPIM stalls. Therefore, the magnitude of the sensitivity of voltage to *Vstall* at bus LB2 is considerably high at the time instant when the SPIM connected at this bus stalls.

The sensitivities of the voltage to the SPIM stall parameters are high at the time of stall and decrease rapidly as time progresses. This is expected since the stall parameters *Vstall* and *Tstall* only affect the time instant and the duration taken for the SPIM to transition from a running state to a stall state. *Vstall* and *Tstall* are not present in the algebraic equations describing the power consumption of the SPIM in the performance model. In

terms of the mathematical formulation of the composite load model, *Vstall* and *Tstall* are present only in *S* of (2.2), which are the algebraic equations defining the switching conditions of the SPIM. On the other hand, *Rstall*, *Xstall*, *Fmd* are present only in *G* of (2.2) which are the algebraic equations defining the behavior of the SPIM in the running and stalled conditions.

Table 3.1 Parameters of motor D examined in this study

Parameter	**Value**	**Description**
Fmd	-	Fraction of motor D (SPIM) load in composite load model (in pu)
Rstall	0.124 pu	Stall conductance in pu
Xstall	0.114 pu	Stall susceptance in pu
Tstall	0.033 s	Time after which the SPIM stalls due to under-voltage
Vstall	0.7 pu	Voltage below which SPIM stalls

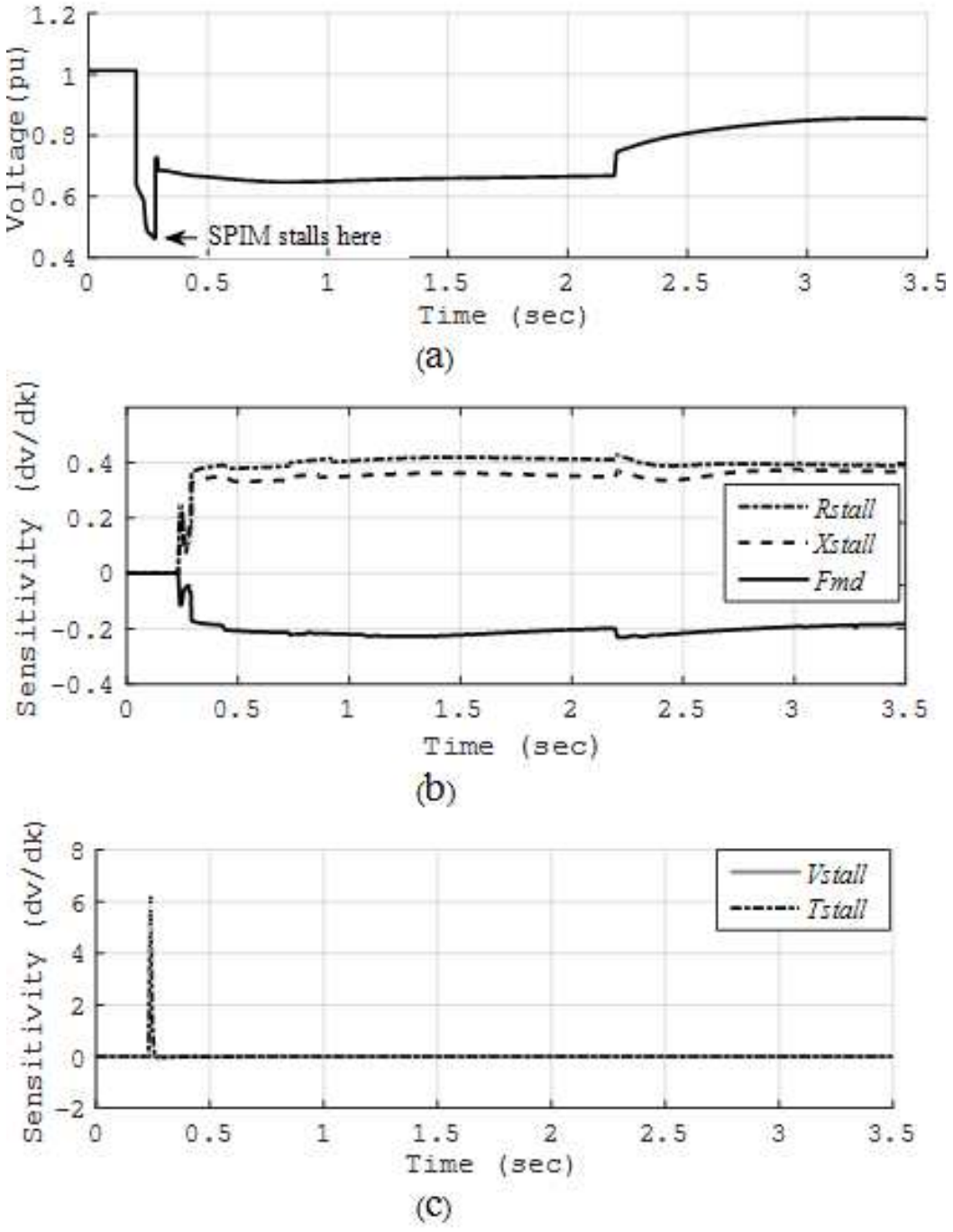

Figure 3.5 Sensitivities of voltage trajectory at bus LB1 to the different load parameters at bus LB1

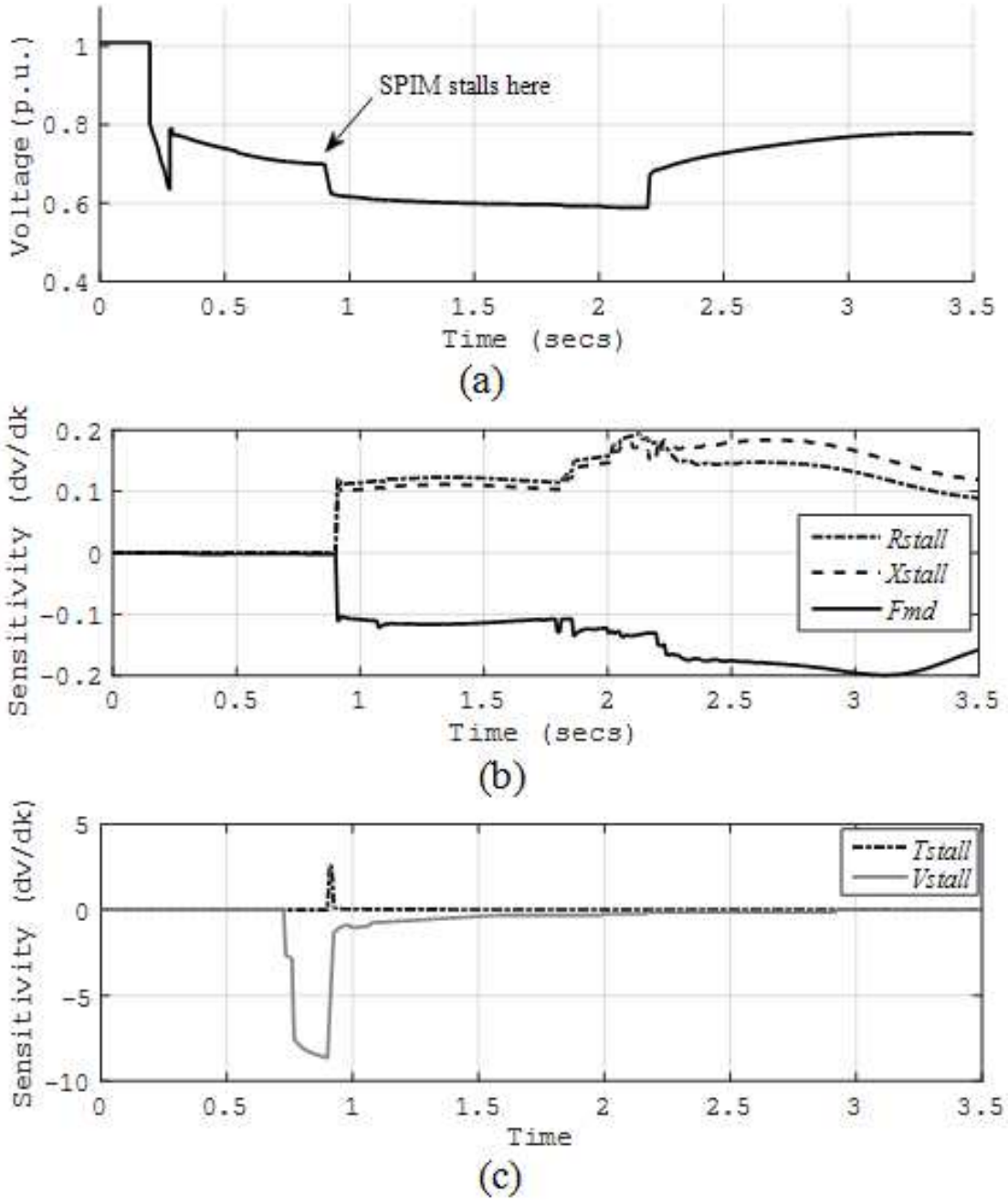

Figure 3.6 Sensitivities of voltage trajectory at bus LB2 to the different load parameters at bus LB2

3.4 Application of trajectory sensitivity to estimate the impact of parameter uncertainty

A simulation-based approach can be used to assess the impact of the uncertainty in parameter values on the system behavior. In this approach, a different value for the uncertain parameter is selected from its range of uncertainty, and a TDS is performed each time. Although accurate, a simulation-based approach is computationally burdensome due to the need for multiple TDSs. Moreover, this method does not provide any information about the importance of the uncertain parameter in the system response.

TS analysis provides a systematic approach to study the impact of the uncertainty in load parameters on system response to disturbances. Trajectory sensitivities quantify the variation of output trajectories based on small variations in parameters and/or initial conditions. Once the sensitivities are evaluated, the system response can be estimated by a linear approximation for a small change in the parameter.

A TS analysis based approach is demonstrated here to estimate the change in the system response due to the uncertainty in load parameters. It is assumed that the parameter *Fmd* of the SPIM in the composite load model is uncertain and may vary. This is a valid premise, as the composite load model is an aggregation of different types of load, the percentage of each type of load is likely to be uncertain [15], [16]. From Figure 3.5 and Figure 3.6, it can be seen that the bus voltages are sensitive to the parameter *Fmd*, only after the SPIM stalls. Therefore, it is reasonable to conclude that the uncertainty in *Fmd* at those buses, where the SPIM stalls will have any effect on the system voltages.

To simulate a large grid disturbance, a three-phase 5-cycle fault was applied on one of the major 500 kV lines in the southwestern WECC system. This is the same disturbance considered in the preceding section. It was observed that the SPIM component of the composite load connected at 20 load buses, located close to the fault, stalled due the voltage dip. The uncertainty in *Fmd* was considered at these 20 load buses. Since an increase in *Fmd* results in poorer voltage recovery, a positive increase in the parameter *Fmd* is of concern from a power system planning viewpoint. It is therefore assumed that the parameter *Fmd* at the selected load buses may increase by 5%. The change in *Fmd* is referred to as ΔFmd in the rest of this report. The sensitivities were evaluated using (2.5)-(2.6) and the estimated trajectories for the system voltages were computed using (2.15) and (2.16). Figure 3.7 and Figure 3.8 show the estimated voltage trajectory at buses LB1 and LB3 respectively, for a ΔFmd of 5% at the 20 selected buses. From Figure 3.7 and Figure 3.8 it can be seen that the estimated trajectory provides a reasonably accurate estimate of the actual voltage trajectory. The actual voltage trajectory is obtained by repeating the TDS by changing the parameter *Fmd*. In addition, Figure 3.9 to Figure 3.11 shows the actual and estimated trajectories of the voltage, frequency and the rotor angle at a generator bus GB1 in the area of interest. From the simulation studies, it can be seen that, a TS based method can be used to estimate the change in the system response to a parameter change without the need for repeated TDSs.

3.5 Comparison of computation time with repeated TDS

Table 3.2 presents the time required to run the various routines for trajectory estimation. In addition, the total time required to estimate the trajectories using the TS based

method is compared to the time required for conducting repeated TDS. From Table 3.2, it can be seen that using the TS based method the system response can be estimated quite accurately with reduced computation time.

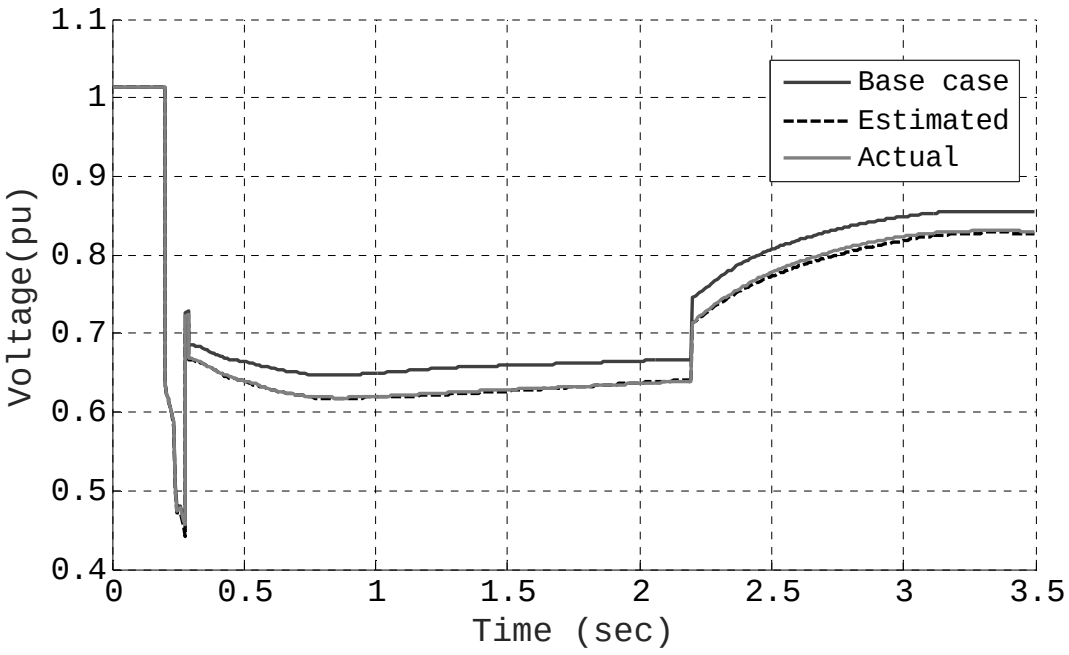

Figure 3.7 Actual and estimated voltage trajectories at bus LB1 for a Δ*Fmd* of 5% at 20 load buses

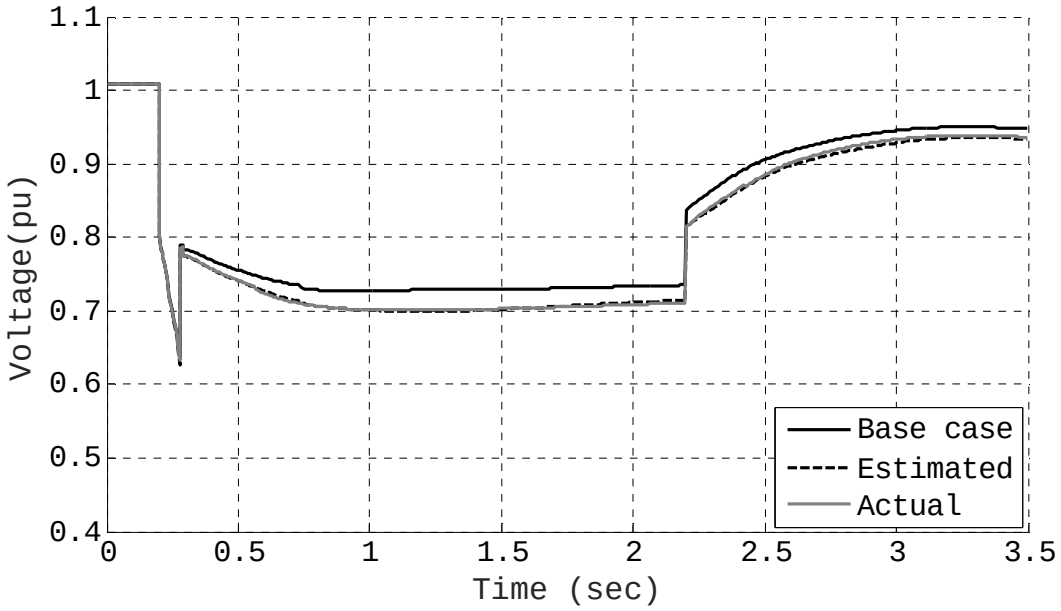

Figure 3.8 Actual and estimated voltage trajectories at bus LB3 for a Δ*Fmd* of 5% at 20 load buses

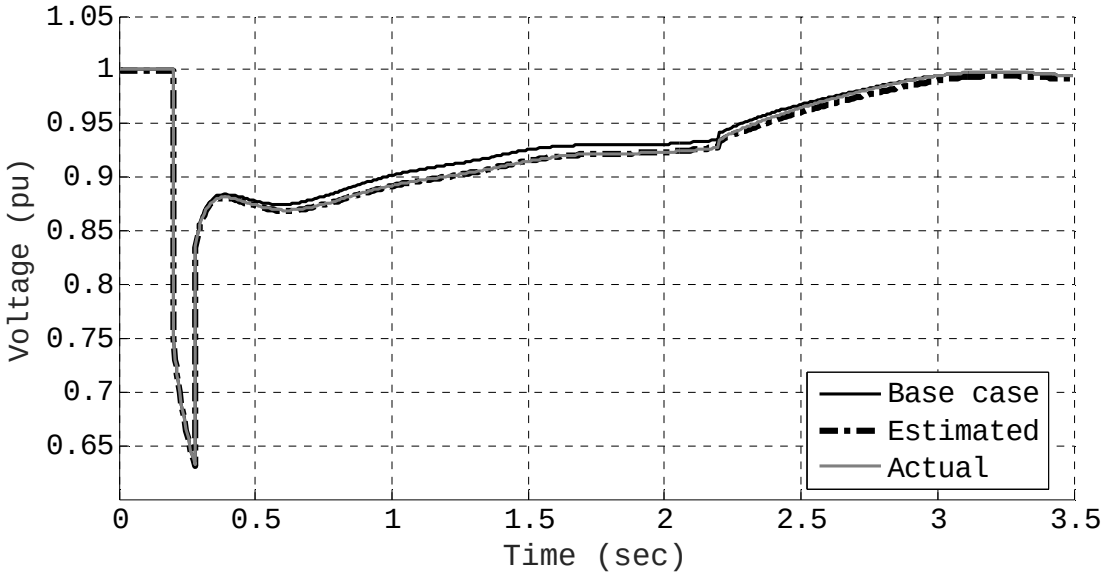

Figure 3.9 Actual and estimated voltage trajectories at bus GB1 for a Δ*Fmd* of 5% at 20 load buses

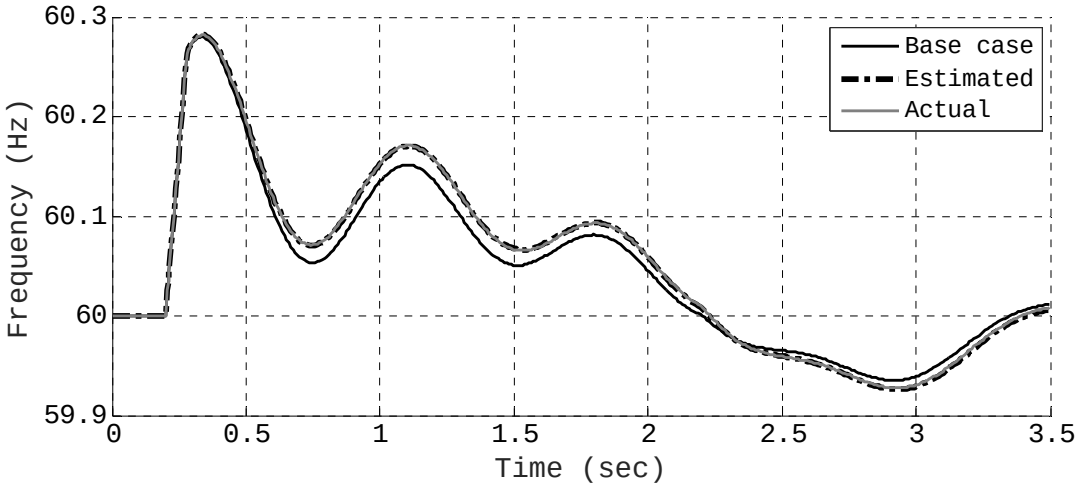

Figure 3.10 Actual and estimated frequency trajectories at bus GB1 for a Δ*Fmd* of 5% at 20 load buses

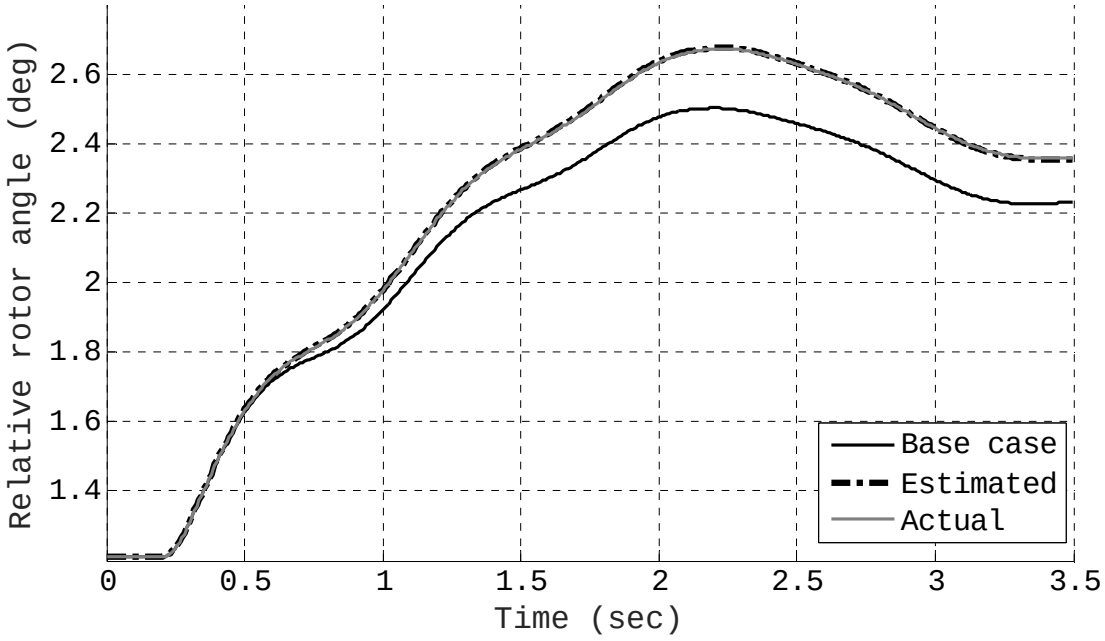

Figure 3.11 Actual and estimated relative rotor angle trajectories at bus GB1 for a Δ*Fmd* of 5% at 20 load buses

Table 3.2 Simulation metrics for TS analysis and repeated TDS in PSAT

Solution metrics (3.5 sec simulation with 0.0083 sec time step)		
Time domain simulation (Evaluating base case including storing the Jacobian entries)	789.201 sec	Needs to be done once
Calculate initial values of sensitivities	1.708 sec	To be done in parallel
Calculate the sensitivities	143.72 sec	To be done in parallel
Create the final trajectory	32.29 sec	Can be done in parallel for different values of delta change
Total time for TS based estimation	966.919 sec	
Total time for two repeated TDS	1575.402 sec	
Savings in computation time	**608.483 sec**	

3.6 Summary

This chapter demonstrated the application of TS to study the impact of load parameter uncertainty on the dynamic response of the system. The sensitivities of a few selected parameters of the SPIM component of the composite load model were discussed. The application of TS to study parameter uncertainty was demonstrated on the WECC system, which is a realistic large power system. The results show that the TS based estimation of the system response is reasonably accurate for the considered uncertainty in the particular load parameter. Furthermore, the chapter compares the computation time of the TS based method to the repeat TDS method for estimating the effect of parameter uncertainty. The comparison results indicate that application of the TS based method results in a substantial savings in computational effort.

CHAPTER 4: PARAMETER SENSITIVITY STUDIES IN POWER SYSTEMS WITH NON-SMOOTH LOAD BEHAVIOR

TS based methods rely on linear approximations based on the first order partial derivatives of the state and algebraic variables with respect to the parameters of interest. It is therefore important to analyze the limit of the perturbation size for which TS based estimations are reasonably accurate. Trajectory estimation using linear approximation has been found to be effective for small perturbations. References [32], [33] have reported that the linear approximation is reasonably accurate when the power system is far from instability. However, the non-smooth nature of the SPIM part of the composite load model presents additional challenges for trajectory estimation. This chapter presents a discussion on the limitations of perturbation sizes while using TS based analysis for power system studies with non-smooth load models. Similar analysis could be extended to find perturbation size limits while dealing with any other non-smooth component model.

4.1 Effect of switching hypersurface on TS analysis in hybrid dynamical systems

Consider the description of the power system given by (2.1)-(2.2) in chapter 2. The equations are repeated here for convenience.

$$\dot{x} = F(x, y, \lambda), \text{ and} \tag{4.1}$$

$$\left.\begin{aligned} G^{-}(x, y, \lambda) = 0 \ for \ S(x, y, \lambda) < 0 \\ G^{+}(x, y, \lambda) = 0 \ for \ S(x, y, \lambda) \geq 0 \end{aligned}\right\}. \tag{4.2}$$

The power system is a hybrid dynamical system where the switching hypersurface is defined by

$$S(x, y, \lambda) = 0. \tag{4.3}$$

If this hybrid dynamical system is represented by a flow map, (4.1) and (4.2) can be re-written as

$$x(t) = \phi_1(x_0, \lambda, t) \text{ for } S(x, y, \lambda) < 0, \text{ and} \tag{4.4}$$

$$x(t) = \phi_2(x_0, \lambda, t) \text{ for } S(x, y, \lambda) \geq 0, \tag{4.5}$$

where, the flow map ϕ is a function that maps the initial condition x_0, parameter λ and the time t to the value of x at time t given by $x(t)$. Mathematically, the function ϕ is defined by (4.6)

$$\phi(x_0, \lambda, t) = x_0 + \int_{t0}^{t} F(x, y, \lambda) \text{ and } G(x, y, \lambda) = 0. \tag{4.6}$$

As mentioned earlier, the analysis presented in this work does not consider discrete jumps in states. References [27] and [29] contain a detailed discussion for systems with discrete jumps in states. Figure 4.1 shows an example phase portrait of the system described by (4.4) to (4.6). The four curves shown in are for four different values of the parameter λ. The two dotted curves, 1 and 2 do not cross the switching hyper-plane given by (4.3), while the two bold curves, 3 and 4 cross the switching hyper-plane given by (4.3). The switching surface introduces a qualitative change in the dynamics of the system [44], [45], [46] and hence the parts of the bold curves (3 and 4) in region 1 and region 2 are qualitatively different. The qualitative difference arises due to the different flow maps in region 1 and region 2. Qualitative changes include change in equilibrium points, as well as change in the nature of the equilibrium. Change in the nature of the equilibrium points due

to such switching in discrete dynamic systems are referred to as border collision bifurcations or grazing bifurcations [44], [45], [46].

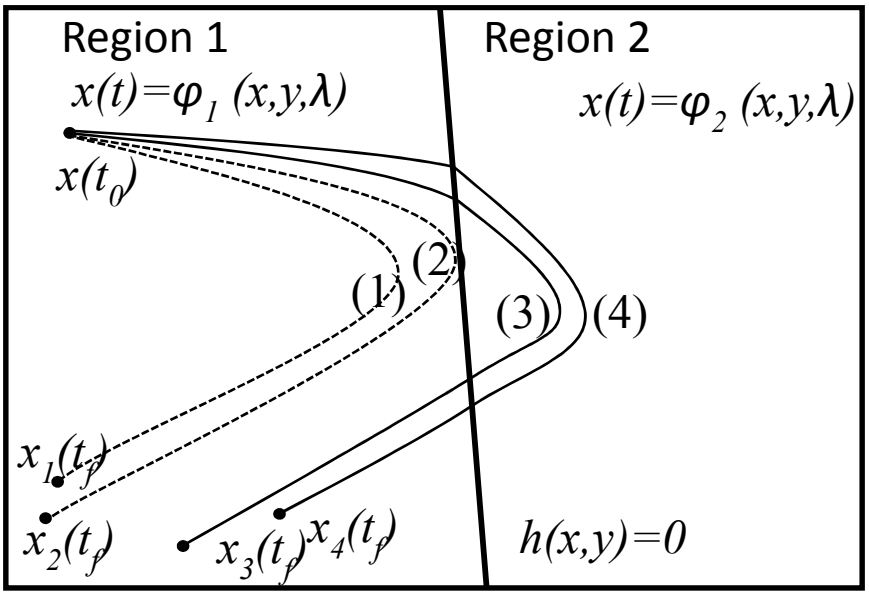

Figure 4.1 Phase portrait of a hybrid dynamical system

In the context of trajectory sensitivity analysis, a linear prediction of curve 2 from curve 1 or curve 4 from curve 3 and vice versa is possible in Figure 4.1. However, due to the qualitative difference introduced by the switching hypersurface, a linear prediction of curve 3 from curve 2 or vice-versa is not possible. To have linear prediction of one trajectory from a nominal trajectory, both of them should traverse the same switching hypersurfaces in the same sequence [27], [44], [45].

4.2 Effect of non-smooth load model on linear trajectory estimation

In sensitivity studies involving the composite load model, the perturbation size for which linear approximations are accurate, is often limited due to the non-smooth nature of

the SPIM part of the composite load model [42]. The discontinuities in the SPIM model are due to

1. The discrete change in the SPIM active and reactive power consumption when the SPIM transitions from a running condition to a stall condition

2. The disconnection of a SPIM from service by an undervoltage trip contactor

As discussed in the foregoing section, it is required that both the base case trajectory and the actual trajectory to be estimated, encounter the same set of discontinuities. In addition, both the trajectories should satisfy the conditions of transversality [27]. The transverality condition at the hyper-surface is given by [27] (4.7).

$$\left.\begin{array}{c} \left[\dfrac{\partial S}{\partial x} \quad \dfrac{\partial S}{\partial y}\right] \cdot \begin{bmatrix} \dot{x} \\ \dot{y} \end{bmatrix} \neq 0 \\ S(x, y) = 0 \\ G(x, y) = 0 \end{array}\right\}. \tag{4.7}$$

If the transversality condition is satisfied, then the jump conditions and the sensitivities at the point of discontinuity can be calculated. The detailed description of the evolution of the trajectory sensitivities at the switching hypersurfaces can be found in [27].

4.2.1 Estimation error introduced by the non-smooth load models

To elucidate the limit set on linear approximation, consider the trajectory estimation at bus LB3. The voltage response at bus LB3 for a ΔFmd of 6% at the 20 selected buses is estimated by using TS analysis. Figure 4.2 shows the actual and the estimated trajectories at bus LB3. The voltage dip at bus LB3 due to the fault does not cause the SPIM connected

at this bus to stall in the base case. However, if the simulation is re-run after incrementing *Fmd* by 6% at the 20 selected buses, the SPIM connected at this bus stalls at t = 0.9 s. The effect of the stalling of this additional SPIM in the actual case manifests as an estimation error beyond t = 0.9 s in Figure 4.2. From this example, it can be seen that for this particular case the computed sensitivities do not provide an accurate estimate of the actual response if the expected variation in *Fmd* is 6% or more. Nonetheless, a careful inspection of the estimated trajectory indicates that for the considered perturbation, the estimated voltage at bus LB3 dips below 0.7 pu for more than 0.033 s. Under this condition, the SPIM connected at bus LB3 is expected to stall. Hence, an estimation error is expected at bus LB3. This shows that the non-smooth nature of load models may impose stricter limits on the size of variability that can be studied by the sensitivity based approach [42].

Although TS based analysis has been applied to systems with non-smooth models [27], [28], [29], the occurrence and analysis of the estimation error shown in Figure 4.2 has not been discussed at length. Most of the work presented previously assumes that both the base case and the actual cases to be predicted encounter the same switching events for reasonable perturbation sizes. The limit of the perturbation size for which linear analysis holds in non-smooth systems is yet to be quantified. In the context of load sensitivity studies, it is possible that an additional switching event, like the stalling of an additional SPIM, does not occur in power systems models where loads are lumped at buses separated by long lines. This is typical for test cases or simplified representations of large power systems where distributed loads are aggregated and represented at a single bus and the buses are connected by transmission lines with relatively high impedance. The high impedance of the connecting branches reduces the impact of a parameter change at a bus on the voltage

of the neighboring buses. Thus, it is unlikely that a small perturbation in a parameter (e.g *Fmd*) will result in a voltage dependent switching event like the stalling of an additional SPIM at a nearby bus. However, in actual power system representations (e.g the WECC system) the load is typically distributed on buses connected by short transmission lines with relatively smaller impedances. Due to the smaller impedance on the connecting branches, small changes in the perturbation sizes can sufficiently change the voltage at adjacent buses to cause stalling of an additional SPIM. As seen from the example discussed here, a small change in *ΔFmd* from 5% to 6% results in the stalling of an additional SPIM at bus LB3. Such events were found to be a common occurrence in the WECC system.

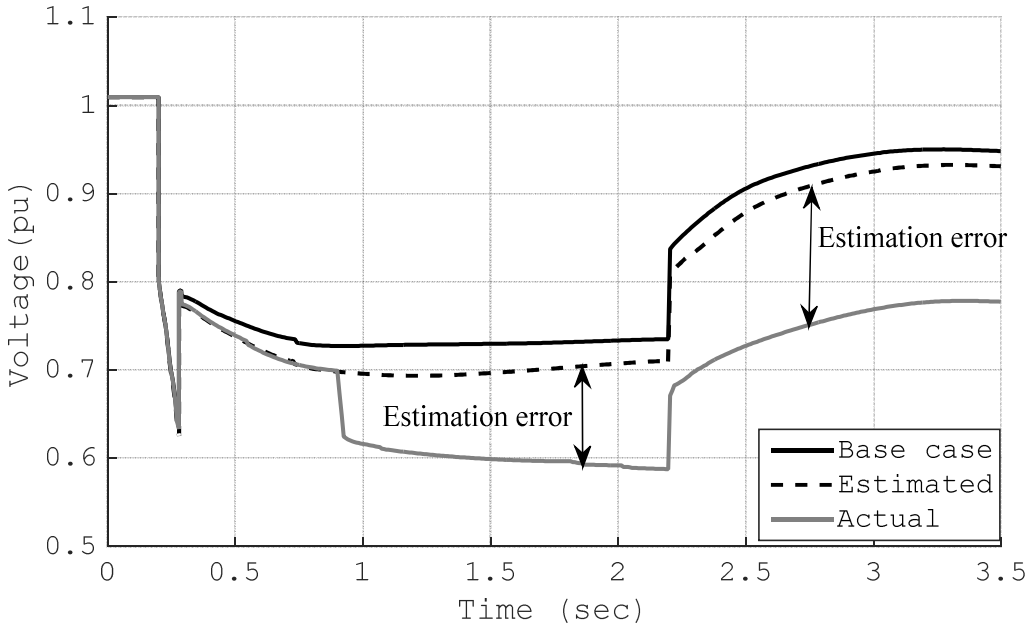

Figure 4.2 Estimation error in voltage response at bus LB3 due to additional AC unit stalling at bus LB3

4.2.2 Estimation error analysis

As discussed in the previous section, the non-smooth behavior of the load model introduces significant error in the trajectory estimation process. Therefore, it is worthwhile to investigate

1. The magnitude of error introduced by a switching event at a bus that affects the trajectory estimation at other buses

2. The perturbation size for which linear approximation is reasonably accurate for power systems with non-smooth load models

Figure 4.3 shows the actual and estimated trajectory at bus LB1 for a ΔFmd of 6% at the 20 selected buses. Bus LB1 is in the same load area as bus LB3 and hence electrically close to each other. It should be noted that the total load represented by SPIM at bus LB3 is 35.3 MW in this case. The maximum estimation error at bus LB1 due to the stalling of an additional SPIM at bus LB3 is less than 5%. This indicates that the error introduced by the load model is localized in nature. The trajectory estimation at bus LB1 is repeated by increasing the amount of load represented by SPIM at bus LB3 to 65.9 MW. Figure 4.4 shows the estimation errors at bus LB1 as the load represented by SPIM at bus LB3 is increased. From Figure 4.4 it can be seen that an increase in the SPIM load at bus LB3 results in an increase in the estimation error at bus LB1. The increase in the error is due to the larger discrete change in the voltage caused by the increase in the size of the SPIM load at bus LB3. This example shows that the estimation error due to the non-smooth nature of the load model may be localized in nature. However, the error propagation will depend on

the topology of the system and the magnitude of the change introduced by the additional switching event [42].

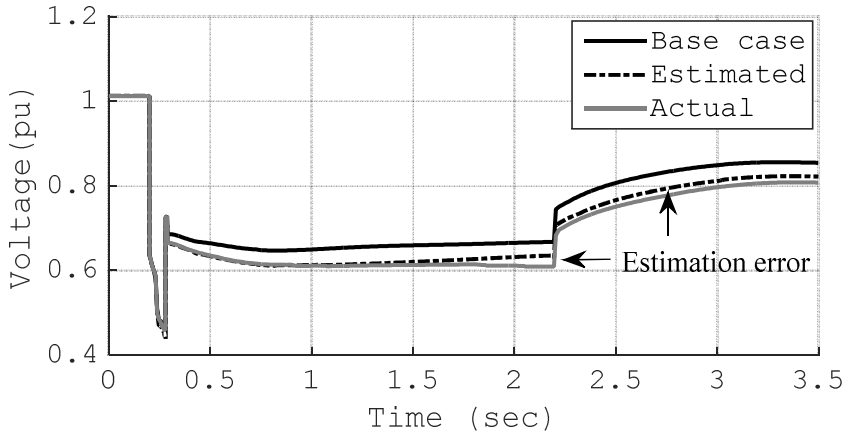

Figure 4.3 Estimation error at bus LB1 due to stalling of an additional Motor D at bus LB3

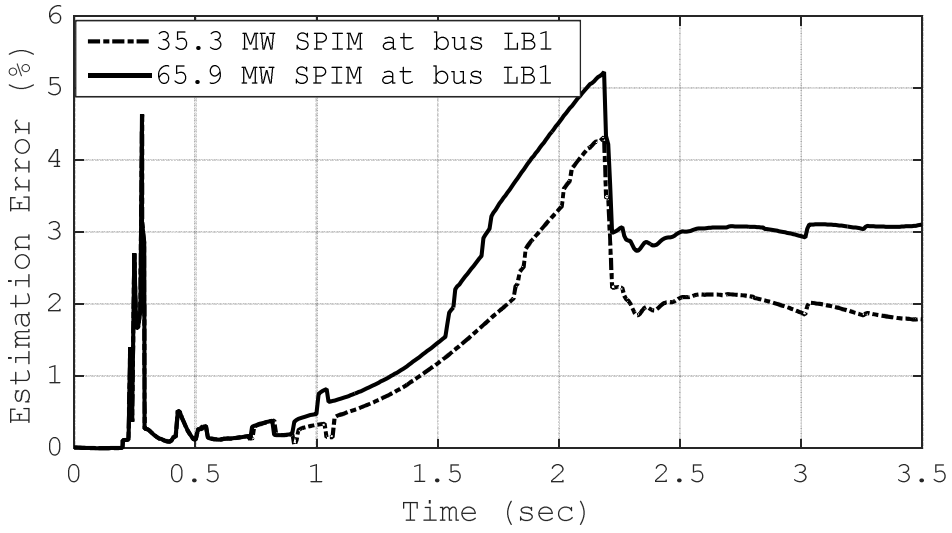

Figure 4.4 . Estimation error at bus LB1 for different size of SPIM at bus LB3

4.3 Perturbation size limit for linear accuracy including non-smooth load models

The inclusion of non-smooth load models puts additional restrictions on the limit of linear analysis in power system. Nevertheless, such inclusions make the power system models more realistic and the simulation results more reliable. It is therefore important to include these models and find a limit for the perturbation size that can be used for linear approximation of trajectories. References [37] and [38] describe a method to estimate the maximum perturbation size for accurate linear estimation. The maximum perturbation size is given by:

$$\Delta\lambda = A / S_{\max}, \tag{4.8}$$

where,

A is a constant evaluated as 1.1 experimentally [37], [38]

$\Delta\lambda$ is the maximum perturbation size for linearity to hold

$S_{\max}$ is the infinite norm of the normalized sensitivity for all variables evaluated during the base case simulation. $S_{\max}$ is typically high when the system is close to instability and small otherwise. Therefore, the maximum perturbation sizes obtained are smaller for stressed power systems and higher when power systems are well within the stability limits [37], [38]. However, only continuous equipment models were considered in [37], [38]. To account for the non-smooth nature of the load models, the maximum perturbation size for which the system undergoes an additional discontinuity needs to be evaluated. The computed value of the perturbation size is compared to that obtained by (4.8), and the smaller of the two is chosen as the maximum perturbation limit. It should be noted that the error

introduced due to linear approximation in continuous systems are a function of the higher order terms that are neglected [35]. The error introduced due to the switching events depends on the type of change introduced by the jump in the operating conditions.

The process of finding the maximum perturbation size that causes the system to undergo an additional discontinuity can be framed as a boundary value problem (BVP) [47]. A shooting method is a well-known approach for solving BVPs [46]. Reference [48] provides details of the application of the shooting method to find grazing points in power system studies. In following through with the previous analysis, computation of the maximum perturbation size of *Fmd* is considered here. The problem of an additional SPIM stalling is formulated as a time difference event trigger problem [27]. To find the maximum perturbation ΔFmd at the 20 selected buses the following assumptions are made:

Assumption 1: The perturbation size ΔFmd, at each bus should be related to each other by some function [42]. This implies that

$$\Delta Fmd_2 = f_1(\Delta Fmd_1), \Delta Fmd_3 = f_2(\Delta Fmd_1)...\Delta Fmd_n = f_{n-1}(\Delta Fmd_1), \qquad (4.9)$$

where, n is the number of buses where a perturbation in *Fmd* is considered. This assumption is needed since a single degree of freedom is available for varying parameters to find the points where a trajectory grazes the switching conditions [32], [48]. Since the application of trajectory sensitivity in load modeling is primarily to circumvent the effect of parameter uncertainty, it is logical that the perturbation size in parameters will be same across different buses or share some algebraic relation. Thus, the relation given by (4.9) would occur

normally in a practical problem without imposing any additional conditions. For this study n is 20 as 20 load buses were selected to apply the perturbation ΔFmd.

Assumption 2: The bus at which the first additional SPIM stalls is known. This can be determined by monitoring the perturbed trajectory and checking if the perturbed trajectory meets the criteria for SPIM stall when that particular SPIM does not stall in the base case. By using this method, the first bus where an additional SPIM stalls, can be identified. This assumption is necessary because the perturbation size should be limited such that the voltage at the first bus where an additional unit stalls should just graze the stalling criteria. If an additional SPIM stalls, it depresses the system voltage. The dip in the system voltage may subsequently cause SPIMs connected at other buses to stall later in the simulation.

As listed in Table 3.1, the SPIM stalls if the voltage at its terminal dips below 0.7 pu and fails to recover above 0.7 pu in 0.033 secs. The shooting method is then used to find the maximum ΔFmd such that the voltage at the particular bus dips below 0.7 pu and recovers above 0.7 pu in 0.033 secs. If a power system is represented as a dynamical system given by (4.1)-(4.6), then the condition when the voltage at a bus marginally recovers without the SPIMs stalling can be represented by [42]

$$\phi(x_0, Fmd, t_1) - x(t_1) = 0, \tag{4.10}$$

$$\phi(x_0, Fmd, t_2) - x(t_2) = 0, \tag{4.11}$$

$$G(x(t_1), y(t_1), Fmd) = 0, \tag{4.12}$$

$$G(x(t_2), y(t_2), Fmd) = 0, \tag{4.13}$$

$$S(x(t_1), y(t_1)) = 0, \tag{4.14}$$

$$S(x(t_2), y(t_2)) = 0, \text{ and} \tag{4.15}$$

$$t_2 - t_1 = \tau, \tag{4.16}$$

where,

ϕ defines a flow map given by (4.6)

t_1, t_2 represent the time instants when the switching conditions given by (4.14) and (4.15) are satisfied

τ is the duration of time between t_1 and t_2 required for the event to trigger

If the voltage of the bus b, with the first instance of additional SPIM stalling is given by V_b, then (4.14)-(4.16) can be re-written as

$$V_b(t_1) - 0.7 = 0, \tag{4.17}$$

$$V_b(t_2) - 0.7 = 0, \text{ and} \tag{4.18}$$

$$t_2 - t_1 = 0.033. \tag{4.19}$$

The equations given by (4.10)-(4.16) are a set of nonlinear equations of the form

$$f\left(\begin{bmatrix} x(t_1) \\ x(t_2) \\ y(t_1) \\ y(t_2) \\ Fmd \\ t_1 \\ t_2 \end{bmatrix}\right) = 0\,. \tag{4.20}$$

(4.10)- (4.16) can be solved iteratively by using the Newton-Raphson (NR) method. The generic form of the Jacobian required for solving time difference event trigger problems can be found in [42], [48]. In this specific problem, the Jacobian required to solve (4.11) is given by [42]

$$\begin{bmatrix} -I & 0 & 0 & 0 & \left.\frac{\partial x}{\partial \lambda}\right|_{t_1} & F(x,y,\lambda)\big|_{t_1} & 0 \\ 0 & -I & 0 & 0 & \left.\frac{\partial x}{\partial \lambda}\right|_{t_2} & 0 & F(x,y,\lambda)\big|_{t_2} \\ G_x\big|_{t_1} & 0 & G_y\big|_{t_1} & 0 & G_\lambda\big|_{t_1} & 0 & 0 \\ 0 & G_x\big|_{t_2} & 0 & G_y\big|_{t_2} & G_\lambda\big|_{t_2} & 0 & 0 \\ S_x\big|_{t_1} & 0 & S_y\big|_{t_1} & 0 & 0 & 0 & 0 \\ 0 & S_x\big|_{t_2} & 0 & S_y\big|_{t_2} & 0 & 0 & 0 \\ 0 & 0 & 0 & 0 & 0 & 1 & -1 \end{bmatrix}, \tag{4.21}$$

where, $\lambda = Fmd$ and $S(x,y) = V_b(t) - 0.7 = 0$.

From (4.21) it can be seen that all the elements of the Jacobian are already available as a by-product of the TDS and TS analysis routines. No additional computations are required for setting up the problem defined by (4.10)-(4.16). However, at every step of the NR iteration, a time domain simulation needs to be performed to solve the flow maps in (4.10) and (4.11). In addition, appropriate starting values for the solution variables need to

be determined before starting the NR iteration. To find the appropriate initial conditions for the shooting method the following comments are in order [42]:

1. The initial values x_o and y_o for computing the flows remain unchanged within iterations.

2. The initial values of *Fmd*, t_1 and t_2 can be found while determining the load bus where the first additional SPIM stalls. This can be done by noting down the value of *Fmd* for which the additional SPIM is about to stall and the approximate time instants t_1 and t_2 when the SPIM is about to stall.

Once the final value of *Fmd* is computed, the maximum value of ΔFmd can be obtained by

$$Fmd - Fmd_0 = \Delta Fmd \,, \tag{4.23}$$

where, Fmd_0 is the initial guess or the base value for starting the iterative procedure. The value of ΔFmd thus obtained gives the maximum perturbation size such that the voltage trajectory $V_b(t)$ marginally grazes the SPIM stalling conditions. It should be noted that the same method could be used for computing the maximum perturbation size for any other load parameter. The only effort involved is to find an appropriate starting condition for the NR iterations required for solving the BVP by the shooting method.

Figure 4.5 shows the voltage trajectories obtained by subsequent iterations and the final voltage trajectory when the SPIM stalling conditions are grazed. The maximum perturbation size ΔFmd obtained by this method is 5.47%. Table 4.1 lists the perturbation sizes obtained by using (4.8) and (4.10)-(4.16). In addition, the final perturbation size that can

be used to ensure estimation accuracy is listed in Table 4.1. Figure 4.6 shows the voltage trajectories at bus LB3 when a Δ*Fmd* of 5.4% and 5.5% is applied at the 20 selected load buses respectively. From Figure 4.6 it can be seen that the SPIM does not stall at bus LB3 for a Δ*Fmd* of 5.4%. However, when Δ*Fmd* is increased to 5.5% the SPIM at bus LB3 stall, thus confirming that the maximum Δ*Fmd* cannot exceed 5.47% for TS based analysis in this case.

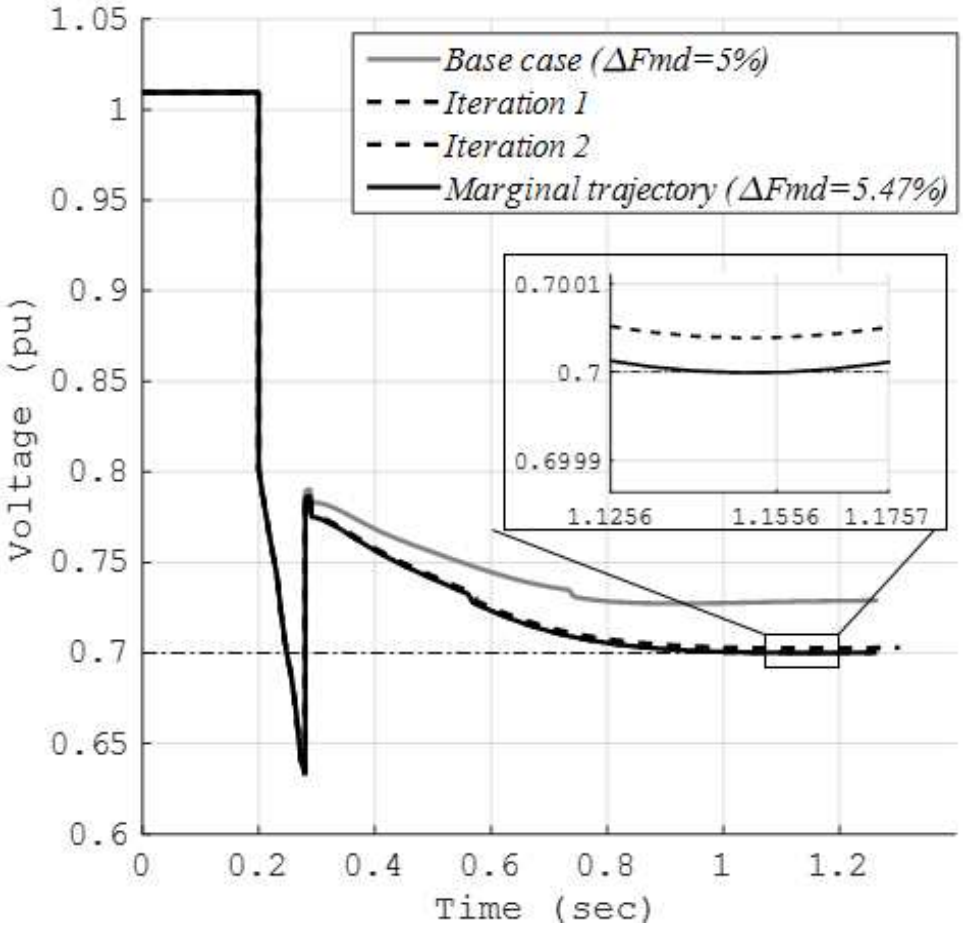

Figure 4.5 Voltage trajectories at bus LB3 for different iterations of the shooting method

Table 4.1 Maximum perturbation size considering linear estimation accuracy

Perturbation size obtained by (4.8)	
S_{max}	0.0666
ΔFmd_{max1} (at the 20 selected buses)	16.52 %
Perturbation size obtained by (4.10)-(4.16)	
ΔFmd_{max2} (at the 20 selected buses)	5.47%
Maximum perturbation size: min(ΔFmd_{max1}, ΔFmd_{max2}) = 5.47	

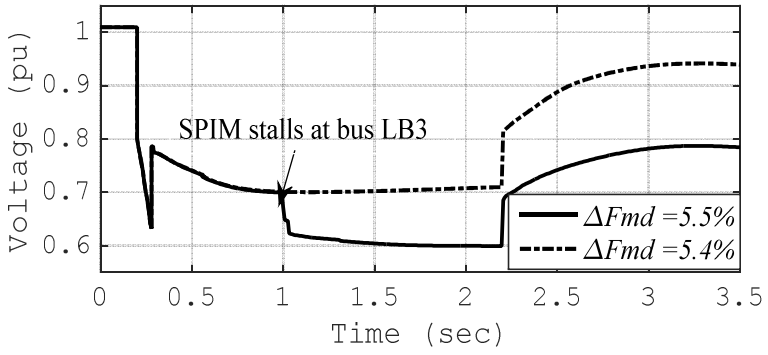

Figure 4.6 Voltage trajectories at bus LB3 for ΔFmd of 5.5% at 20 selected buses

4.4 Summary

This chapter presented the analysis of the linear approximation accuracy limit for TS analysis, when non-smooth load models are present. A brief introduction to the impact of switching hypersurfaces on TS analysis for hybrid dynamical systems is also provided. The chapter further discussed the additional limitation placed on the perturbation size due to the inclusion of the non-smooth load model. For the particular case discussed here, the perturbation size of the parameter is limited due to the non-smooth characteristics of the SPIM component of the composite load. In addition, a shooting method is presented here

to compute the maximum perturbation size, while taking into account the non-smooth behavior of the load model.

CHAPTER 5: COMMERCIAL IMPLEMENTATION OF TRAJECTORY SENSITIVITY ANALYSIS

The previous chapters presented the application of TS analysis to quantify the impact of load model parameter uncertainty on the power system algebraic and state variable trajectories during dynamic simulations. The TS analysis module was implemented in PSAT, which uses an implicit integration algorithm based TDS routine. It was shown in Chapter 2 that using an analytical method for TS analysis in conjunction with an implicit integration based TDS results in additional saving in computational time due to the structure of the problem. However, not all power system simulators are equipped with implicit integration techniques. A majority of the commercially available power system simulators like GE-PSLF and Siemens PSS/E use explicit integration based methods to perform the dynamic simulations [22], [23]. As such, it is important to investigate the implementation of the TS analysis module in commercial power system simulators, which use explicit integration routines. This chapter presents the implementation of a TS analysis in conjunction with an explicit integration routine in PSAT. A comparison of the performance of TS with explicit and implicit integration routine is also presented here. Furthermore, TS analysis is implemented in GE-PSLF and the results are presented here.

5.1 Implicit versus explicit methods of numerical integration

A detailed discussion of implicit and explicit methods of integration can be found in [36]. A brief discussion of the two methods in relation to solving differential algebraic equations is presented in this section.

Consider a dynamic system described by

$$\dot{x} = F(x, y, \lambda) \text{, and} \tag{5.1}$$

$$G(x, y, \lambda) = 0 . \tag{5.2}$$

where, the description of the variables are the same as those given in (2.1) and (2.2). When (5.1) and (5.2) are solved using an implicit method like the trapezoidal method [36], the state variables $x(t+\Delta t)$ and the algebraic variables $y(t+\Delta t)$ for the next time step are obtained by solving

$$x(t+\Delta t) - x(t) - \frac{\Delta t}{2}(F(x(t+\Delta t), y(t+\Delta t), \lambda) + F(x(t), y(t), \lambda)) = 0 \text{, and} \tag{5.3}$$

$$G(x(t+\Delta t), y(t+\Delta t), \lambda) = 0 . \tag{5.4}$$

Since (5.3) and (5.4) are both nonlinear in $x(t+\Delta t)$ and $y(t+\Delta t)$, (5.3) and (5.4) is solved iteratively. When a Newton-Raphson method is employed to solve (5.3) and (5.4), the Jacobian required at each step of the iteration is given by

$$\begin{bmatrix} I - F_x \frac{\Delta t}{2} & F_y \frac{\Delta t}{2} \\ G_x & G_y \end{bmatrix}. \tag{5.5}$$

When (5.1) and (5.2) are solved using an explicit method of integration like a forward Euler method [36], the state variables $x(t+\Delta t)$ and the algebraic variables $y(t+\Delta t)$ for the next time step is obtained by solving

$$x(t+\Delta t) = x(t) + \Delta t(F(x(t), y(t), \lambda)) \text{, and} \tag{5.6}$$

$$G(x(t+\Delta t), y(t+\Delta t), \lambda) = 0\,. \tag{5.7}$$

In the explicit method, (5.6) is linear in $x(t+\Delta t)$ and $y(t+\Delta t)$ and can be solved directly to obtain $x(t+\Delta t)$. However (5.7) is still nonlinear and has to be solved iteratively. When a Newton-Raphson method is used to solve (5.6), the Jacobian at every step of the iteration is given by G_y. In the context of power system TS analysis, G_y is the power flow Jacobian. A comprehensive description of other explicit and implicit methods of integration can be found in [36].

Both the explicit and the implicit methods of integration have their advantages and disadvantages. The implicit methods of integration are preferred when the underlying dynamic system has fast transient responses [36]. The method is more stable even with larger simulation time steps Δt, as compared to an explicit method. Explicit methods of integration are recommended for systems with comparatively slower dynamics if a reasonably large simulation time step Δt is to be used. The appropriate simulation time step Δt, is dependent on the time constants of the dynamic system. Implicit methods of integration require more computation for each time step of the simulation as compared to the explicit methods. However, since a larger time step can be used for the implicit methods, the overall computational burden can be significantly reduced when compared to explicit methods, while integrating a fast dynamic system. Reference [36] provides a detailed discussion of the time step selection, and the stability and accuracy of various explicit and implicit methods of integration. Electromagnetic transient programs (EMTP) which handle faster elec-

trical transients, use implicit methods of integration. The electromechanical transient simulators like PSLF and PSS/E which handle comparatively slower electromechanical transients, use explicit methods of integration.

5.2 Computing sensitivities using explicit integration

The sensitivity equations are repeated here for convenience. The sensitivity equations are given by

$$\frac{d\dot{x}}{d\lambda_i} = \frac{dF}{d\lambda_i} = \frac{dU_i}{dt} = F_x U_i + F_y W_i + F_{\lambda_i}, \text{ and} \tag{5.8}$$

$$0 = \frac{dG}{d\lambda_i} = G_x U_i + G_y W_i + G_{\lambda_i}. \tag{5.9}$$

In Chapter 2, the sensitivity equations (2.5) and (2.6) were integrated using the trapezoidal method. When an explicit method of integration like the forward Euler method is used to compute the sensitivities, $U_i(t+\Delta t)$ and $W_i(t+\Delta t)$ are obtained by solving

$$U_i(t+\Delta t) = U_i(t) + \frac{\Delta t}{2}(F_x U_i + F_y W_i + F_{\lambda_i}), \text{ and} \tag{5.10}$$

$$G_x U_i(t+\Delta t) + G_y W_i(t+\Delta) = -G_{\lambda_i}. \tag{5.11}$$

(5.9) and (5.10) can be re-written as a linear matrix equation given by

$$\begin{bmatrix} I & 0 \\ G_x(t+\Delta t) & G_y(t+\Delta t) \end{bmatrix} \begin{bmatrix} U_i(t+\Delta t) \\ W_i(t+\Delta t) \end{bmatrix} = \begin{bmatrix} U_i(t) + \frac{\Delta t}{2}(F_x(t)U_i(t) + F_y(t)W_i(t) + F_{\lambda_i}(t) \\ - G_{\lambda_i}(t+\Delta t) \end{bmatrix}. \quad (5.12)$$

For solving (5.12), the entries $F_x(t)$, $F_y(t)$, $F_{\lambda i}(t)$, $G_x(t+\Delta t)$ and $G_{\lambda i}(t+\Delta t)$ need to be evaluated additionally. The entry $G_y(t+\Delta t)$ is obtained as a byproduct of solving (5.7) during the TDS. Unlike the implicit integration based TS analysis, not all entries in the coefficient matrix and the right hand side vector of (5.12) are available as a byproduct of the TDS routine when an explicit integration algorithm is used. However, the additional evaluation of those entries does not necessarily make the explicit integration based TS analysis computationally more expensive. If an implicit integration method is used, the sub matrices F_x, F_y, G_x and G_y, are computed at every iteration in each time step while solving (5.3) and (5.4). The converged values of F_x, F_y, G_x and G_y are then used for evaluating the trajectory sensitivities. In contrast, if an explicit integration method is used, the sub matrices F_x, F_y and G_x are computed once every time step after the values of the algebraic and state variables for that time is obtained. Therefore, the computational burden in an explicit integration method would depend on the time step of simulation that can be permitted, which is dependent on the underlying dynamic system.

5.2.1 Application of explicit integration based TS analysis in PSAT

The publicly available version of PSAT does not have an explicit integration routine. The explicit integration based TDS and the TS analysis routine was implemented in PSAT based on (5.9)-(5.12). To compare the performance of the TS analysis using both

integration methods, the same study performed in Chapter 3 is repeated here. Accordingly, the WECC 2012 HS case is used here. Figure 5.1 and Figure 5.2 shows the comparison of the simulated voltages at bus LB1 and LB3 respectively, by using an explicit and an implicit integration based TDS. From Figure 5.1 and Figure 5.2 it can be seen that using either integration method results in similar voltage trajectories with minor differences. The explicit integration based TS analysis is used to estimate the effect of a 5% increase in *Fmd* at 20 selected buses on the system voltages during a fault. The fault simulated here is the same as that simulated in Chapter 3. Figure 5.3 shows the base case, estimated and actual voltage trajectories at bus LB1. Figure 5.4 shows the base case, estimated and actual voltage trajectories at bus LB3. From Figure 5.3 and Figure 5.4 it can be seen that the estimated voltage trajectories closely follow the actual response of the system.

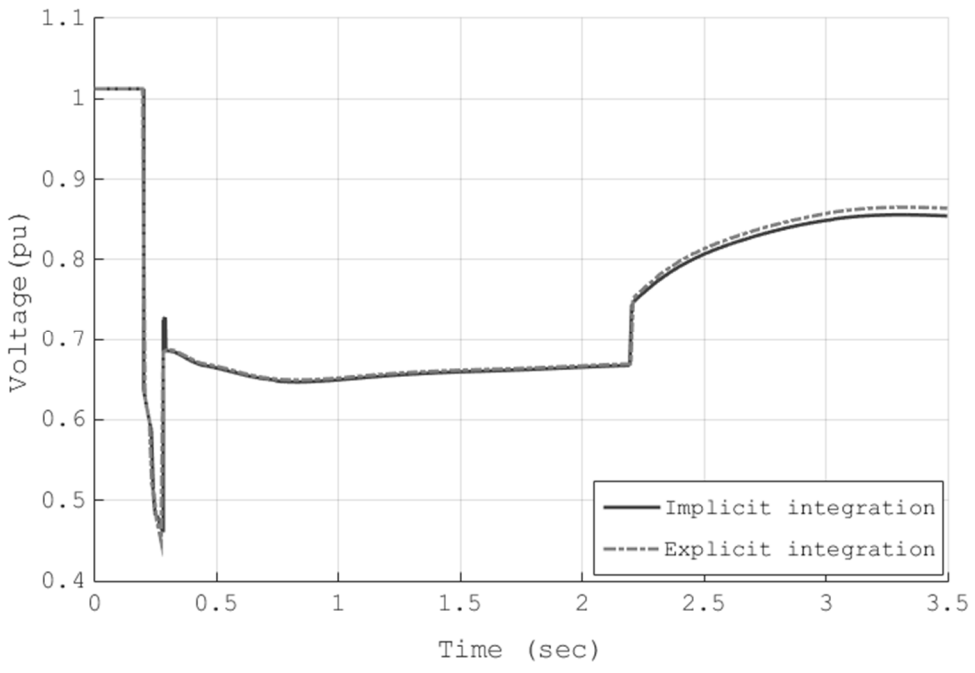

Figure 5.1 Comparison of simulated voltage at bus LB1 using explicit and implicit integration based TDS

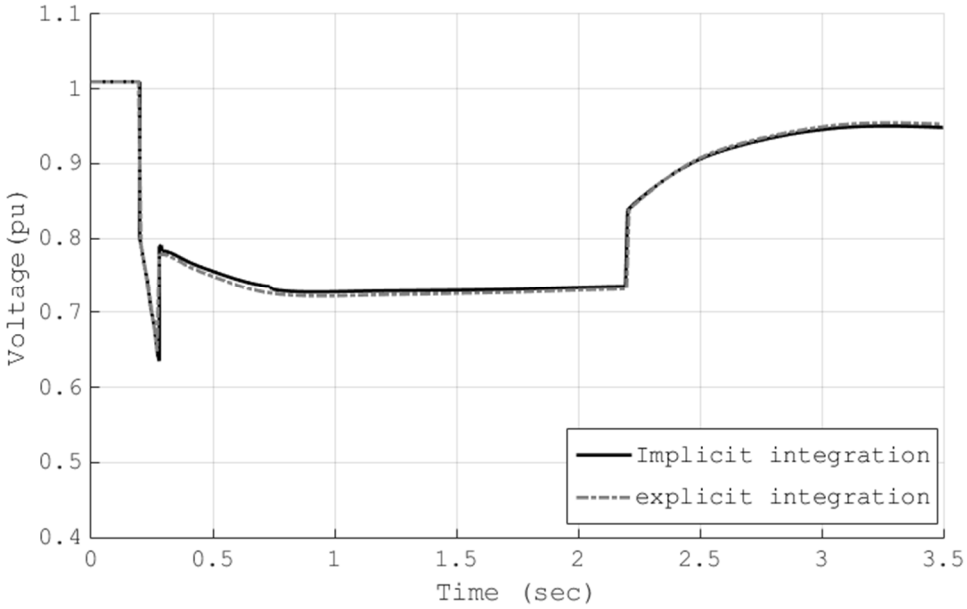

Figure 5.2 Comparison of simulated voltage at bus LB3 using explicit and implicit integration based TDS

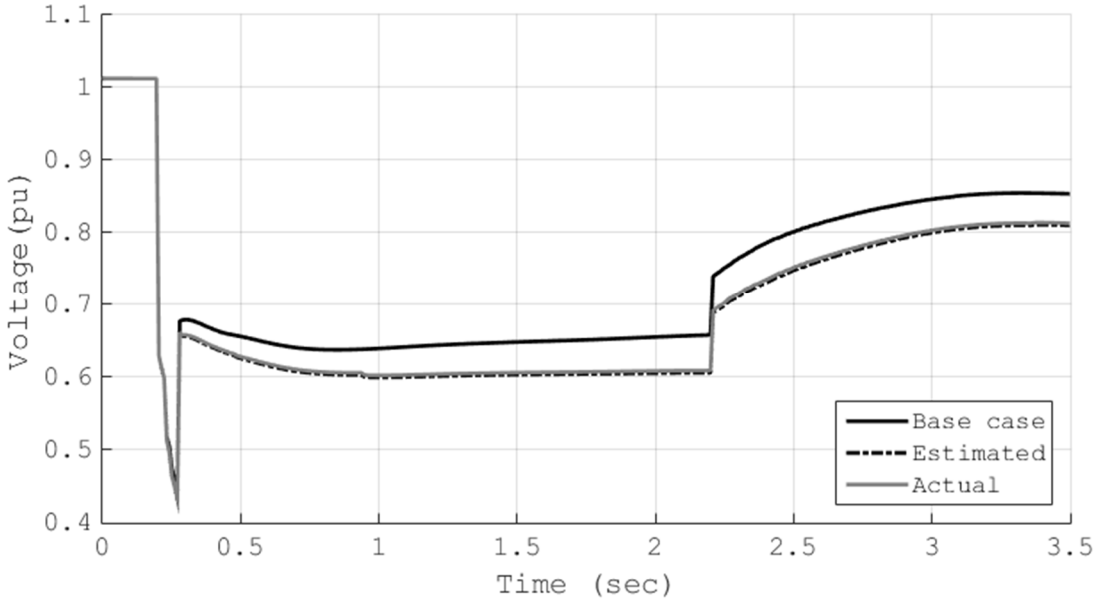

Figure 5.3 Actual and estimated voltage trajectories at bus LB1 for a Δ*Fmd* of 5% at 20 load buses (explicit integration based TS analysis)

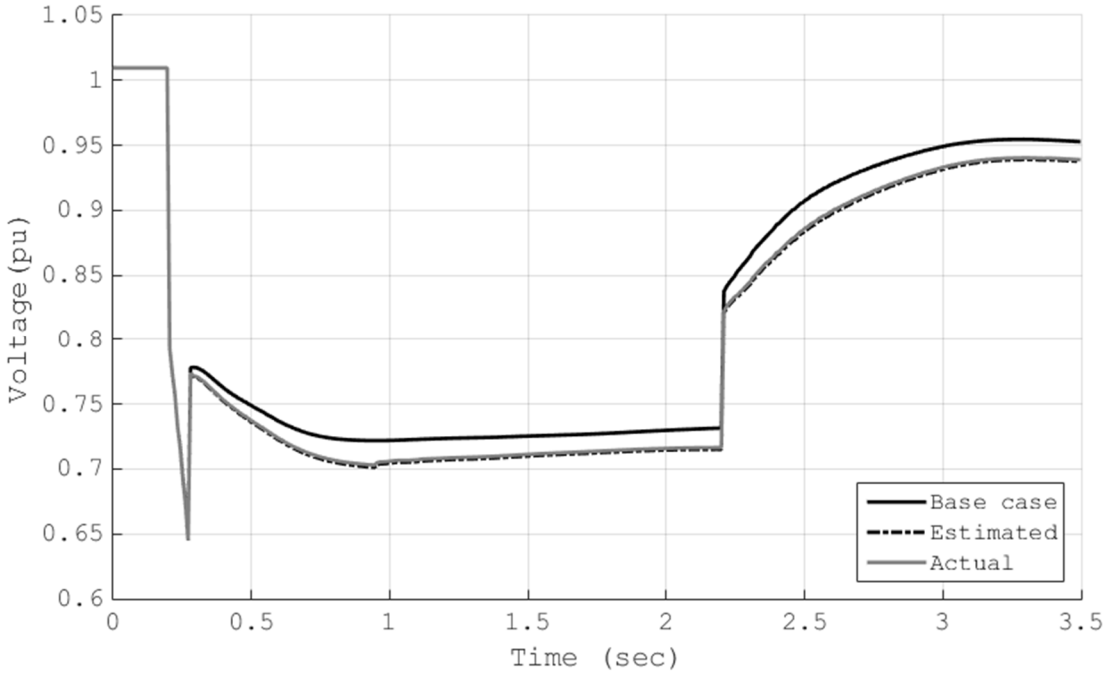

Figure 5.4 Actual and estimated voltage trajectories at bus LB3 for a Δ*Fmd* of 5% at 20 load buses (explicit integration based TS analysis)

Table 5.1 shows a comparison of the performance TS analysis using an explicit and an implicit integration method. It can be seen that some savings in computation time can be obtained by switching to an explicit integration based TS routine. However, the savings in the computation time are not quite significant in this case. This is because in the explicit integration based TDS a larger number of iterations are required to solve the network solution given by (5.7). PSAT uses a power injection formulation for the network solution given by

$$V.I^* = V.(YV)^*, \tag{5.12}$$

where, V are the vector of system bus voltages, I is the vector of current injection at each bus and Y is the full network admittance matrix and the '.' Symbolizes elementwise multiplication. It was observed that a larger number of iterations were needed to solve the network equations during the depressed voltage condition as shown in Figure 5.1 and Figure 5.2

Table 5.1 Performance metric comparison between implicit and explicit integration based TS analysis

Subroutine	**Implicit integration (Trapezoidal rule)**	**Explicit integration (Forward Euler)**
Time domain simulation	789.201 sec (time step 0.0083 sec)	746.52 sec (time step 0.002 sec)
Calculate initial values of sensitivities	1.708 sec	1.708 sec
Calculate the sensitivities	143.72 sec	105.2 sec
Create the final trajectories	32.29 sec	32.29 sec

5.3 Implementation of TS analysis in GE-PSLF

Section 5.2 presented the implementation of TS analysis in PSAT using an explicit integration based routine. This section describes the implementation of a TS analysis module in GE-PSLF, which is a commercially available power system simulator. In GE-PSLF, the TDSs are performed using the Adam-Bashforth method, which is a second order explicit integration method. Presently, most commercial power system simulators do not provide any access to the differential equations describing the equipment models. Therefore, a numerical approach to compute the trajectory sensitivities is implemented here. Although

computationally burdensome, the numerical method for evaluating the trajectory sensitivities is easy to implement as compared to the analytical method. A discussion of the numerical method for computing derivatives is provided in Chapter 2. Since the numerical approach for evaluating sensitivities is based on the perturbation of the trajectories, it is independent of the type of numerical integration technique used to create the trajectories. Therefore, a numerical method can be used in conjunction with any commercially available power system simulator irrespective of the integration method being used. In this work, MATLAB was used along with GE-PSLF to implement the TS analysis module. Figure 5.4 shows a block diagram of the implementation of TS analysis using GE-PSLF and MATLAB. As shown in Figure 5.4, GE-PSLF and MATLAB work independently of each other and either could be easily replaced by any other similar program.

The forward differencing method was used in MATLAB to compute the trajectory sensitivities numerically. The trajectories of the state and algebraic variables are obtained as outputs from GE-PSLF and a MATLAB based program was used to externally compute the sensitivities and construct the estimated trajectories. As described in Chapter 2, two sets of TDS need to be performed to compute the trajectory sensitivities. Therefore, this method is computationally more expensive compared to the analytical method.

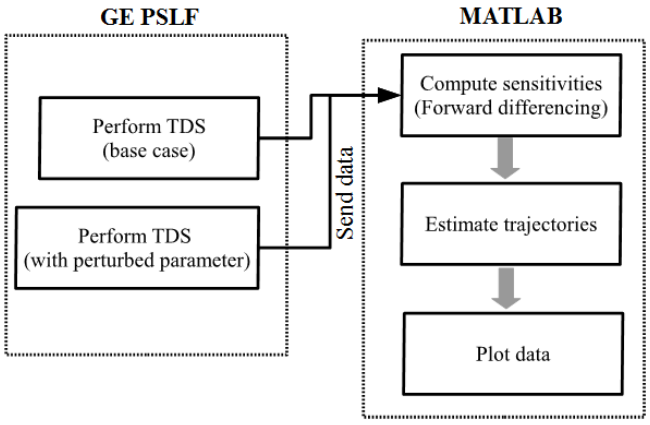

Figure 5.5 Implementation of TS analysis using GE-PSLF and MATLAB

5.3.1 Application of TS analysis in GE-PSLF

Continuing with the previous work, TS analysis is used to study the effect of load parameter uncertainty on the power system response. The WECC 2012 HS case used in Chapter 3 has been used here for performing the study. The loads at load buses are represented by a composite load model '*cmpldw*'. The original WECC 2012 HS case, available through the WECC website, does not use a composite load model to represent the loads. The composite load model has been added to the WECC 2012 HS case separately. The composition of the composite load model connected at a load bus was determined based on the season/hour of day and the region where the load bus was located. The region where the load bus is located can be ascertained by the long identifier associated with every load bus in the load data table of PSLF. Table A.2 in Appendix A, lists the composition of load models used for load buses in the different regions.

The developed GE-PSLF TS analysis module is used to estimate the effect of a 5% increase in *Fmd* at 20 selected buses on the system voltages during a fault. A three-phase

five-cycle fault is applied on a major 500 kV line in the southwestern U.S. The fault simulated here is the same as that simulated in Chapter 3. Figure 5.6 shows the base case, actual and the estimated voltage trajectory at bus LB1. Figure 5.7 shows the base case, actual and the estimated voltage trajectory at bus LB3. From Figure 5.6 and Figure 5.7, it can be seen that the TS based trajectory estimation provides an accurate approximation of the system without the need of repeated TDS. It should be noted that the voltage responses in PSAT and GE-PSLF are different due to the difference in the implementation of dynamic models and the algorithms used in performing the dynamic simulations.

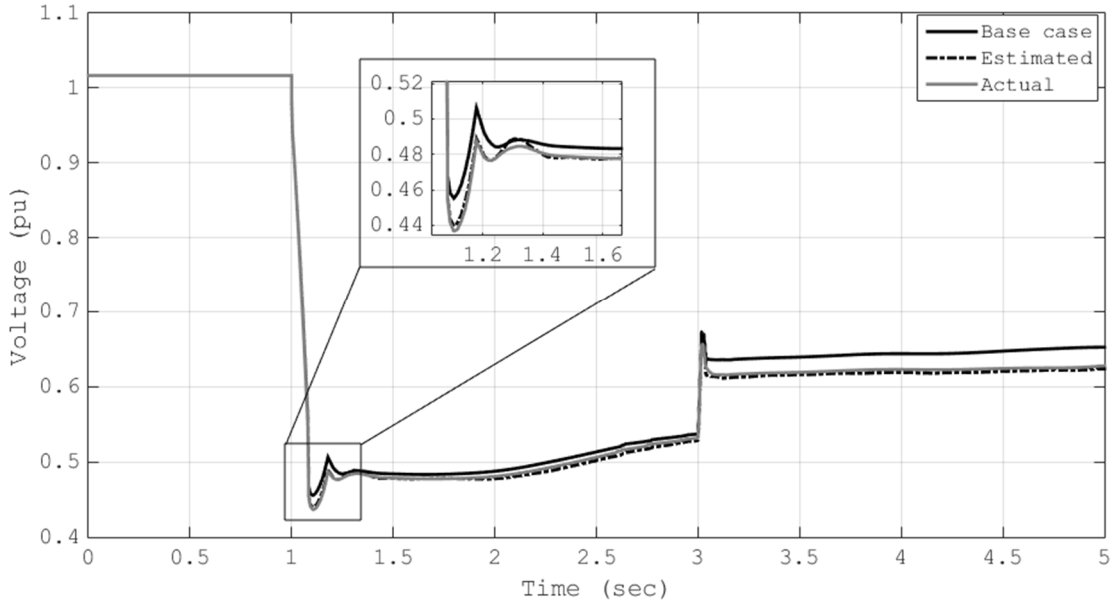

Figure 5.6 Actual and estimated voltage trajectories at bus LB1 for a Δ*Fmd* of 5% at 20 load buses (TS analysis in GE-PSLF)

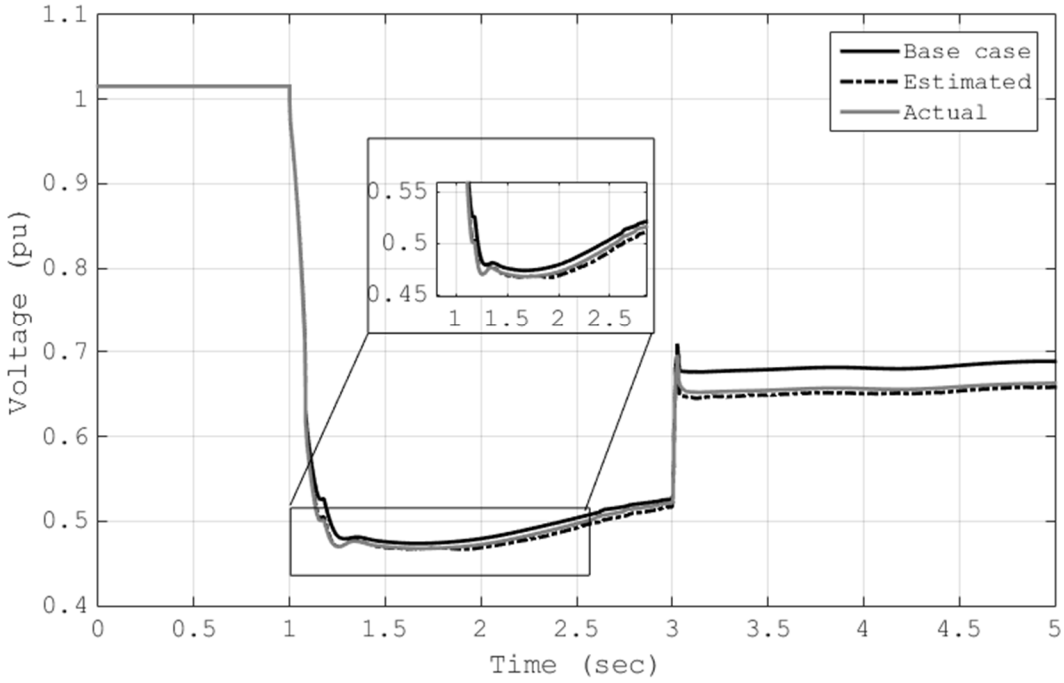

Figure 5.7 Actual and estimated voltage trajectories at bus LB3 for a Δ*Fmd* of 5% at 20 load buses (TS analysis in GE-PSLF)

5.3.2 Comments on implementation of TS analysis for hybrid systems in commercial power system simulators

For implementing the TS analysis module in GE-PSLF, the dynamic simulations were performed separately in GE-PSLF. The rest of the computation involved in evaluating the sensitivities is done in MATLAB. Although easy to implement, there exists some limitations in the capabilities of this tool. The limitations arise because the commercial power system simulators do not provide any access to the differential equations of the dynamic models. As discussed in section 4.3 in Chapter 4, the discontinuous nature of the load model limits the perturbation size of the parameters for which trajectories can be estimated with sufficient accuracy. Therefore, an important part of TS analysis is to compute

the limit on the perturbation size for which trajectory estimation is valid. However, in the numerical approach to TS analysis, substantial additional computation is required for evaluating the maximum perturbation size by the shooting method as given by (4.10) – (4.20). Due to the inability to access to the model differential equations, all entries of the Jacobian given by (4.21) have to be computed numerically by a finite differencing method. This requires multiple perturbed TDSs, thereby substantially increasing the computational burden. It is therefore important to implement the TS analysis using the analytical method in commercial power system simulators. This can be done in the same way as TS analysis was implemented in PSAT using an explicit integration in section 5.2. It should however be pointed out that PSAT uses a power injection model for representing the network equations given by (5.12). In contrast, most commercial power system simulators use a current injection model for the representing the network equations in the TDS modules. In the current injection model, only the active nodes in the network are retained for solving network equations. The generators and nonlinear loads with voltage dependent current injections are represented by their Norton's equivalent. The network equations using the current injection model is given by

$$I = (Yred)V \tag{5.13}$$

where, *Yred* is the reduced *Y* matrix of (5.12), which retains only the active nodes of the system. This formulation is particularly favored because the size of the matrix *Yred* is less than the complete admittance matrix *Y*. Additionally, (5.13) is typically solved using Gauss-Jacobi iterations instead of the Newton-Raphson method, as used in PSAT. While

implementing the TS analysis module in this framework, unlike PSAT, the entry G_y is not available and needs to be evaluated separately.

5.4 Summary

This chapter describes the implementation of TS analysis using an explicit integration based TDS. A comparison of the explicit integration based TS analysis with an implicit integration based TS analysis is presented here. Furthermore, the implementation of TS analysis in GE-PSLF a commercially available power system simulator using the present infrastructure is presented here. This chapter also presents an additional discussion on the limitation of the current implementation of TS analysis in the existing commercial power system simulators. It highlights the need to move to an analytical approach for TS analysis rather than pursuing a numerical approach.

CHAPTER 6: SENSITIVITY BASED PARAMETER ESTIMATION

Simulation studies play a crucial role in power system operations and planning. Simulation studies enable system operators and planners to study the behavior of key transmission and generation components under different operating conditions, and to ensure the security and reliability of the system. These studies rely heavily on the accuracy of the mathematical models used to represent the various transmission and generation equipment. The simulation models are expected to replicate the behavior of the actual component in a reasonably accurate manner. Therefore, estimating the model parameters precisely is of paramount importance. Parameter estimation techniques for generators and other major transmission and distribution components are well-established [49-52]. The model parameters are typically estimated based on field-testing of these components as well as from manufacturers' data [49-52]. In recent years, parameter estimation in load modeling has gained considerable importance [15], [53], [54]. This is due to the increasing focus on the development of accurate load models for power system studies. Since the consumer loads (both commercial and residential) are represented as aggregated loads at the distribution substation, determination of parameters for the aggregated load model is challenging [15], [53], and [54]. Presently, the utilities determine such load models based on the measurements made at substations and by testing the performance of common consumer loads like induction motors and electronic loads [15]. However, aggregated load models have a large number of tunable parameters, which makes the task of parameter estimation challenging. This chapter describes a tool that can be used to estimate model parameter, which focuses on aggregated load model parameter estimation. The tool presented here uses a sensitivity-based approach to estimate multiple model parameters based on recorded measurements of

voltage, active and reactive power at the substation bus of interest. A nonlinear least squares minimization method is used to estimate the parameters. The output of the model (active and reactive power) based on the terminal voltage and an initial guess of the parameters is compared to the actual measurements. The parameters are then adjusted iteratively to reduce the error between the model output and the actual measured output. The proposed tool provides a convenient method to estimate the model parameters such that the simulation results can replicate the actual system response.

Apart from tuning model parameters based on measurements, the tool can be useful in tuning parameters such that comparable results can be obtained between different simulation tools. This can be done by using the simulation output of a reliable tool and then using this output as measurements to tune the model parameters in a different tool. This is particularly significant as the power system simulation industry is seeing a surge in open source simulation tools. One of the main issues with open source tools is replicating the results of simulations with the established commercial power system simulators. One of the main reasons for the observed discrepancies is the difference in the mathematical implementation of the various equipment models across different simulation tools. Tuning the model parameters, such that open source tools can replicate the simulation outputs could be a significant step towards the advancement of such open source tools. However, this is envisaged as a secondary use of the tool and the primary use remains for parameter estimation based on actual field measurements.

The following sections present brief discussions on the nonlinear least squares minimization and the sensitivity based parameter estimation process. A numerical example

showing the application of the tool to estimate the composite load model parameters is also presented here.

6.1 Nonlinear least squares minimization

The nonlinear least squares minimization technique is a common method used for curve fitting. The curve-fitting problem can be framed as least square minimization problem given by [55]

$$\arg\min_{\lambda} e(\lambda) = [m - F(\lambda)]^t [m - F(\lambda)], \tag{6.1}$$

where,

m is the vector of data points corresponding to the measured data,

$F(\lambda)$ is the vector of values of the curve to be fitted, evaluated for a particular value of λ,

$e(\lambda)$ is the λ dependent square of the error, which is the objective function being minimized, and

λ is the vector of variables that are updated to minimize $e(\lambda)$

The trust region methods are established algorithms to solve the nonlinear least squares problem given by (1) [55]. Detailed descriptions of these methods can be found in [55]. The Gauss-Newton [55] and Levenberg-Marquardt [55] are the most popular and effective trust region methods used for solving the nonlinear least squares problem. In the Gauss-Newton method, the parameter set λ is updated by an amount $\Delta\lambda$ at each iteration of the optimization process, where $\Delta\lambda$ is given by [55]

$$\Delta\lambda = (J^t J)^{-1} J^t (m - F(\lambda)), \tag{6.2}$$

$$J = \frac{\partial F(\lambda)}{\partial \lambda}, \tag{6.3}$$

where, J is the Jacobian with respect to the parameter set λ. The main drawback of the Gauss-Newton method is that it requires the matrix J^tJ to be invertible.

The Levenberg-Marquardt method works better than the Gauss-Newton method when the matrix J^tJ is ill conditioned or singular. In the Levenberg-Marquardt method, the parameter set λ is updated by [55]

$$\Delta\lambda = (J^t J + \mu \,\mathrm{diag}(J^t J))^{-1} J^t (m - F(\lambda)), \tag{6.4}$$

where, μ is a damping factor that is computed adaptively at each step of the iteration based on the computed error between m and $F(\lambda)$. The additional term $\mu diag(J^tJ)$ prevents the inverted part of (6.4) to be singular [55], [56]. The Jacobian matrix given by (6.3) can be computed either numerically using a finite differencing approach or analytically.

6.2 Effect of parameter sensitivity on the estimation process

The Jacobian matrix provides useful information about the parameter estimation process. For the load model parameter estimation problem, the elements of the Jacobian matrix are the sensitivities of the consumed active and reactive power to the parameters to be estimated. Since the number of data points obtained by measurements is typically more than the number of parameters to be estimated, the Jacobian matrix has more rows than columns. For the parameter estimation to be accurate, the Jacobian given by (6.3) should

have full column rank. For a column rank deficient Jacobian matrix, not all parameters in the parameter set can be identified uniquely. The Jacobian can be rank deficient or close to rank deficiency for two reasons:

1. A particular parameter being estimated may have little or no impact on the measurements used. Therefore, the sensitivity of the particular measurement/model output to the parameter is zero or nearly zero, thereby making the Jacobian rank deficient.
2. A set of parameters may have identical impact on the measurement/model output and hence two or more columns of the Jacobian matrix may be linearly dependent. The linear dependence of the columns makes the Jacobian matrix rank deficient in this case.

In both the conditions described here, certain parameters of the load model cannot be estimated uniquely. When the Jacobian is column rank deficient or close to being column rank deficient the term,

$$J^t J + \mu \,\mathrm{diag}(J^t J)\,, \tag{6.5}$$

may be ill conditioned. A detailed discussion on solving nonlinear least squares problem with a rank deficient Jacobian can be found in [56].

In the context of model parameter estimation, analyzing the Jacobian J reveals if the measurements made are sufficient for estimating a desired set of parameters. For a given mathematical model of the load, the measurements recorded for parameter estimation

should clearly reflect the influence of the individual parameters, such that they can be estimated uniquely. When columns of the Jacobian matrix J are zero, the parameters associated with those particular columns will retain the initial guess values at the end of the estimation process. These parameters do not have any influence on the dynamic behavior of the model for a particular event, for which, the measurements have been made. If two or more columns are linearly dependent on each other, the parameters associated with those columns may or may not have significant effect on the model behavior. However, even if the effect is significant the parameters cannot be identified uniquely because small changes in the parameters have a similar impact on the dynamic behavior of the model for the particular event.

For the estimation error to be minimum, the Jacobian J should have full rank and the matrix J^tJ should not be ill-conditioned. When these conditions are satisfied, the parameters can be estimated uniquely with minimum error. As a practice both these indices, rank of Jacobian J and the condition number JtJ, should be investigated prior to proceeding with the parameter estimation process. J^tJ is the approximate Hessian matrix in the least square minimization process. This matrix provides information about the curvature of the problem at any step of the iteration; that is, the rate of change of the sensitivities.

6.3 The composite load model parameter estimation

An example of load model parameter estimation is presented here. The parameters of the composite load model developed in PSAT [40], a MATLAB based open source power system simulator, is estimated here. This model is similar to the WECC composite

load model '*cmpldw*' in GE-PSLF [22]. The example presented here serves to test the proposed tool rather than present an actual case of measurement based parameter estimation. In the absence of actual field measurements, the composite load model parameters are estimated based on surrogate voltage and, active and reactive power recorded from a detailed three phase electromagnetic transient simulator. To obtain the measurements, a detailed model of the composite load was used in PSCAD/EMTDC [57]. Furthermore, the entire system in PSCAD/EMTDC is simulated in its full three phase details using a point on wave simulation. As such, the measurements made in PSCAD/EMTDC serve as an efficient surrogate for actual field measurements. The parameter estimation problem presented here, serves as a good example to test the efficiency of the proposed tool. In PSCAD, the single-phase induction motor (SPIM) driven air-conditioners (A/C) and the three phase induction motors are represented by detailed differential equations describing the behavior of the internal flux linkages in full three-phase details. However, the composite load model in PSAT is represented by positive sequence models of three-phase induction motors and a performance model of a SPIM driven A/C. The performance model of the SPIM driven A/C is described by algebraic equations governing the active and reactive power consumption depending on the terminal voltage. A detailed description of the SPIM driven A/C model in PSCAD can be found in [58].The detailed description of the SPIM driven A/C in PSAT can be found in [41]. The example highlights the efficiency of estimating the parameters of an approximate positive sequence load model from a detailed three-phase model load model.

The IEEE 9 bus system was used in PSCAD to simulate a disturbance scenario and record the voltage, active and reactive power at the load bus. Figure 6.1 shows the one line

diagram of the IEEE 9 bus system designed in PSCAD. Figure 6.2 shows the details of the composite load model connected at bus 5 in PSCAD. The total load at bus 5 in Figure 6.2 is equally divided on the three 12.47 kV distribution feeders. Table 6.1 lists the composition of the load connected on each 12.47 kV feeder. As discussed in the previous section, the disturbance should be chosen such that all the parameters to be estimated are expected to have some impact on the dynamic behavior. For example, if the parameters affecting the stalled behavior of an induction motor is to be estimated, the recorded measurements should correspond to an event where the induction motor stalls. To achieve this, a three-phase fault for 0.05 s was applied on bus 5. The fault creates a voltage dip sufficiently long for the SPIM driven A/C to stall thereby resulting in a delayed voltage recovery. Figure 6.3 shows the voltage recorded at the low voltage side of the transformer connected at bus 5 in PSCAD. Figure 6.4 and Figure 6.5 show the active and reactive power consumed by the load connected at bus 5 respectively. These recorded measurements serve as inputs to the parameter estimation tool presented here. Figure 6.6 shows the individual components of composite load model in PSAT. The parameters of this model are estimated using the measurements made from the detailed three-phase model in PSCAD. To estimate the load parameters:

1. The voltage recorded in PSCAD is played in at the terminal bus of the load model in the estimation tool as shown in Figure 6.6,
2. The active and reactive power consumed by the load model based on the initial guess of the parameters is computed; and

3. The parameter values are then updated such that the least square error between the computed active and reactive power and the recorded active and reactive power in PSCAD is minimized.

Table 6.1 Component wise consumption of the composite load model

Load component	**Steady state load (MW/MVAr)**
1-Φ A/C motor	24.3 + j6.5 MVA
3-Φ, constant torque motor (A) (torque proportional to square of speed)	2.5 + j1.2 MVA
3-Φ, variable torque and low inertia motor (B) (torque proportional to square of speed)	4.1 + j2.1 MVA
Static load	8.1 + j6.8 MVA
Total load	40+j16.6 MVA

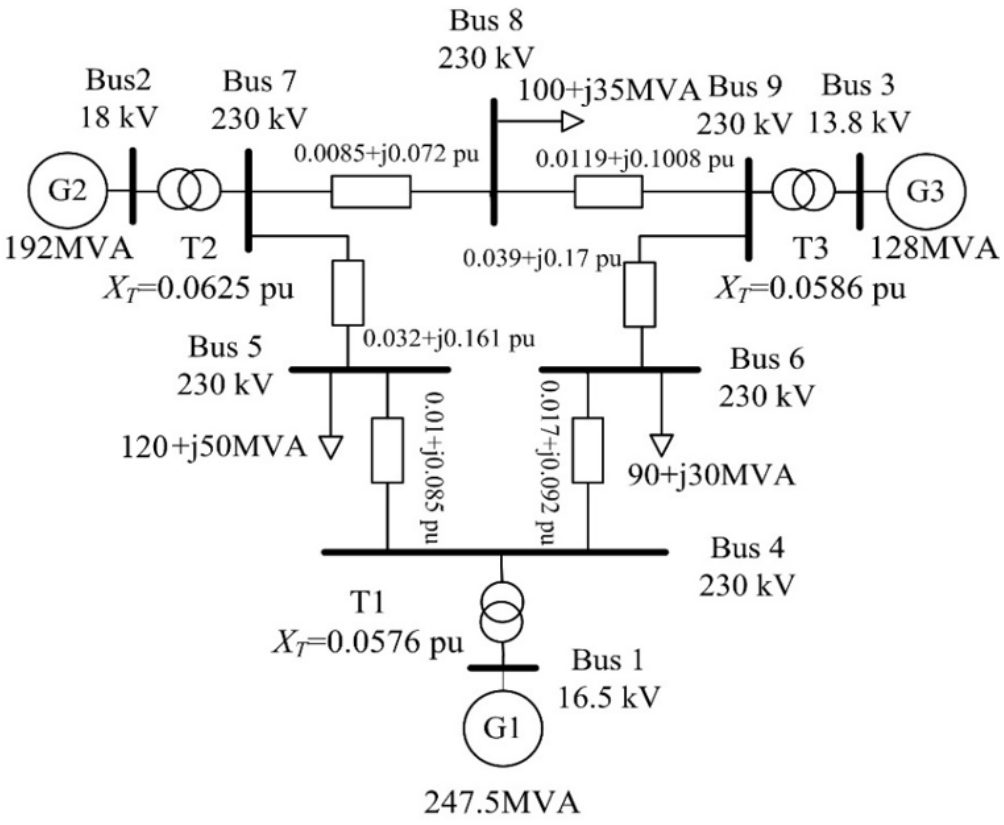

Figure 6.1 One-line diagram of the IEEE 9 bus system

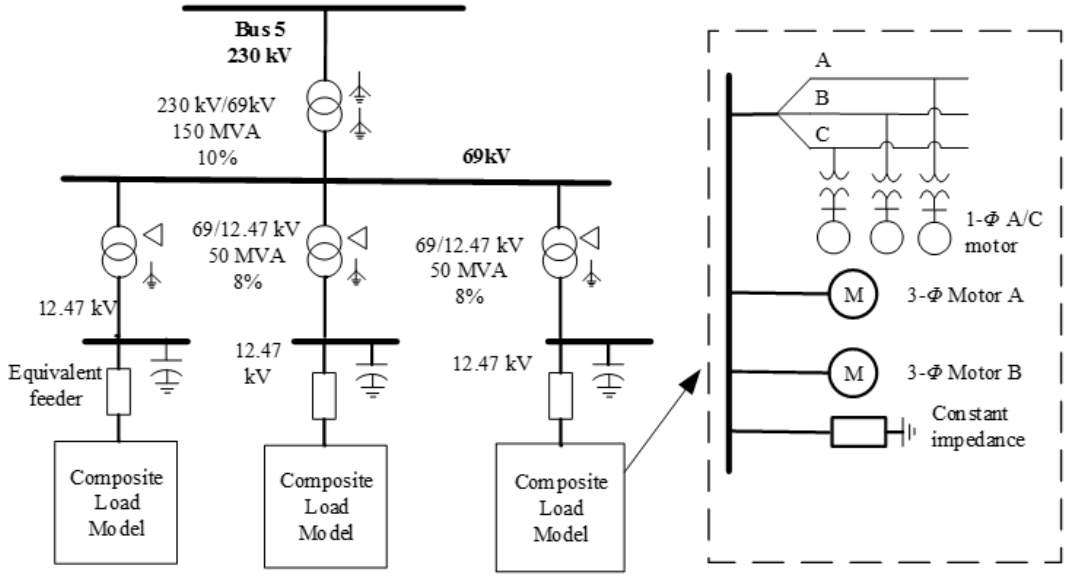

Figure 6.2 Detailed load distribution at bus 5

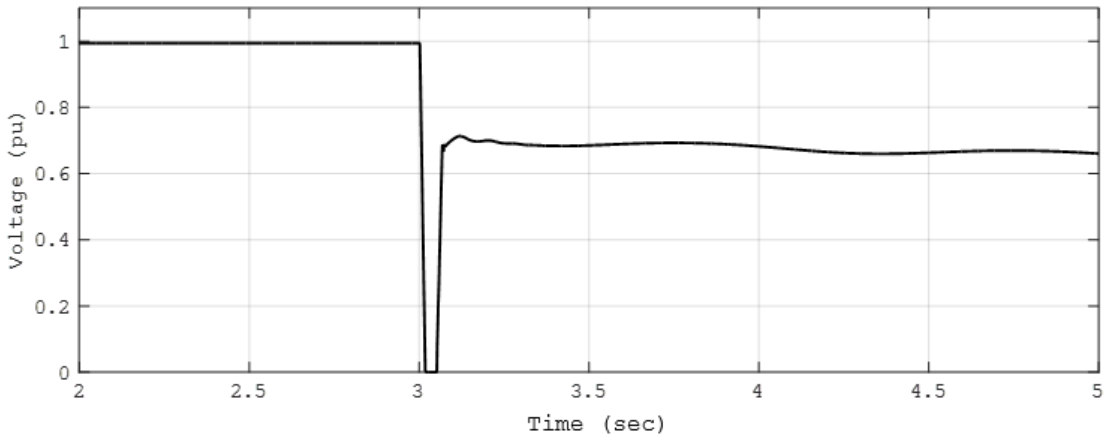

Figure 6.3 Measured voltage (in pu) at 12.47 kV level at bus 5

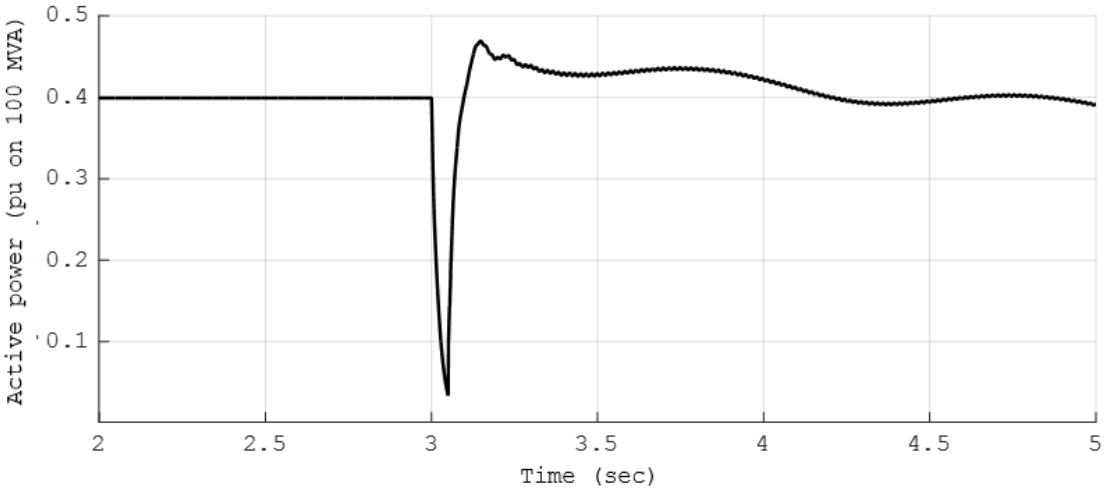

Figure 6.4 Measured active power (in pu) at 12.47 kV level at bus 5

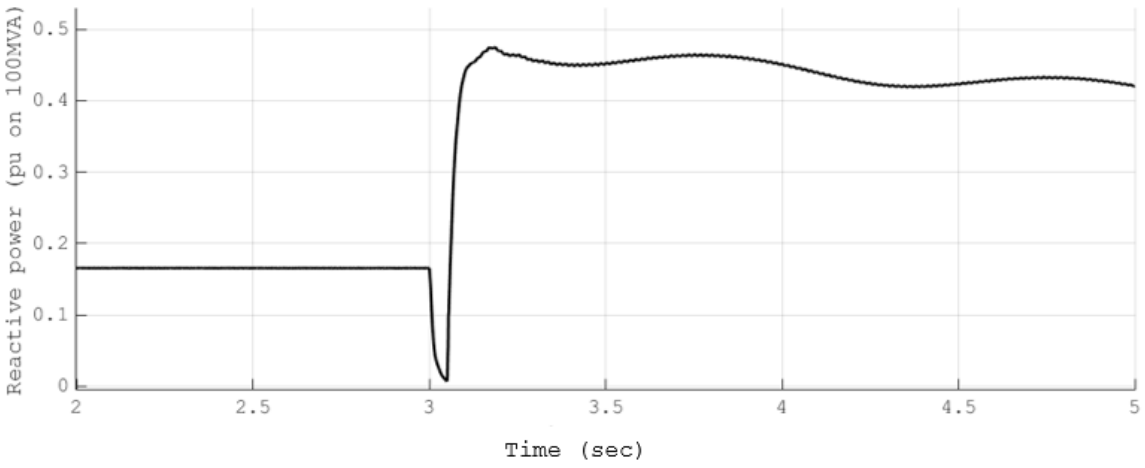

Figure 6.5 Measured reactive power (in pu) at 12.47 kV level at bus 5

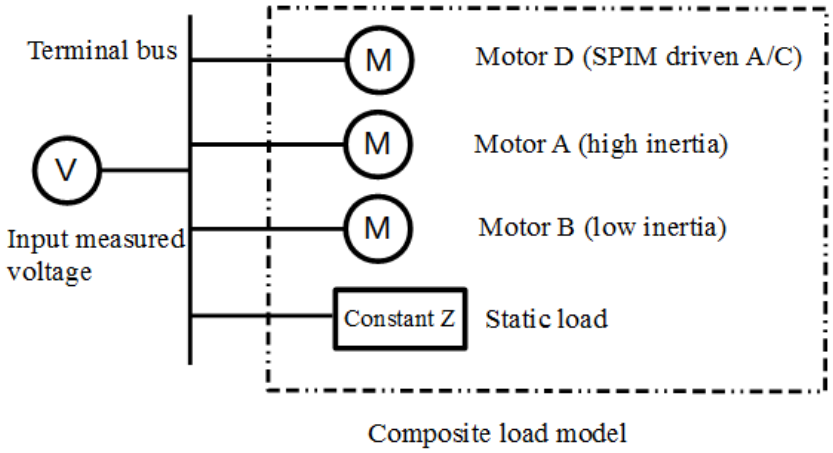

Figure 6.6 Composite load model in the parameter estimation tool

To formulate the parameter estimation problem as a nonlinear least squares minimization problem F and m in (1) is given by

$$F(\lambda) = \begin{bmatrix} P(\lambda) \\ Q(\lambda) \end{bmatrix}, m = \begin{bmatrix} Pmeas \\ Qmeas \end{bmatrix}, \tag{6.6}$$

where,

Pmeas is the recorded active power consumption of the detail load model implemented in PSCAD shown in Figure 6.3,

P(λ) is the computed active power consumption in the parameter estimation tool for a particular value of λ,

Qmeas is the recorded reactive power consumption of the detail load model implemented in PSCAD shown in Figure 6.4,

$Q(\lambda)$ is the computed reactive power consumption in the parameter estimation tool for a particular value of λ,

λ is a vector of parameters to be estimated, and the Jacobian J in (3) for the load model parameter estimation is given by

$$J = \left[\frac{\partial P(\lambda)}{\partial \lambda} \quad \frac{\partial Q(\lambda)}{\partial \lambda} \right]^t . \tag{6.7}$$

J is computed analytically for this work as it saves the additional computations required in the finite differencing approach. However, a provision to compute the Jacobian by finite differencing is included in the tool, which is useful when it is cumbersome to compute certain entries of the J analytically.

Table 6.2 lists the parameters of the composite load model that are estimated in this example. As shown in Table 6.2, 27 parameters are estimated in this example. The 27 selected parameters are the key parameters in the composite load model. The parameters relating to contactor trip or relay tripping are excluded here as these parameters introduce discontinuities in the minimization problem.

Table 6.3 lists the initial guess used for the parameters in the estimation process. Table 6.4 lists the upper and the lower bound on the parameter values. It is important to set the upper and lower bounds properly based on some survey or prior experience. In the absence of upper and lower bounds, the minimization routine can return unrealistic values for the various parameters being estimated. The Levenberg-Marquardt method in the least

square minimization routine, *lsqnonlin* [59] in MATLAB was used for solving the minimization problem. However, the Levenberg-Marquardt routine in *lsqnonlin* cannot handle upper and lower bounds. To circumvent this problem, an additional internal parameter set P_{int}, which is supplied to the load is defined as

$$P_{\text{int}} = lb + (\sin(P_{ext}) + 1)(ub - lb)/2, \tag{6.8}$$

where, P_{ext} is the parameter set updated by the optimization routine in an unbounded parameter space. *lb* and *ub* are the lower and the upper bounds on the parameter set. From (6.8), it can be seen that the P_{int}, which is used in the load model is always bounded, even when P_{ext} is unbounded. P_{ext} is related to P_{int} by

$$P_{ext} = \frac{\arcsin(2(P_{ext} - lb))}{ub - lb}. \tag{6.9}$$

A detailed discussion about the formulation given by (6.8) and (6.9) can be found in [60]. It should be noted that although the Levenberg-Marquardt is comparatively more robust than the Gauss-Newton method, imposing bounds using (6.8) and (6.9) adds additional computational burden [55], [59]. The maximum number of iterations has been set to 30. During the testing process, no further improvement was observed after the 30 iterations. However, the maximum number of iterations required is dependent on the model as well as the measurements that are recorded. The maximum number of iterations needed is therefore problem dependent and needs adjustment for individual cases.

Table 6.2 Parameters of the composite load model

<table>
<tr><th>Motor A and B</th><th>Motor D (SPIM driven A/C</th><th>Static load</th></tr>
<tr><td>Stator resistance (rs)</td><td>Active power coefficient for running state 1 (kp1)</td><td>Constant P part (Pp)</td></tr>
<tr><td>Stator reactance (xs)</td><td>Active power exponent for running state 1 (np1)</td><td>Constant Q part (Qp)</td></tr>
<tr><td>Rotor resistance (rr)</td><td>Reactive power coefficient for running state 1 (kq1)</td><td rowspan="9">2 parameters</td></tr>
<tr><td>Rotor reactance (xr)</td><td>Reactive power exponent for running state 1 (nq1)</td></tr>
<tr><td>Magnetizing reactance (xm)</td><td>Active power coefficient for running state 2 (kp2)</td></tr>
<tr><td>Inertia constant (h)</td><td>Active power exponent for running state 2 (np2)</td></tr>
<tr><td>Percentage composition (Fm)</td><td>Reactive power coefficient for running state 2 (kq2)</td></tr>
<tr><td rowspan="5">14 parameters (7 parameters each for motors A and B</td><td>Reactive power exponent for running state 2 (nq2)</td></tr>
<tr><td>Stall resistance (rstall)</td></tr>
<tr><td>Stall reactance (xstall)</td></tr>
<tr><td>Percentage composition Fmd</td></tr>
<tr><td>11 parameters</td></tr>
<tr><td colspan="2">Total number of parameters estimated</td><td>27</td></tr>
</table>

Table 6.3 Initial guess for the parameter estimation process

Common parameters for motor A and B	**Initial guess (pu)**	**Motor D**	**Initial guess (pu)**
rr	0.02	*kp1*	0.001
xs	0.04	*np1*	1
rr	0.004	*kq1*	6
xr	0.1	*nq1*	2
xm	3	*kp2*	12
Individual parameters for motor A, B and C	**Initial guess (pu)**	*np2*	3
Fma	5	*kq2*	11
ha	0.8	*nq2*	2
Fmb	8	*rstall*	0.1
hb	0.3	*xstall*	0.1
		Fmd	40
		Static load	**Initial guess (pu)**
		Pp	1.5
		Qp	0.8

Table 6.4 Upper and lower bounds on the parameters for the estimation process

Common parameters for motor A and B	**Range (pu)**	**Motor D**	**Range (pu)**
rs	0.1 – 0.005	*kp1*	5
xs	0.1 – 0.005	*np1*	5 – 0
rr	0.01 – 0.001	*kq1*	10 – 0
xr	0.1 – 0.01	*nq1*	10 – 0
xm	4 - 2	*kp2*	20 – 0
Individual parameters for motor A and B	**Range (pu)**	*np2*	5 – 0
Fma	0.15 – 0.07	*kq2*	20 – 0
ha	1.5 – 0.5	*nq2*	5 – 0
Fmb	0.1 – 0.02	*rstall*	0.5 – 0.01
hb	0.5 – 0.1	*xstall*	0.5 – 0.01
		Fmd	0.7 – 0.3
		Static load	**Range (pu)**
		Pp	1 – 0
		Qp	1 – 0

Figure 6.7 shows the measured active power and the fitted active power at bus 5. Figure 6.8 shows the measured reactive power and the fitted reactive power at bus 5. From Figure 6.7 and Figure 6.8 it can be seen that the active and reactive power output of the composite load model matches the measured quantities closely except during the fault. The composite load model in the parameter estimation tool exhibits sudden jumps in its behavior, whereas the output of the PSCAD model is considerably smooth. This is shown in the

insets of Figure 6.7 and Figure 6.8. The discrepancy can be attributed to the modeling differences in the SPIM driven A/C model in PSCAD and PSAT. As mentioned before, in PSCAD the flux decay in the SPIM and the rotation of its shaft is described by differential equations. However, in PSAT, the SPIM is represented by a performance model, which is purely algebraic and has discontinuities. The sharp jumps in the output of the tuned PSAT model are due to the transition of the SPIM from one operating state to another. However, before the fault and approximately 0.4 s after the fault is removed, the output of PSAT model with the estimated parameters closely matches with the PSCAD model. The estimated values of the parameters are listed in Table 6.4. The estimation process was repeated using the Gauss-Newton algorithm in *lsqnonlin*. The Gauss-Newton algorithm supports the upper and lower bounds on the parameters values. The estimated values of the parameter are listed in Table 6.6.

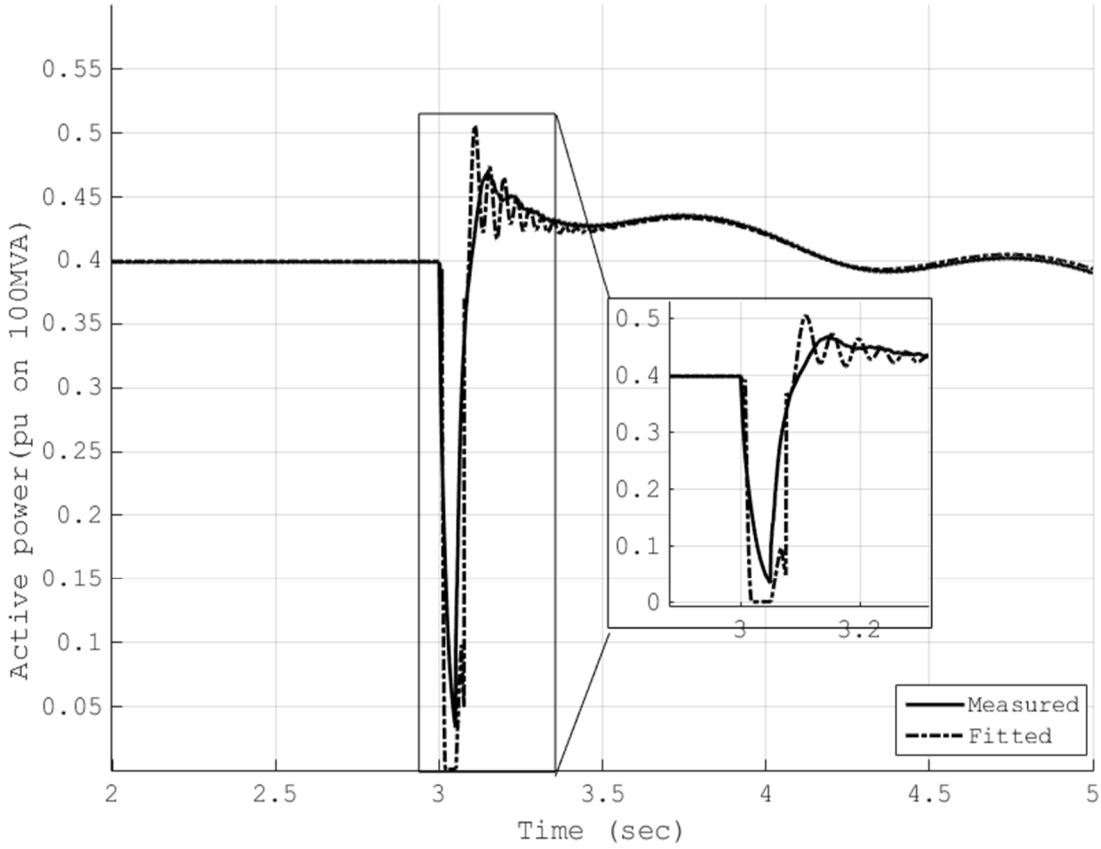

Figure 6.7 Measured and fitted active power consumption of the composite load model

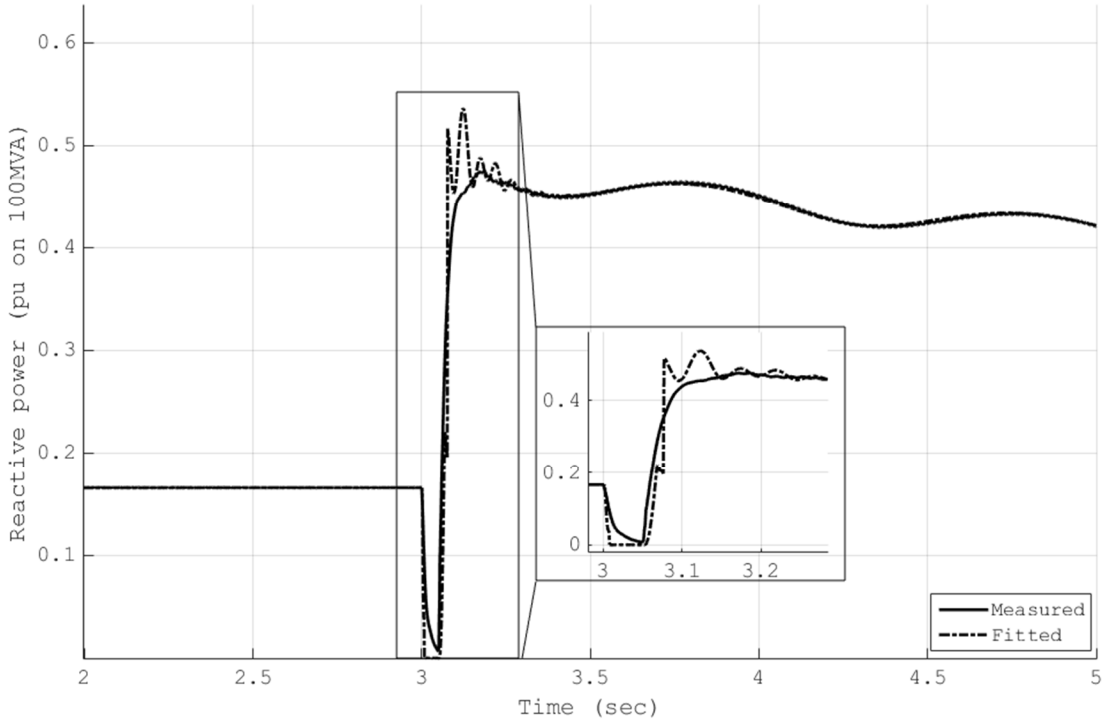

Figure 6.8 Measured and fitted reactive power consumption of the composite load model

Table 6.5 Estimated parameters of the composite load model using Levenberg-Marquardt method with upper and lower bounds on the parameters

Motor A	**Estimated value**	**Motor d**	**Estimated value**
rsa	0.0087	*np1*	~ 0
xsa	0.021	*kq1*	6
rra	0.0098	*nq1*	2.01
xra	0.1705	*kp2*	9.86
xma	3.16	*np2*	1.05
ha	0.98	*kq2*	8.8
Fma	5.06	*nq2*	0.95
Motor B	**Estimated value**	*rstall*	0.174
rsb	0.0674	*xstall*	0.157
xsb	0.0354	*Fmd*	65.63
rrb	0.0049	**Static load**	**Estimated value**
xrb	0.1273	*Pp*	0.39
xmb	2.93	*Qp*	0.17
hb	0.2		
Fmb	10		

Table 6.6 Estimated parameters of the composite load model using Gauss-Newton method with upper and lower bounds on the parameters

Motor A	**Estimated value**	**Motor d**	**Estimated value**
rsa	0.0083	*np1*	~ 0
xsa	0.041	*kq1*	6
rra	0.0078	*nq1*	2.03
xra	0.153	*kp2*	9.72
xma	2.99	*np2*	1.05
ha	0.88	*kq2*	8.802
Fma	6.26	*nq2*	0.95
Motor B	**Estimated value**	*rstall*	0.1735
rsb	0.0611	*xstall*	0.16
xsb	0.0375	*Fmd*	64.51
rrb	0.0040	**Static load**	**Estimated value**
xrb	0.137	*Pp*	0.39
xmb	3.01	*Qp*	0.17
hb	0.202		
Fmb	10		

6.3.1 Load model parameter sensitivity and dependency

The entries of the matrix *J* are the sensitivities of the active and reactive power consumed by the load to the load model parameters being estimated. As discussed before, a low column rank of *J* may introduce error in the parameter estimation process. In this particular case of load model parameter estimation, a low column rank of *J* indicates that

1. the recorded measurements of active and reactive power may not be sensitive to the load parameters of interest, or
2. two or more parameters may have similar sensitivities for the recorded measurements.

Analyzing and understanding the implications of these two different conditions, provides additional insight into the parameter estimation process. References [53] and [54], uses the Jacobian to reduce the parameter space by removing the less sensitive parameters. However, a systematic method is not introduced in [53] or [54]. To analyze the Jacobian *J*; the pairwise condition number for each column of *J* with all other columns is computed. A large condition number indicates either that the entries of one column is nearly zero or that the two columns are linearly dependent. Figure 6.9 and Figure 6.10 shows the pairwise condition numbers of the important parameters of the composite load model for the active and reactive power measurements respectively. The parameters *kp1*, *np1*, *kp2*, *np2*, *kq1*, *nq1*, *kq2*, and *nq2* are left out of Figure 6.9 and Figure 6.10 because these parameters did not significantly affect the model. The condition numbers were computed for the Jacobian *J* at the beginning of the iteration with the initial guesses for the parameters.

The relatively large pairwise condition numbers are highlighted in both Figure 6.9 and Figure 6.10. The key observations from Figure 6.9 and Figure 6.10 are as follows:

1. In Figure 9, the pairwise condition numbers for the parameter *Qp* are very high. This is because the column entries of *J* corresponding to the parameter *Qp* is zero for the active power measurements. *Qp* has no impact on the active power consumption of the composite load model. Changes in the parameter *Qp* only impacts the reactive power consumption of the model. Figure 11 and Figure 12 show the sensitivity of the active and reactive power consumed by the load to the parameters *Pp* and *Qp*. From Figure 11 and Figure 12 it can be seen that both the active and reactive power consumption is sensitive to *Pp*. However, the parameter *Qp* only affects the reactive power consumption.
2. In Figure 6.9 and Figure 6.10, the pairwise condition numbers of the parameters *xma* and *xmb* are high. This is because the magnetizing reactance of the induction motor model does not have any significant effect on the active or reactive power consumed by the model. The Jacobian entries for the active and reactive power corresponding to these parameters are nearly zero. Figure 6.13 and Figure 6.14 show the sensitivities of the active and reactive power to the parameters *xma*, *xra* and *xsa*. From Figure 6.13 and Figure 6.14 it can be seen that the active and reactive power consumption of the motor is not affected by changes in the magnetizing reactance as compared to the stator and rotor reactance of the three-phase induction motor.

3. In Figure 6.9 and Figure 6.10, the pairwise condition numbers of *Fmd*, *Fma* and *Fmb* are relatively high. This is because the sensitivity of active and reactive power to the percentage of different types of induction motors is comparatively much less than the sensitivities to the physical parameters of these motors. Figure 6.15 and Figure 6.16 show the sensitivities of the active and reactive power to the parameters *Fmd*, *Fma* and *Fmb*. Figure 6.17 and Figure 6.18 show the sensitivities of the active and reactive power to the parameters *Rstall* and *Xstall*. A comparison of Figure 6.15 and Figure 6.17, and Figure 6.16 and Figure 6.18 shows that the sensitivity of active and reactive power consumed by the load to *Rstall* and *Xstall* is considerably higher than the percentage of each motor in the load model.
4. Finally, in Figure 6.9 and Figure 6.10, the pairwise condition number between *xs* and *xr* is high. From Figure 6.13 and Figure 6.14, it can be seen that the parameters *xra* and *xsa* have a significant effect on the active and reactive power consumption. However, the effects of these two parameters on the active and reactive power are similar. Since the sensitivities are similar, the columns of the Jacobian corresponding to these parameters are linearly dependent, resulting in a high condition number.

The investigation of the Jacobian reveals that using the disturbance measurements given in Figure 6.4, Figure 6.5, and Figure 6.6 may not be sufficient to estimate the parameters accurately. The high pairwise condition numbers cause the approximate Hessian J^tJ

to be close to singular leading to errors in the optimization process. The condition number of $J'J$ in the first iteration is 1.08e15.

	Fmd	*Rstall*	*Xstall*	*rsa*	*xsa*	*rra*	*xra*	*xma*	*ha*	*Fma*	*rsb*	*xsb*	*rrb*	*xrb*	*xmb*	*hb*	*Fmb*	*Pp*	*Qp*
Fmd		$< 10^7$	$< 10^7$	**216.4**	**408.8**	**331.5**	**372.0**	2.6	3.2	11.3	85.8	96.2	**611.6**	94.8	15.3	20.8	38.8	**656.7**	$< 10^7$
Rstall			$< 10^7$	12.9	24.3	19.7	22.1	40.3	6.4	128.6	5.4	6.7	36.3	6.9	**256.8**	1.2	**579.5**	39.0	$< 10^7$
Xstall				3.3	2.3	1.7	2.4	**1383.4**	**218.4**	**4408.6**	17.4	39.6	1.1	48.4	**8818.0**	27.8	**19888.1**	3.5	$< 10^7$
rsa					15.0	3.2	14.8	**2630.8**	**248.2**	**290.2**	3.9	5.7	3.1	6.4	**2166.4**	9.5	**601.4**	2.1	$< 10^7$
xsa						2.4	**169.3**	**6447.3**	**363.2**	**531.7**	7.1	10.6	1.8	11.8	**3916.3**	16.5	**1133.0**	1.6	$< 10^7$
rra							2.4	**1018.9**	**224.0**	**478.3**	6.2	8.8	1.8	9.8	**3470.3**	16.0	**925.7**	1.1	$< 10^7$
xra								**6577.5**	**341.2**	**484.0**	6.5	9.6	2.0	10.8	**3567.7**	15.0	**1031.1**	1.7	$< 10^7$
xma									24.1	1.7	**119.4**	87.0	**1241.3**	78.5	5.6	42.3	1.9	**855.7**	$< 10^7$
ha										4.2	19.5	13.9	78.9	12.5	31.6	7.2	8.7	**139.3**	$< 10^7$
Fma											**119.0**	**125.7**	**872.0**	**121.6**	10.6	29.6	12.5	**908.0**	$< 10^7$
rsb												7.5	13.3	7.0	**565.8**	2.6	**235.3**	9.3	$< 10^7$
xsb													16.9	49.2	**429.0**	1.8	**263.4**	15.4	$< 10^7$
rrb														18.6	**9535.3**	32.6	**1705.6**	1.6	$< 10^7$
xrb															**392.3**	1.6	**256.6**	17.5	$< 10^7$
xmb																**222.5**	5.6	**4948.3**	$< 10^7$
hb																	58.1	18.3	$< 10^7$
Fmb																		**1822.3**	$< 10^7$
Pp																			$< 10^7$

Figure 6.9 Pairwise condition numbers for the active power measurement

	Fmd	*Rstall*	*Xstall*	*rsa*	*xsa*	*rra*	*xra*	*xma*	*ha*	*Fma*	*rsb*	*xsb*	*rrb*	*xrb*	*xmb*	*hb*	*Fmb*	*Pp*	*Qp*
Fmd		$< 10^7$	$< 10^7$	**322.73**	**439.07**	**351.77**	**399.38**	4.9623	4.4109	6.2166	46.794	**101.23**	**441.84**	**100.1**	21.172	14.827	**171.183**	**7148.6**	**212.5**
Rstall			$< 10^7$	4.6717	3.5639	1.1684	3.7259	**1851.1**	**274.38**	**1370.7**	17.125	38.74	1.1165	47.327	**8639.8**	27.64	**20287.9**	**95.212**	2.7776
Xstall				27.121	36.838	29.471	33.518	53.952	8.2021	40.151	4.1764	9.4903	37.017	9.646	**251.65**	1.2423	**601.094**	**601.15**	17.822
rsa					40.413	2.3915	43.675	**6234.7**	**227.07**	**510.63**	6.6412	9.1082	2.4593	10.266	**3017.9**	12.116	**206.422**	3.4336	1.5776
xsa						1.8647	**164.88**	**6392**	**285.82**	**660.24**	9.2655	12.397	1.7368	13.975	**4214.7**	17.18	**280.806**	3.389	1.7567
rra							1.9881	**1097.5**	**173.97**	**391.56**	10.494	10.727	1.2528	11.93	**4374.3**	23.738	**224.389**	1.8169	1.9288
xra								**6553.3**	**267.32**	**605.53**	8.4675	11.312	1.8992	12.745	**3845**	15.702	**255.425**	3.2905	1.6667
xma									22.865	7.6352	**107.16**	**136.14**	**1166.3**	**124.27**	6.3627	39.185	7.37863	**905.83**	**530.1**
ha										7.4865	16.504	20.405	**181.22**	18.608	39.317	6.0904	3.28134	**134.15**	81.937
Fma											46.882	79.254	**463.87**	74.572	18.568	15.57	7.07709	**707.4**	**219.32**
rsb												1.5854	16.817	1.6678	**421.1**	2.303	29.8954	8.1983	5.8539
xsb													14.609	60.019	**1363.4**	2.2315	64.6961	18.687	6.4088
rrb														16.025	**7172.7**	33.68	**281.885**	2.2806	2.4179
xrb															**1112.8**	2.002	63.9013	22.74	7.1401
xmb																**187.98**	33.1322	**4090.1**	**2490.5**
hb																	9.45722	13.089	12.298
Fmb																		**4480.1**	**135.54**
Pp																			1.7701

Figure 6.10 Pairwise condition numbers for the reactive power measurement

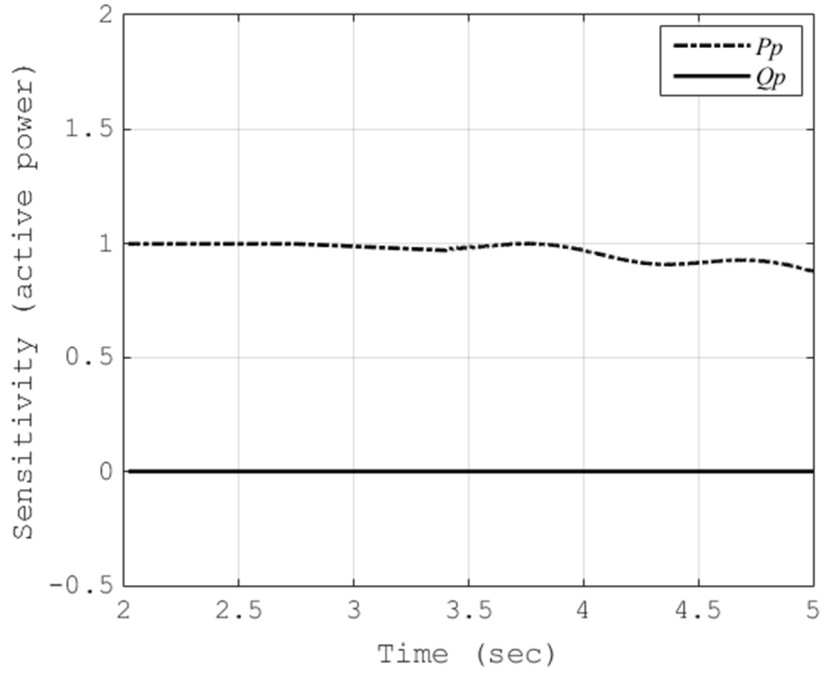

Figure 6.11 Sensitivity of active power consumption to *Pp* and *Qp*

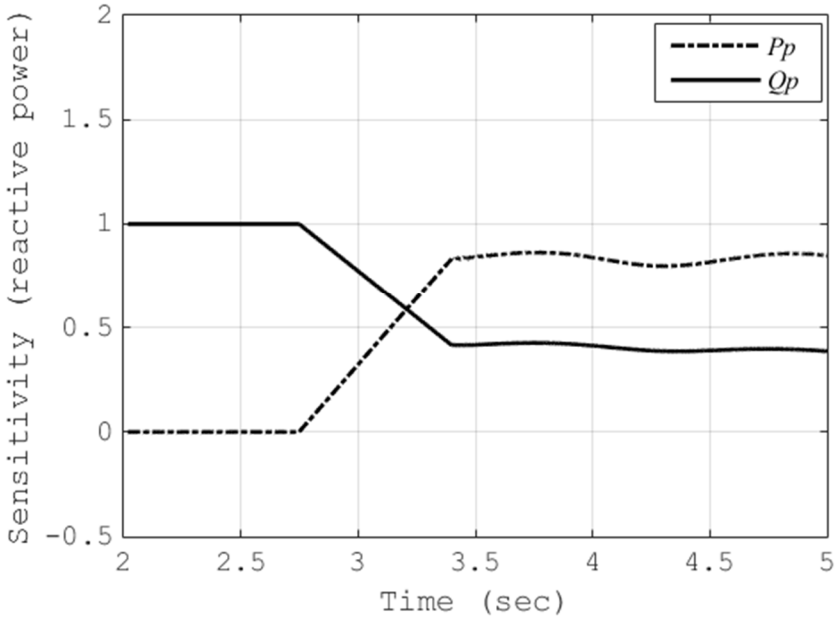

Figure 6.12 Sensitivity of reactive power consumption to *Pp* and *Qp*

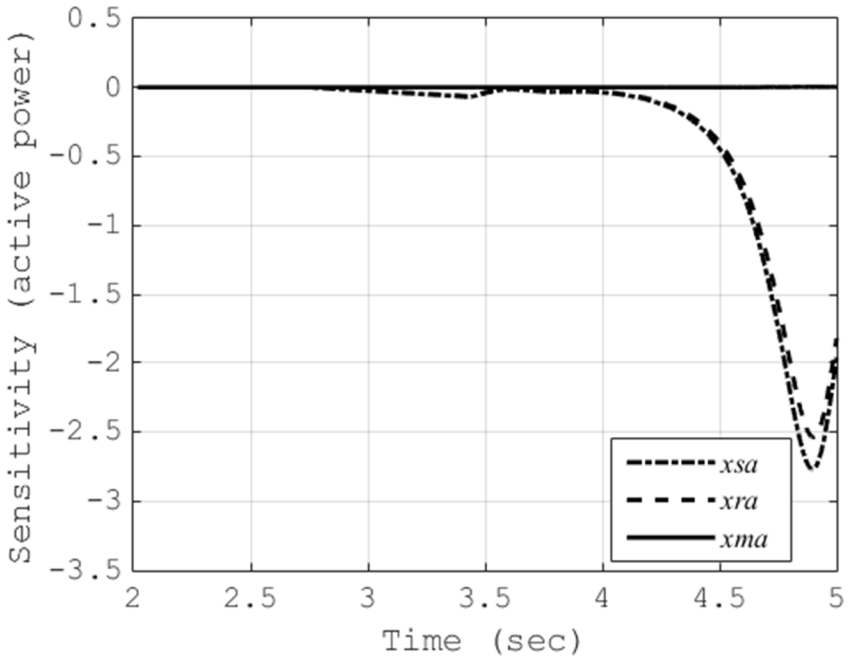

Figure 6.13 Sensitivity of active power consumption to *xsa*, *xra* and *xma*

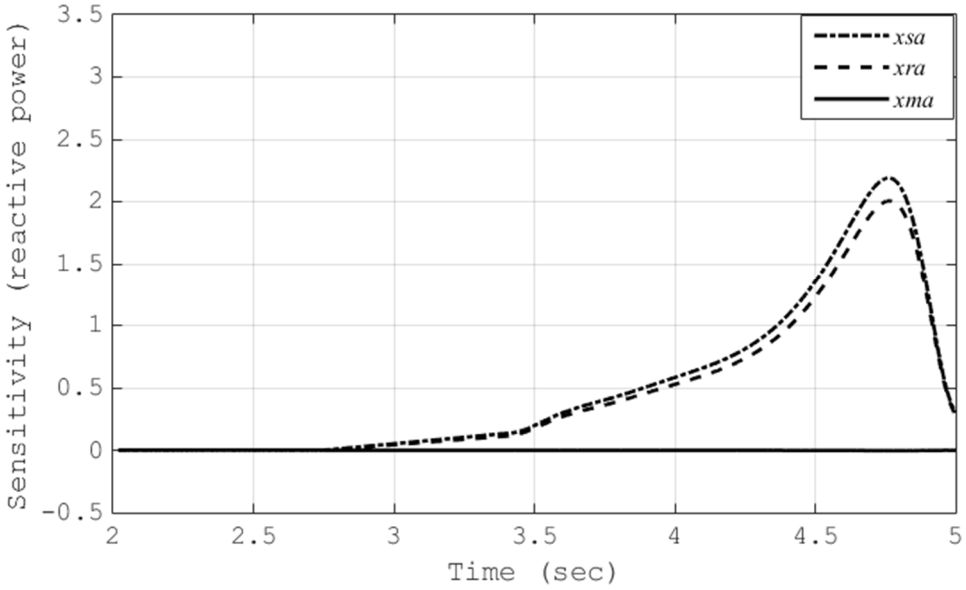

Figure 6.14 Sensitivity of reactive power consumption to *xsa*, *xra* and *xma*

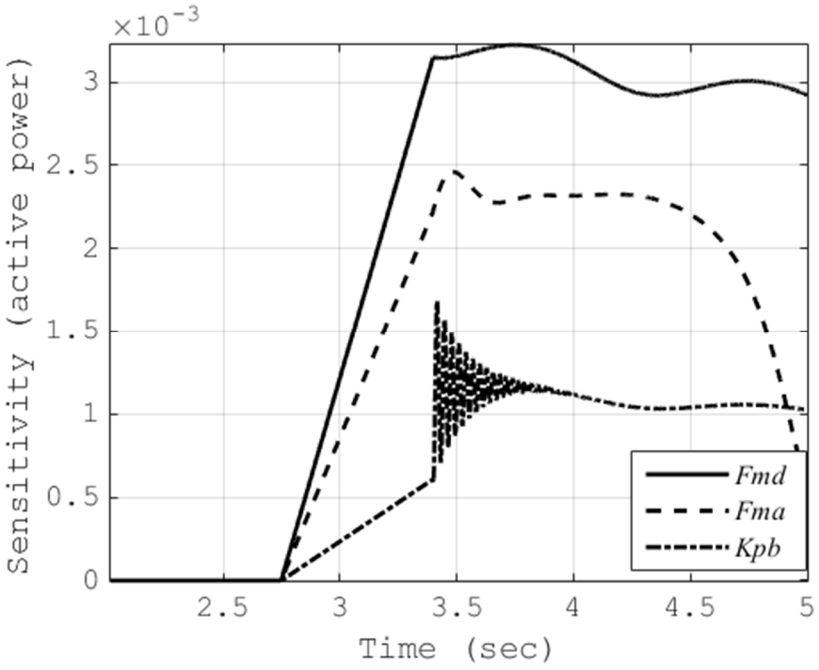

Figure 6.15 Sensitivity of active power consumption to *Fmd*, *Fma* and *Fmb*

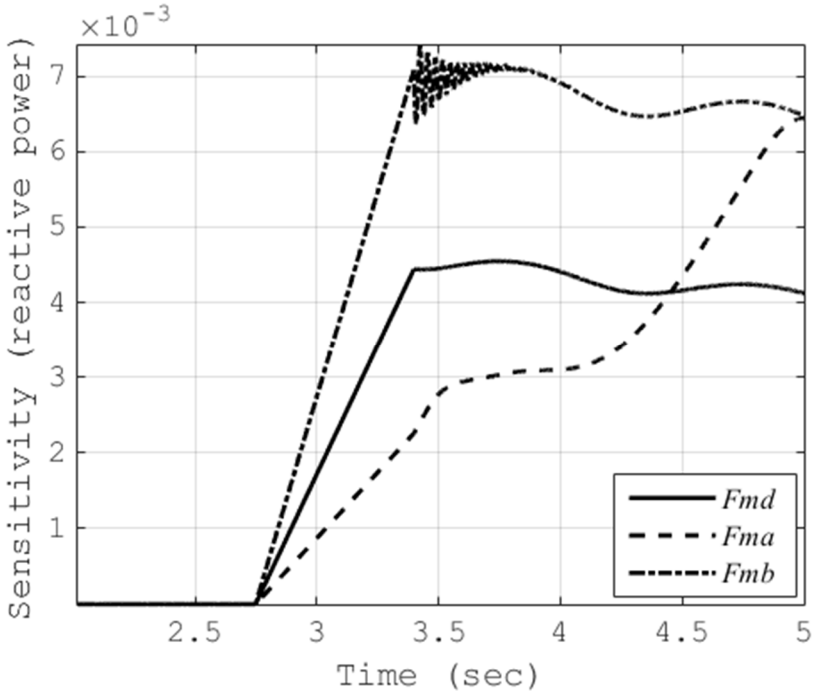

Figure 6.16 Sensitivity of active power consumption to *Fmd*, *Fma* and *Fmb*

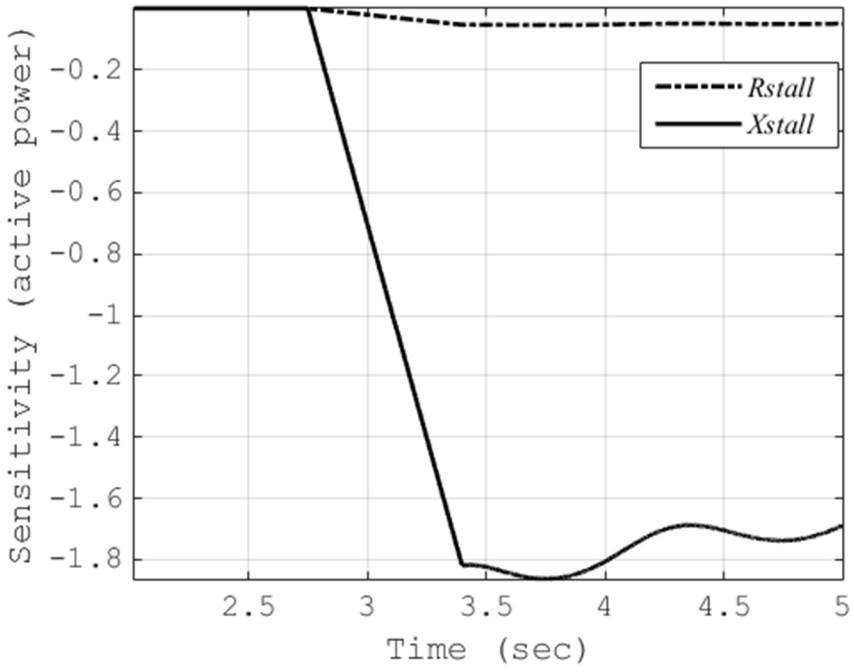

Figure 6.17 Sensitivity of active power consumption to *Rstall* and *Xstall*

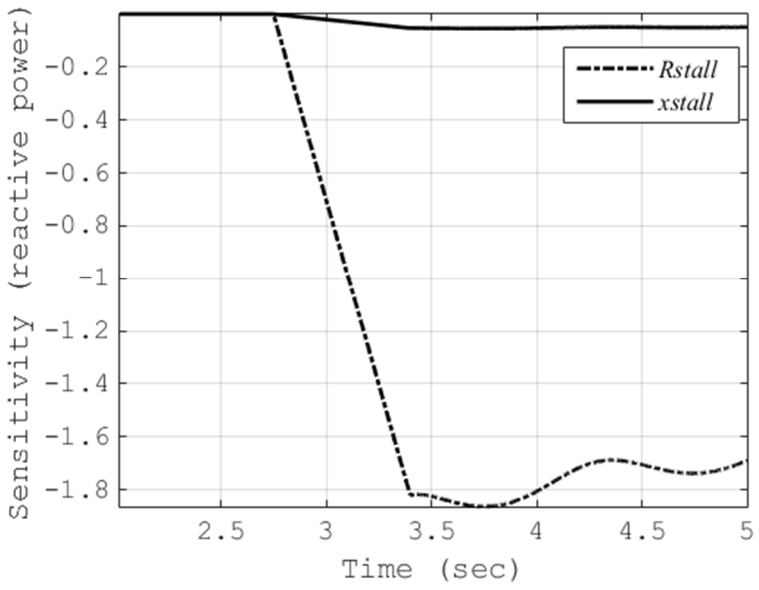

Figure 6.18 Sensitivity of reactive power consumption to *Rstall* and *Xstall*

For nonlinear least squares problem, with an ill conditioned J^tJ, the Levenberg-Marquardt algorithm is more efficient as compared to the Gauss-Newton method. Apart from using a different algorithm, the sensitivity information can be used to make the parameter estimation process more efficient. The sensitivity of the active and reactive power consumption of the composite load model to the parameters *Fmd*, *Fma*, and *Fmb* is much less as compared to the physical parameters of the models like the stator and the rotor impedance. Since the parameter vector is updated based on the gradient, the parameters *Fmd*, *Fma* and *Fmb* would not change much from the initial guess with every iteration, whereas the physical parameters of the model like *xs*, *xr*, *rr*, *rs* will change substantially. This might result in the estimation tool returning unrealistic values for the physical parameters of the model. To avoid such error in this example, one approach consists of fixing the values of the percentage of individual components of the composite load model based on additional knowledge about the load and then estimate the remaining parameters of the model based on the measurements. Another approach to avoid error in parameter estimation is to set appropriate upper and lower bounds on the parameters. A method for implementing parameter bounds while using the Levenberg-Marquardt method is given by (6.8) and (6.9). The parameter *xm* does not have any impact on the active or reactive power consumption of the model. This parameter can be fixed at the beginning of the estimation process. For parameters like *xr* and *xs*, whose sensitivities are linearly dependent, a fixed ratio could be assumed between these two parameters as given by

$$\delta xr = \frac{xr}{xs}, \tag{6.10}$$

where, δxr is the increment in *xr* corresponding to an increment in *x*s.

6.3.2 Parameter estimation with reduced number of parameters

Based on the analysis presented in the previous section the parameter estimation process is repeated by fixing certain parameters of the model. The parameters *Fmd*, *Fma*, *Fmb*, and *xm* are fixed before the estimation process. Table 6.6 shows the values of the fixed parameters for the reduced parameter estimation process. Since this is a test example, the parameters are kept close to the values obtained in Table 6.5. The ratio between *xs* and *xr* is fixed to 8 for motor A and 4 for motor B. The initial guess for the remaining parameters are kept the same as given in Table 6.3. As the number of parameters is reduced, the parameter estimation process is faster, since the dimensions of the optimization problem is reduced. Furthermore, with the reduced set of parameters the condition number of $J'J$ is 2286, which shows that the reduced problem is not ill-conditioned. The problem can now be solved easily using the Gauss-Newton algorithm in *lsqnonlin*. Figure 6.21 and Figure 6.22 show the measured as well as the fitted active and reactive power. The estimated composite load parameters are listed in Table 6.4. The parameters that were fixed in the beginning of the estimation process are marked in bold italics.

Table 6.7 Fixed values of parameters used in the reduced parameter estimation process

Parameter	**Fixed value**
Fma	6
Fmb	12
Fmd	62
xma	3 pu
xmb	3 pu

Table 6.8 Estimated parameters of the composite load model with reduced parameter

Motor A	**Estimated value**	**Motor D**	**Estimated value**
rsa	0.012	*np1*	~ 0
xsa	0.015	*kq1*	6
rra	0.0072	*nq1*	2.01
xra	***0.120***	*kp2*	9.5
xma	***3.00***	*np2*	1.07
ha	0.94	*kq2*	8.3
Fma	***6***	*nq2*	0.95
Motor B	**Estimated value**	*rstall*	0.1506
rsb	0.062	*xstall*	0.1519
xsb	0.04	***Fmd***	***62***
rrb	0.0039	**Static load**	**Estimated value**
xrb	***0.16***	*Pp*	0.39
xmb	***3.00***	*Qp*	0.164
hb	0.211		
Fmb	***12***		

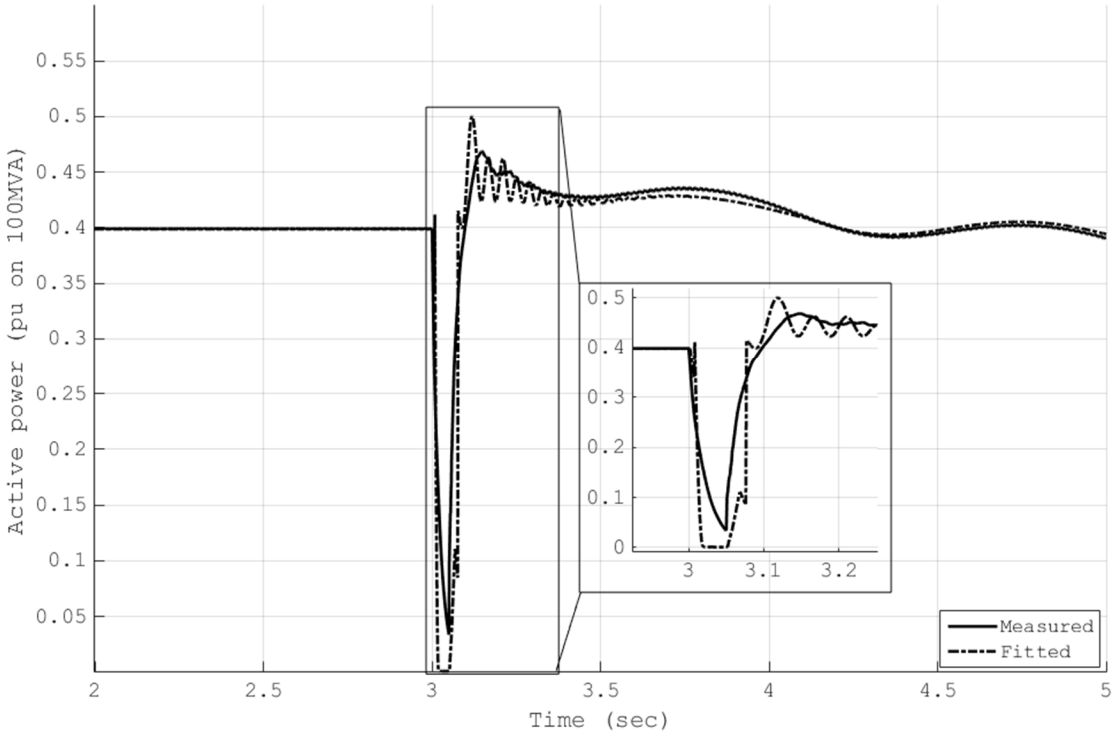

Figure 6.19 Measured and fitted active power consumption of the composite load model with reduced parameters

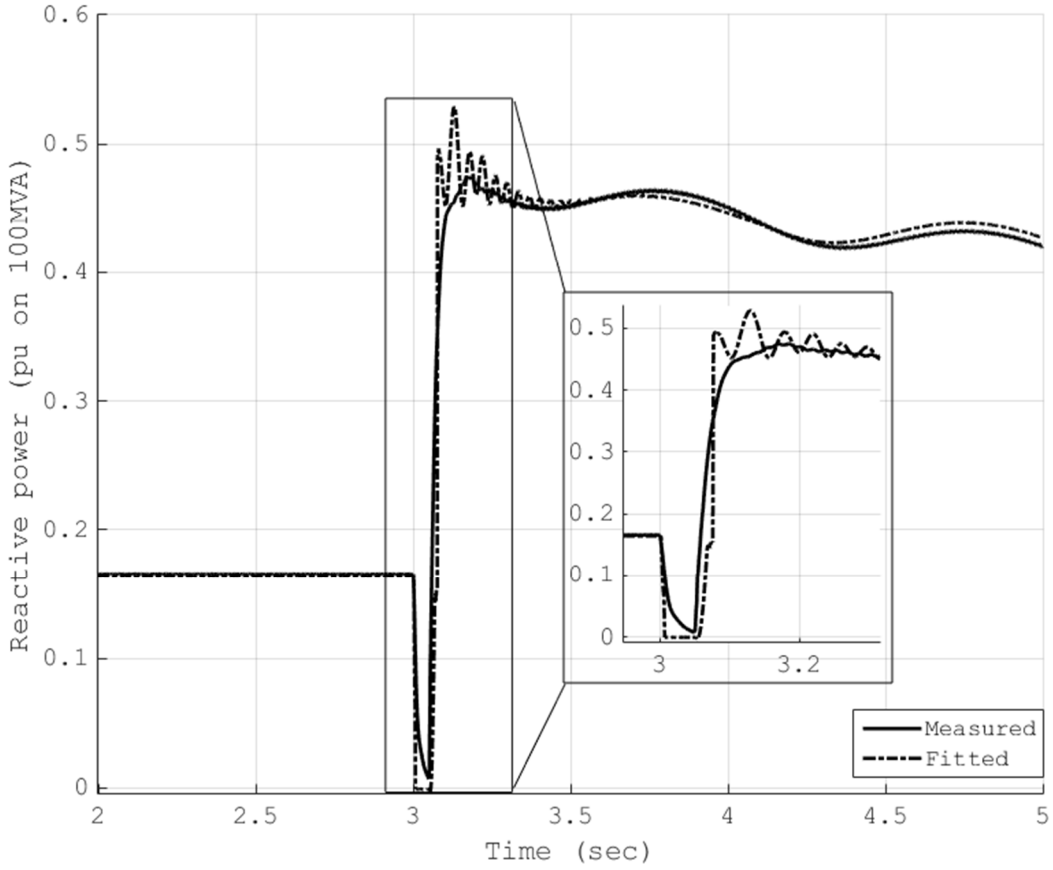

Figure 6.20 Measured and fitted reactive power consumption of the composite load model with reduced parameters

6.4 Summary

A detailed description of the development of a sensitivity based parameter estimation tool was presented in this chapter. Furthermore, the importance of analyzing the parameter sensitivities was demonstrated and the impact of various composite load parameters was discussed. It is shown that examining the sensitivities can help in reducing the model parameters to be estimated by identifying the redundant parameters for a particular set of data measurements. The sensitivities also indicate whether the disturbance recordings

are sufficient to identify the parameters of interest uniquely. In addition, an example of parameter estimation was presented here. The parameters of a positive sequence composite load model were estimated from a surrogate disturbance measurement recorded from an electromagnetic transient simulator.

CHAPTER 7: CONCLUSIONS AND FUTURE WORK: LOAD SENSITIVITY STUDY

7.1 Conclusions

Load modeling is an important aspect of performing time-domain stability studies for transmission system planning and operations. Due to the stochastic nature of the load, one of the key challenges in load modeling is determining the composition and the aggregate model parameters. Sensitivity analysis provides a systematic approach to analyze the effect of load parameter uncertainty on the power system response. In the work presented in this dissertation, TS analysis was used to study the impact of load model parameter uncertainty on the power system response. However, the present day commercial power system simulators do not have the capability to perform TS analysis. To this end, the implementation of TS analysis was presented using an explicit integration method, which is commonly used in all commercial simulators. In addition, a TS analysis was implemented in GE-PSLF using a numerical method. The chapter further discusses some of the drawbacks of using a numerical method for TS analysis when non-smooth load models are used. Chapters 2 to 5 of this dissertation document the work done on the application of TS analysis in load modeling.

Due to the aggregated nature of the load models, parameter estimation is a challenging task in load modeling. Sensitivity analysis can be used to perform load model parameter estimation in a much more efficient and insightful manner. Chapter 6 presents the development of a sensitivity based parameter estimation tool. Furthermore, a discussion on utilizing the sensitivities to identify the suitability of the measurement and parameter

redundancy is presented in chapter 6. The main conclusions of the work presented in chapter 2 to chapter 6 are as follows:

1. A TS based method estimates the change in system response due to a change in a parameter by a linear approximation. Therefore, this method allows a planner to study multiple scenarios with uncertain load parameters without the need of multiple TDS.

2. To evaluate the trajectory sensitivities, a single linear matrix equation needs to be solved in addition to the computation required for the TDS. Furthermore, the factors of the coefficient matrix in the linear matrix equation are obtained as a by-product of the TDS procedure. Hence, the TS based method enables considerable savings in computation time while analyzing the impact of parameter uncertainty.

3. The computation of individual parameter sensitivities are independent from each other and can be done in parallel. Parallel computation of various sensitivities enables further savings in computation time.

4. It was shown that the different parameters in the load model have markedly different effect on the behavior of the system. Parameter sensitivities help the planner/operator to understand the contribution of different parameters to the system response. Parameters like *Vstall* and *Tstall*, which effect the time instant and the duration required for a SPIM to stall, affect the system very differently from parameters like *Rstall*, *Xstall* and *Fmd*.

5. The linear estimates of the actual system variable trajectories were found to be reasonably accurate for small perturbations in parameter size.

6. Although the perturbation size for linear accuracy has been explored for continuous equipment models, the non-smooth behavior of the load models was found to impose additional constraints on the parameter perturbation size.

7. The error introduced due to the non-smooth nature of the load is primarily localized in nature. However, the impact on the trajectory estimation in other parts of the system is dependent on the magnitude of the discrete change caused by the switching event in the non-smooth load model.

8. The computation of the maximum perturbation size considering a switching event can be framed as BVP and can be solved using the shooting method. The formulation of the problem does not require any additional computation. However, the shooting method is an iterative procedure, requiring multiple TDS.

9. The TS analysis can be implemented using an explicit integration routine. However, additional computational effort is required to perform TS analysis and the entries of the linear matrix equation required to compute the sensitivities are not available as a byproduct of the TDS routine.

10. Although additional computation is required, the entire process of estimating the perturbed trajectories using an explicit integration may not require

more computation time as compared to implicit integration based TS analysis. The computation time depends on the problem and the time step of integration used.

11. TS analysis can be implemented using present day commercial power system simulators using a numerical finite differencing method. This can be done irrespective of the integration method employed in the power system simulator as the trajectories are computed numerically. However, the numerical approach is not suitable for computing the maximum perturbation size when non-smooth load models are used.

12. Parameter sensitivities provide useful insight into the measurement based parameter estimation process. An inspection of the Jacobian matrix can reveal whether the measurements made are sufficient to estimate all the parameters of interest. Furthermore, the Jacobian entries convey information as to whether two or more parameters have similar impact on the measurements used for parameter estimation. In this case, it is difficult to identify the parameters uniquely as the estimation problem is ill conditioned.

13. Based on the parameter sensitivities the dimension of the parameter estimation problem can be reduced by fixing the values of some redundant parameters. Sensitivity analysis enables the identification of the redundant parameters for a particular disturbance measurements used.

7.2 Future work

The findings of the study highlight the importance of adopting sensitivity-based techniques in mainstream analysis. In terms of the application of TS analysis in load modeling studies, the future work includes implementation of this module in a commercial power system simulator. An implementation of the TS analysis is shown here using an explicit integration algorithm, which is most commonly used in commercial power system simulators. However, as the formulation of the TDS routines in commercial simulators is different from PSAT, further work is needed for commercialization of the TS module

For sensitivity based parameter estimation, the results presented in this work are based on surrogate measurements made from simulations performed in EMTDC/PSCAD. The next step would be to use actual disturbance recordings for parameter estimation. It was shown that the disturbance measurements might not be sufficient to identify all the parameters of the load model uniquely. The sensitivity-based approach can be utilized to determine the type of disturbance measurements that may be needed to identify all the parameters in the composite load model. Furthermore, if a particular type of disturbance is of interest, the sensitivity-based approach can also be utilized to derive a reduced parameter load model. These areas of parameter estimation can greatly improve load modeling and require further research.

CHAPTER 8: POWER SYSTEM SECURITY ASSESSMENT FOR *N*-1-1 CONTINGENCIES

Power system security is the ability to maintain uninterrupted supply of power from the generation sources to the load centers, especially when subjected to a disturbance [21], [60], [61]. Disturbances could be due to faults in the system resulting in the loss of a line or generator or simply due to scheduled maintenance activities by utilities [61]. Such events, leading to the loss of lines/transformers or generators are termed as contingencies. Power system security assessment deals with examining whether the system is capable of serving the loads after the occurrence of such contingencies.

The September 2011, blackout in San Diego and parts of the southwestern U.S. has highlighted the need to examine *n*-1-1 contingencies in which, the second outage is not related or dependent on the initiating outage [18], [17]. The identification of critical *n*-1-1 contingencies is an important step in the planning process. It helps the utilities to identify and plan for IROLs, which may affect the system operating limits [18]. The work done in this part of the report proposes a systematic approach to *n*-1-1 security assessment considering both steady state as well as the dynamic response of the system. In the following sections, key concepts related to power system security assessment are introduced and the need for a new approach is highlighted.

8.1 Contingency analysis

Contingency analysis serves as a tool to assess, whether a power system can be operated within security limits after the occurrence of planned or unplanned outages [62]. An *n*-1 contingency analysis involves, studying the impact of outage of a single component

on the system voltages and the branch flows [18], [60]. Similarly, an *n-k* contingency analysis involves studying the impact of simultaneous outage of *k* components on the system voltages and the branch flows [18], [60]. For *n*-1-1 contingency analysis, the two contingencies are applied sequentially rather than simultaneously. System adjustments if needed are made after the first outage, prior to applying the second outage [18]. An *n*-1-1 contingency differs from an *n*-2 (*n-k* with $k = 2$) contingency in the manner the two outages are simulated.

8.2 Power system security assessment

Power system security assessment can be broadly classified into two categories, namely static security assessment (SSA) and dynamic security assessment (DSA) [21], [60], [61]. Both the steady state performance and the transient behavior of the system need to be accounted for in determining the system operating thresholds [17].

Static security assessment (SSA) deals with examining whether the post-contingent steady state operating state is acceptable from a power system operations viewpoint [21], [60]. A post-contingent operating state is acceptable when all bus voltages in the system are within an allowable range and all transmission lines and transformers are loaded within their short-term emergency limits. During SSA, it is assumed that the fast acting controls in the system have acted and reached a steady state and the slow acting controls and human actions have not responded yet. Multiple power-flow analyses are performed for different contingencies to compute the post-contingent system voltages and branch flows. The voltages and branch flows are then compared with set thresholds to gauge the severity of the outages.

Dynamic security assessment (DSA) on the other hand deals with examining the transition of the system from the old equilibrium point to the new equilibrium point following the outage [21], [60]. If the transition is stable and the new equilibrium point is acceptable from a system operations viewpoint the contingency is termed secure and otherwise insecure [63]. TDS is the method of choice while performing DSA. The outages are simulated as a disturbance and the evolution of the system variables are recorded to determine whether the system is stable. DSA takes into account the behavior of slow and fast acting controls in the system during a disturbance.

A traditional approach to power system security assessment is to inspect all possible contingencies sequentially, and study their impact on the steady state and transient performance of the system [64].This process entails performing multiple power flows for SSA and multiple TDS for DSA to cover all possible contingencies. However, for any well-designed power system, not all contingencies are harmful. To save computation time, it befits a planner or an operator to inspect a smaller subset of contingencies that are deemed critical from a system security viewpoint [64]. If such a subset is chosen solely based on the operator's or the planner's experience, some critical cases might be omitted in the process. To solve the problem of identifying critical contingencies various contingency screening methods have been reported in literature for both SSA and DSA. The contingency screening methods rely on performing approximate computations to identify the severe contingencies before proceeding to a more detailed evaluation. The following subsections present a review of the contingency screening methods presented in literature for SSA and DSA.

8.2.1 Contingency screening for SSA in power systems

The contingency screening and ranking methods presented in the literature for SSA can be broadly classified under explicit methods and implicit methods. Explicit methods for contingency screening define system-wide performance indices (PIs), which capture the voltage and line flow violations, in the system [64, 67-70]. After the appropriate PIs have been defined, the first order sensitivities of the PIs are computed with respect to parameter changes. For outage studies the power system components are modeled to include parameters, which when changed can simulate the outage of the component. References [67-70] describe different modeling approaches for contingency analysis using explicit methods. The magnitude of the first order PI sensitivities to these parameters, serve as indicators of severity and are used to rank the contingencies. References [64, 67-70], lists the various indices that have been developed to rank contingencies using explicit methods. Once the contingencies are ranked in the order of their severity, the top-ranking contingencies are classified as critical. The main drawback of explicit methods is that the PIs defined are highly nonlinear functions of the system parameters [70]. Screening based on the first order sensitivities around a base case often results in inaccurate assessment of contingencies. Moreover, inclusion of additional nonlinearities like load tap changers, generator reactive power limits and nonlinear load models amplify the error associated with contingency screening and ranking [70].

Implicit methods for contingency screening use network solutions to identify voltage and flow violations [65, 56, 71-75]. In the past, due to computational limitations, these

methods have traditionally relied on approximate or partial post-contingent network solutions to estimate the line flows and the bus voltages. Branch overloads could be typically identified by performing dc power-flow and only solving relevant portions of the network [66, 73]. Single iterations of fast-decoupled power flow have been used to estimate the post-contingent system voltages [73]. It is assumed that the effect of a contingency is localized in nature and hence methods have been proposed to find localized solutions to assess the severity of the contingency [71]. Methods have also been proposed to approximate the widespread effects of contingencies along with the local effects [72, 73]. Such methods use sparsity oriented compensation techniques along with partial re-factorization methods to achieve computational efficiency [75]. Although fast, implicit methods can potentially underestimate the widespread effects of contingencies due to the approximations involved.

8.2.2 Contingency screening for DSA in power systems

It is worthwhile to mention that DSA, as discussed in various literatures, primarily deals with evaluating whether a system is able to maintain stability after large disturbances such as a fault on a line and the corresponding protection system action [76-79]. Although, generator outages are a part of DSA, such outages do not pose any immediate threat to the system from a rotor angle stability point of view. As rotor angle stability is being discussed here, analysis of generator outages have not been pursued in this report.

Various contingency screening methods for DSA have been proposed in literature [77-84]. A coherency-based index for contingency screening is described in reference [79]. References [77-82], describe contingency screening techniques based on the transient energy function. Filtering of contingencies using sparse transient energy function is described

in [80, 81]. Extensions of static security analysis techniques coupled with applications of artificial neural networks have also been explored for contingency screening and ranking [83]. Composite indices based on coherency, transient energy conversion and dot products have been proposed for contingency screening [84]. Most of these screening methods compute the required indices by performing short duration time domain simulations only until a few cycles after the disturbance.

8.3 Need for a new contingency screening and ranking method for *n*-1-1 contingencies

As presented in the preceding section, contingency analysis is a mature field and various screening methods for *n*-1 contingency analysis have been proposed for both SSA and DSA. However, applying these techniques for *n*-1-1 contingencies can be problematic. For SSA, the explicit and the implicit contingency screening methods reported in literature have been verified on smaller test systems for single (*n*-1) branch or generator outages. However, since the described methods rely on first order sensitivities or partial network solutions, they might fail to capture the effect of multiple outages, which can be highly nonlinear [85], [86]. Therefore, these methods cannot be reliably extended to *n*-1-1 contingency analysis [87]. Similarly, for DSA, screening *n*-1-1 contingencies using the traditional screening methods can also be impractical [87]. This is due to the staggering number of short duration TDS that need to be performed [87]. To address the problems with reliability and accuracy, a new approach for *n*-1-1 contingency screening and ranking is needed for both SSA and DSA [87]. To this end, this report proposes

1. A method to screen and rank *n*-1-1 contingencies for static security assessment (SSA), and

2. A method to screen and classify *n*-1-1 contingencies for dynamic security assessment (DSA).

Both the proposed methods are intended to be used during the planning phase by planners or operators. One of the important features of the proposed methods is that these methods can be implanted easily with any existing power system simulator without the need of any additional investment.

8.4 Summary

This chapter presented some of the key concepts of contingency analysis for SSA and DSA. A literature survey of the existing methods of contingency screening and ranking for both SSA and DSA is presented here. In addition, the need for a new approach for *n*-1-1 contingency screening and ranking is highlighted in this chapter.

CHAPTER 9: *N*-1-1 CONTINGENCY SCREENING AND RANKING FOR SSA

The majority of contingency screening and ranking methods rely on linear sensitivities or partial local solutions of the network to gauge the severity of the outage. Chapter 8 provided a review of methods that have been proposed in the literature. However, the effect of severe contingencies on bus voltages and branch flows can be highly nonlinear and hence, approximate methods often fail to assess the criticality of severe contingencies. The approximation errors can be substantial for *n*-*k* (for $k > 1$) or *n*-1-1 contingencies.

With the advancement in computational capabilities in terms of hardware, it is possible to perform complete power-flow solutions in a reasonable time for large power systems. It is therefore convenient to use ac power solutions to develop reliable filters to screen and rank contingencies. Such methods have already been adopted in some commercial power system simulators [22], [23]. This chapter describes an existing *n*-1-1 contingency screening method in a commercial power system simulator and proposes a novel *n*-1-1 contingency screening and ranking methodology based on full ac power-flow solutions. The proposed screening and ranking method is designed such that it can be easily implemented with any commercial power system simulator with relative ease. The commercial power system simulator used for this work is GE-PSLF [22].

9.1 Existing method for *n*-1-1 contingency screening in GE-PSLF

The SSTools module in GE-PSLF has an inbuilt routine to generate a list of screened *n*-1-1 contingencies [22], [88], [89]. This routine creates a list of *n*-1-1 contingencies based on a severity index that is computed from the results of the *n*-1 contingency analysis [88], [89]. A brief description of the method is as follows [88], [89]:

3. Power-flow solutions are performed for all *n*-1 cases. The bus voltages and the branch flows are recorded for every outage at user-specified locations in the system. Locations refer to the specific areas or zones within a power system.
4. The branch flows and the bus voltages for each contingency are compared against the user-defined thresholds. These thresholds could be:
    a. The maximum and minimum allowable voltage levels
    b. The change in voltage from pre-contingent condition
    c. The maximum allowable flow on a branch (line or transformer)
    d. The change in branch flows from pre-contingent condition
    e. A combination of (a) and (b) for bus voltages and (c) and (d) for branch flows
5. The severity index for a contingency is incremented by 1 for each branch flow violation or voltage violation. Depending on the number of violations due to an outage, the severity index of the *n*-1 contingency is computed.
6. Once the severity index for each *n*-1 contingency is computed, all *n*-1 contingencies with severity index greater than a user-defined value are considered for *n*-1-1 analysis. The *n*-1-1 contingency list is created by forming all possible combinations of the screened *n*-1 contingencies.

The above-described method in SSTools seeks to identify *n*-1-1 contingencies based on the assumption that if two contingencies individually cause voltage or branch flow violations, the combination of such contingencies can be critical. All combinations of contingencies, which do not cause voltage or flow violations individually, will be ignored

by this screening process. However, some combinations of innocuous contingencies occurring as an *n*-1-1 contingency can be potentially harmful. Such instances of inadequacy of the existing method were observed while analyzing the WECC. The WECC system has 20605 buses, 17056 lines, 7836 transformers and 2737 generators. An example of such a case for the WECC system is as follows:

Case: The outage of the branches 2320-2319 and 2322-2319

A schematic one-line diagram of the region of interest is shown in Figure 9.1. The two branches to be disconnected are marked with dotted crosses. Table 9.1 lists the voltages at some selected buses in the region for the base case and following the individual outages of the marked branches. From Table 9.1, it can be seen that the individual outages do not have a considerable impact on the bus voltages. However, when these contingencies are considered sequentially, severe undervoltages are observed at those buses. Table 9.2 lists the voltages at the load buses due to the sequential outage of the two branches.

When either the branch 2322-2319 or the branch 2320-2319 is disconnected, the power supply to the load area is simply re-routed through the remaining line in service when the other one is disconnected. However, when both these marked lines are disconnected sequentially, the loads in the region are supplied through the only alternate path 2320-1720-1721. The alternate path, marked by a dotted line in Figure 9.1, has considerably higher impedance. The large voltage drop on the higher impedance path and lack of reactive power resources in the region leads to depressed voltages at the load buses.

This example illustrates that the method of screening contingencies based on the impact of individual contingencies may not be sufficient for screening *n*-1-1contingencies.

The combined effect of the two sequential outages can be catastrophic even though the individual outages may be harmless [87].

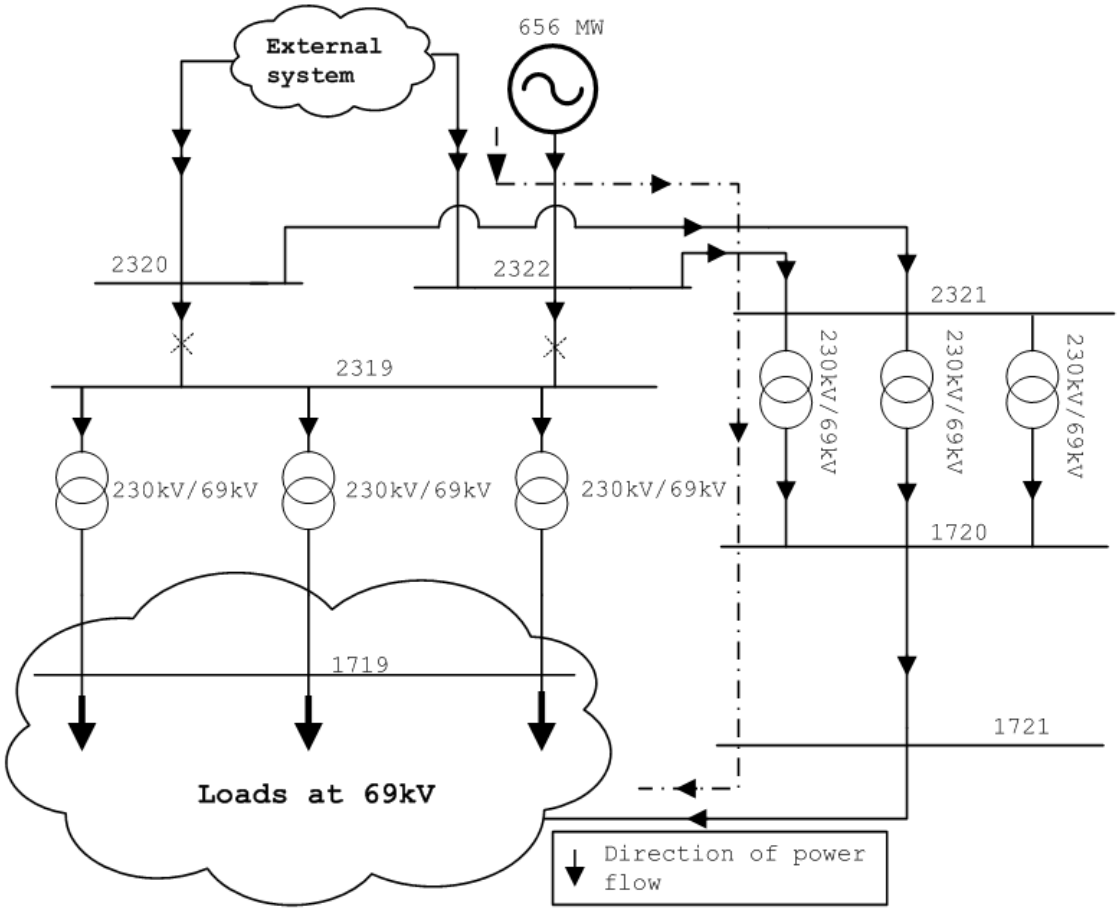

Figure 9.1 Schematic one-line diagram of the load area supplied by branches 2320-2319 and 2322-2319

Table 9.1 Voltage at selected buses in the base case and for the individual outages

Bus no.	Base case voltages (pu)	Voltages after outage of 2322-2319 (pu)	Voltages after outage of 2320-2319 (pu)
2319	1.009	1.007	1.000
1719	1.036	1.034	1.027
1720	1.023	1.021	1.013

1721	1.017	1.015	1.007

Table 9.2 Voltage at selected buses for the sequential outage of the two branches

Bus no.	Voltages after outage of 2322-2319 and 2320-2319 (pu)
2319	0.85
1719	0.86
1720	0.87
1721	0.87

9.2 Contingency screening for *n*-1-1 analysis

In a well-planned interconnected power system, the outage of a single component only affects a few branch flows and generator outputs. The majority of branch flows and generator outputs throughout the system remain practically unchanged. It can be intuitively observed that substantial changes in the branch flows or the generator outputs following an outage indicate that the affected branches and/or generators compensate for the disconnected component. Therefore, to account for the critical *n*-1-1 contingencies, the candidate branches or the generators for the second outage can be screened by analyzing their pre-contingent and post-contingent state (flows for branches and outputs for generators) following the first outage. The following sub-sections describe the methods to generate an *n*-1-1 contingency list for branch-branch, generator-branch, and generator-generator outages with examples and explanations.

9.2.1 Contingency screening for branch-branch outages

To generate a list of *n*-1-1 contingencies involving branch-branch outages, the following steps are followed [87]:

1. Perform a full ac power-flow for all *n*-1 branch contingencies and store all the branch MVA flows.

2. For each branch outage, compute the percentages of MVA flow in the disconnected branch that shows up in all other branches in the system. This percentage is the ac equivalent of the line outage distribution factor (LODF) and will be referred to as *ACLODF* in the rest of this report. As an example, the *ACLODF* in a hypothetical line A for outage of line B is computed as follows:

$$ACLODF_{AB} = \left(\frac{MVA_{n-1,AB} - MVA_{base,A}}{MVA_{base,b}} \right) 100 \ , \qquad (9.1)$$

where,

$ACLODF_{AB}$ is the percentage of MVA flow in line *B* that shows up on line *A*.

$MVA_{n\text{-}1,AB}$ is the MVA flow on line *A* with line *B* disconnected.

$MVA_{base,A}$ is the MVA flow on line *A* in the base case (all lines in service).

$MVA_{base,B}$ is the MVA flow on line *B* in the base case (all lines in service).

3. All branches that have an *ACLODF* more than a set threshold for an *n*-1 contingency are screened as candidate branches for the second outage following that particular *n*-1 contingency.

4. The *n*-1-1 contingency list is updated to include all pairs of the *n*-1 outage and the corresponding screened second outages in step 3. Steps 2 to 4 are performed for all *n*-1 contingencies.

5. For every candidate branch screened in step 3, the MVA flow on that branch due to a combination of any two *n*-1 outage is estimated. The change in flow is linearly approximated by using the already computed *ACLODF*s.
6. The contingency list is updated to include any combination of two *n*-1 contingencies, which may cause the estimated flow on a screened branch computed in step 5, to be above a set percentage of the emergency rating of the branch.
7. Finally, all duplicate *n*-1-1 contingencies are removed from the list and the final list of *n*-1-1 contingency is printed out in GE-PSLF SSTools format.

An example is provided here to illustrate steps 3 to 6. It should be noted that the example is intended to highlight the screening process once an *n*-1 analysis is completed. It is purely demonstrative and numbers quoted are for the sake of illustration. Consider a power system example with lines designated as 'line 1', 'line 2', 'line 3' and so forth. Figure 9.2 shows the list of screened branches due to some *n*-1 branch outages. The *ACLODF* of each branch due to the corresponding *n*-1 branch outage is listed on top of the branch name. It can be seen that the list contains branches with *ACLODF* more than 10 percent. The threshold for screening mentioned in step 3 is set to be 10 percent in this example. The intermediate *n*-1-1 contingency list formed in step 4 is shown in Figure 9.3.

It is assumed that for line 3 in Figure 9.2 the sum total of the base flow and the change in MVA flow due to the outages of line 1 (10.2 percent) line 4 (11.5 percent) is more than 80 percent of its emergency rating. Hence, as indicated in step 6 the combination

of outage of line 1 and line 4 is added to the list. Figure 9.4 shows the updated *n*-1-1 contingency list.

After all the contingencies are added to the list, the duplicate *n*-1-1 contingencies are removed and the final list of contingencies is created. Figure 9.5 shows the final list of *n*-1-1 contingencies with the duplicate contingencies removed. The duplicate entries are outlined and the removed entries are marked with a cross sign beside them.

Branch outage	Branches screened for second outage		
line 1	50.00% line 2	22.00% line 8	10.20% line 3
line 2	47.20% line 1	14.00% line 8	
line 3	60.00% line 9	15.18% line 4	
line 4	11.50% line 3		
line 5	No lines with ACLODF > 10%		
...	...		

Figure 9.2 List of screened branches due to *n*-1 branch outages (step 3)

Intermediate *n*-1-1 contingency list	
first outage	**Second outage**
line 1	line 2
line 1	line 8
line 1	line 3
line 2	line 1
line 2	line 3
line 3	line 9
line 3	line 4
line 4	line 3
...	...

Figure 9.3 Intermediate *n*-1-1 contingency list (step 4)

Updated *n*-1-1 contingency list		
first outage	**Second outage**	
line 1	line 2	
line 1	line 8	
line 1	line 3	
line 1	**line 4**	**Added in step 6**
line 2	line 1	
line 2	line 3	
line 3	line 9	
line 3	line 4	
line 4	line 3	
...	...	

Figure 9.4 Updated *n*-1-1 contingency list (step 6)

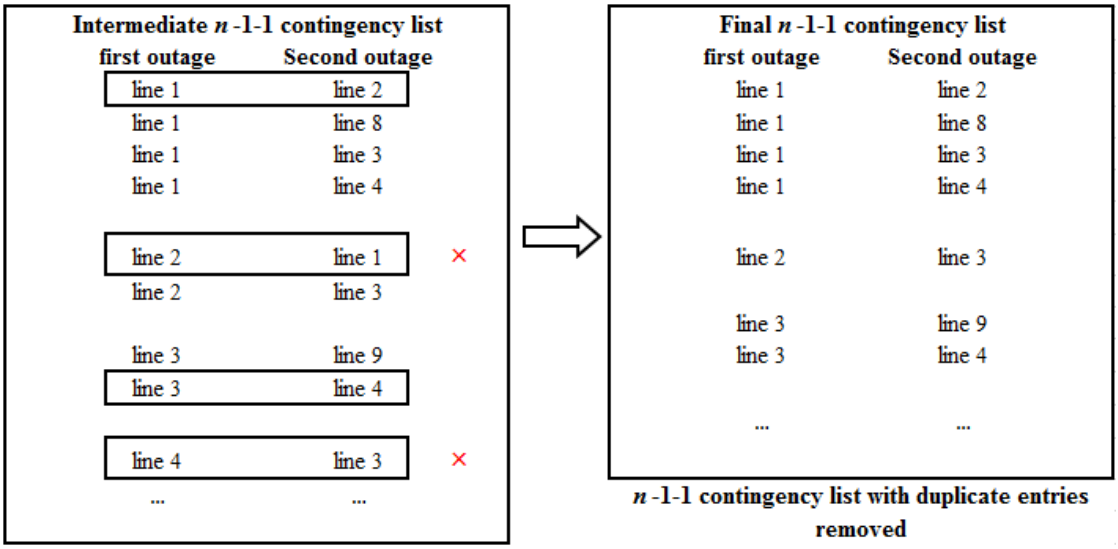

Figure 9.5 Final *n*-1-1 contingency list with duplicate entries deleted (step 7)

9.2.2 Contingency screening for generator-branch outage

To generate a list of *n*-1-1 contingencies involving generator-branch outages, the following steps are followed.

1. A generator is disconnected from the system and the system is re-dispatched based on an operator specified schedule. A power-flow is performed on the re-dispatched system.
2. The branch flows are recorded and the percentage change in MVA flow is computed for all branches in the systems.
3. All branches with a percentage change in MVA flow more than a set thresh-old, are screened as candidate branches for the second outage.

4. The *n*-1-1 contingency list is updated to include all pairs of the *n*-1 generator outage and the corresponding screened second outages in step 3. Steps 2 to 4 are performed for all *n*-1 contingencies.

5. The contingency list is updated to include any combination of two *n*-1 generation outage, which may cause the estimated flow on a screened branch computed in step 5, to be above a set percentage of the emergency rating of the branch.

It should be noted that contingencies added in step 5 are essentially generator-generator contingencies. These contingencies could be omitted from here and later added to the list of generator-generator contingencies. However, these contingencies, if any, were added to the generator-branch contingency list for the purpose of this study. If any such *n*-1-1 contingency re-appeared in the generator-generator contingency list, they were subsequently removed.

To illustrate the steps 3 to 5, consider the power system example of section 9.2.1. The generators are numbered 'gen 1', 'gen 2', 'gen 3' and so forth. Figure 9.6 shows the screened branches due to some *n*-1 generation outages. The percentage change in MVA flow on a branch due to the corresponding *n*-1 generation outage is listed on top of the branch name. It can be seen that the list contains branches with a percentage change in MVA flow more than 10 percent. The threshold mentioned in step 3 is set at 10 percent for this example. The intermediate *n*-1-1 contingency list formed in step 4 is shown in Figure 9.7.

It is assumed that for line 5 in Figure 9.6 the sum total of the base flow and the change in MVA flow due to the outages of gen 2 (28.5 percent) gen 4 (11.5 percent) is more than 80 percent of its emergency rating. Hence, as indicated in step 5 the combination of outage of gen 2 and gen 4 is added to the list. Figure 9.8 shows the final *n*-1-1 contingency list with the updated entries.

Generator outage	**Branches screened for second outage**
gen 1	28.50% line 9 22.00% line 8 10.20% line 6
gen 2	28.50% line 5 14.00% line 2
gen 3	23.80% line 9 15.18% line 4
gen 4	11.50% line 5 13.70% line 6
gen 5	No lines with percentage change in MVA flow > 10%
...	...

Figure 9.6 List of screened branches due to *n*-1 generator outage (step 3)

Intermediate *n*-1-1 contingency list	
first outage	**Second outage**
gen 1	line 9
gen 1	line 8
gen 1	line 6
gen 2	line 5
gen 2	line 2
gen 3	line 9
gen 3	line 4
gen 4	line 5
gen 4	line 6
...	...

Figure 9.7 Intermediate *n*-1-1 contingency list (step 4)

Final *n*-1-1 contingency list		
first outage	**Second outage**	
gen 1	line 9	
gen 1	line 8	
gen 1	line 6	
gen 2	line 1	
gen 2	line 3	
gen 2	**gen 4**	**Added in step 5**
gen 3	line 9	
gen 3	line 4	
gen 4	line 5	
gen 4	line 6	
...	...	

Figure 9.8 Final *n*-1-1 contingency list (step 5)

9.2.3 Contingency screening for generator-generator outage

To generate a list of *n*-1-1 contingencies involving a generator-generator outage, the following steps are followed.

1. A generator is disconnected from the system and the system is re-dispatched based on an operator specified schedule. A power-flow is performed on the re-dispatched system.
2. From the power-flow solution of the *n*-1 analysis, the reactive power generation of each generator is recorded.
3. The generators, which have a reactive power increase of more than a set threshold, are screened as candidate generators for the second outage.
4. Generators, which are on their upper or lower reactive power limits following the *n*-1 generator outage and re-dispatch are also screened as candidate generators for second outage
5. The *n*-1-1 contingency list is updated to include all pairs of the *n*-1 generator outage and the corresponding screened second outages in step 3. Step 2 to step 4 is performed for all *n*-1 contingencies.
6. The duplicate contingencies are removed after the list is formed.

To illustrate steps 3 to 5, consider the power system example of Section 9.2.1. Figure 9.9 shows the screened generators due to some *n*-1 generator outages. The percentage change in reactive power output is listed on the top of the generator names. The threshold mentioned in step 3 is set at 10 percent for this example. Hence, generators with a change

in reactive power output of more than 10 percent are screened as candidate generators for a second outage. Figure 9.9 also lists the generators that are at their maximum and minimum reactive power limits.

Figure 9.10 shows the intermediate *n*-1-1 contingency list and Figure 9.11 shows the final *n*-1-1 contingency list with duplicate entries removed. The duplicate entries are outlined and the removed entries are marked with a cross beside them.

Generator outage	Branches screened for second outage		
	Change in reactive power output > 10%	Generators on Qmax	Generators on Qmin
gen 1	11.30% gen 4 10.10% gen 2	gen 5, gen 3	
gen 2	10.05% gen 1	gen 5	
gen 3	No generators with change in reactive power > 10%		
gen 4	12.20% gen 1	gen 3	
gen 5	No generators with change in reactive power > 10%		
...	...	...	...

Figure 9.9 List of screened generators due to *n*-1 generator outage (step 3)

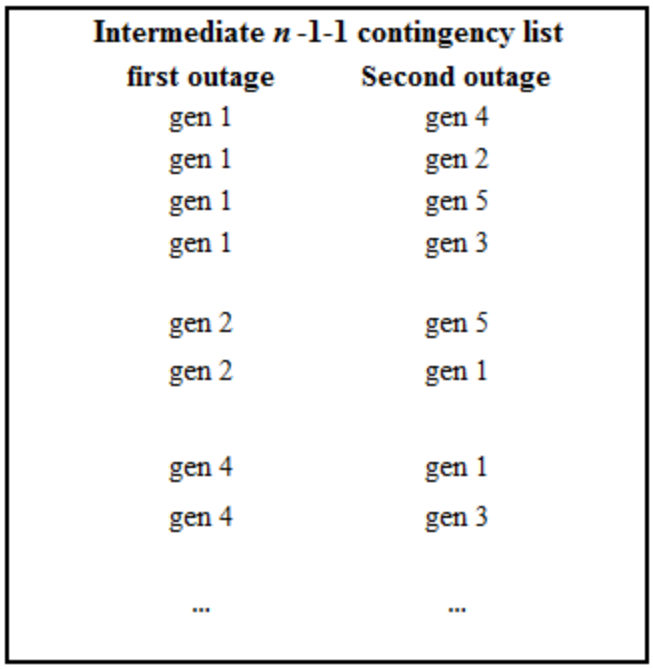

Figure 9.10 Intermediate *n*-1-1 contingency list (step 5)

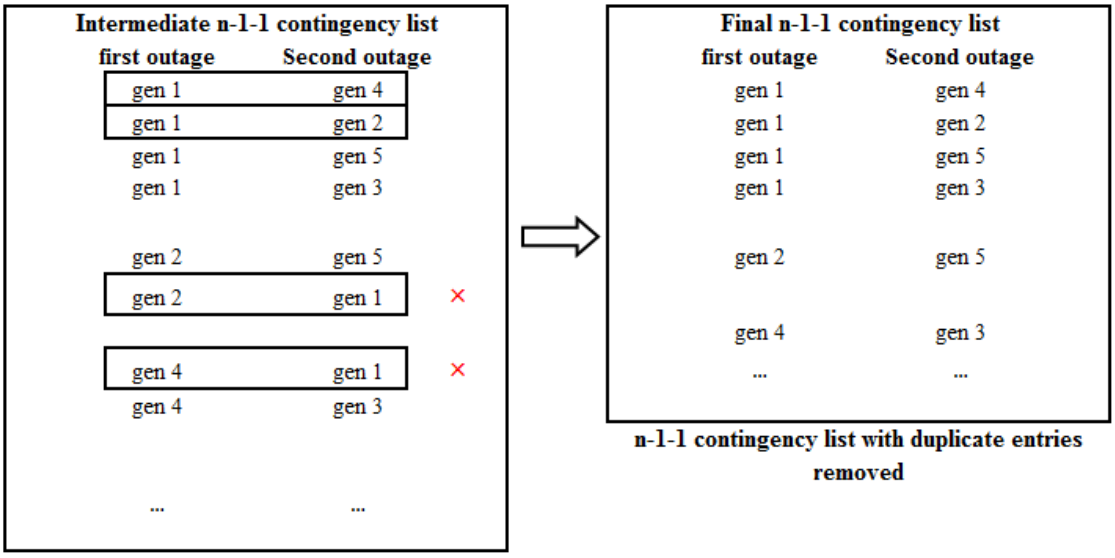

Figure 9.11 Final *n*-1-1 contingency list with duplicate entries deleted (step 6)

9.3 Justification for the contingency screening method

The contingency screening method proposed in the previous section is expected to screen possibly critical second outages following an *n*-1 outage. The screened *n*-1-1 outages may cause voltage or branch flow violations in the system. This section provides an explanation of how the screening method identifies *n*-1-1 contingencies that might be critical from a system operation point of view.

For branch-branch outages, if the outage of a single branch causes the *ACLODF* for another branch to be significantly high, it indicates that this second branch is an important supply route to the same load area. An outage of a branch with a high *ACLODF* can lead to considerable weakening of the transmission path to a load area. The alternate supply route to the load may have substantially higher impedance. This can lead to large voltage drops and possible reactive power problems at the load buses. Close to large generation sources, disconnecting a branch with high *ACLODF* can cause significant reduction in the short circuit ratio, leading to stability issues. Hence, the outage of such a branch may be critical following the corresponding *n*-1 branch outage. Furthermore, if two separate *n*-1 branch outages cause the estimated MVA flow on a branch or branches to increase beyond its emergency rating, the sequential combination of the two *n*-1 outages can also be critical. This is particularly significant in identifying *n*-1-1 contingencies that resulted in overloading of transformers and lines, which were operating near their emergency ratings in the base case. Steps 3 to 6 in the algorithm presented in section 9.2.1 screen *n*-1-1 branch-branch outages based on these ideas.

For generator-branch outages, if the outage of a generator causes a significant increase in MVA flow on a branch, it indicates that a part of the lost reactive power in the area is being imported through this branch. Outage of such a branch may cause voltage violations in the load areas. Hence, the outage of such a branch may be critical following the corresponding *n*-1 generator outage. Furthermore, if two separate *n*-1 generator outages cause the estimated MVA flow on a branch or branches to increase beyond its emergency rating, the sequential combination of the two *n*-1 outages can also be critical. Steps 3 to 5 in the algorithm presented in section 9.2.2 screens *n*-1-1 generator-branch outages based on these ideas.

For generator-generator outages, if the outage of a generator causes the reactive power output of another generator to increase significantly, it indicates that a part of lost reactive power is being supplied by this generator. Outage of such a generator may cause voltage violations due to reactive power shortage. Hence, the outage of such a generator may be critical following the corresponding *n*-1 generator outage. Furthermore, all generators that reach their reactive power limits following the outage of a generator are also included for *n*-1-1 screening. Since these generators are at their reactive power limits disconnecting these generators from the system can lead to voltage violations at their regulated buses. Steps 3 to 5 in the algorithm presented in section 9.2.3 screens *n*-1-1 generator-generator outages based on these ideas.

9.4 Ranking of screened *n*-1-1contingencies based on severity

Ranking contingencies based on their severity enables a planner or an operator to identify the most critical elements in a power system. Additional measures can then be

taken for hardening such elements to prevent future outages. Various indices have been proposed to rank contingencies based on the severity of their impact on the system voltages and the branch flows [64], [66], [70]. For the analysis presented in this report, performance indices as defined in reference [64] are used. The voltage-based index and the flow-based index are defined as follows:

Voltage based index

The voltage-based index ranks the contingencies based on the magnitude of the voltage violations and the number of buses in the system where such violations occur [64]. The voltage-based index is defined by:

$$PI_V = \sum_{i=1}^{nb} \frac{w_{bi}}{2\alpha} \left(\frac{|V_i| - |V_i^{sp}|}{\Delta V_i^{\lim}} \right)^{2\alpha} \tag{9.2}$$

where,

PI_V is the voltage-based index

nb is the total number of monitored buses in the system

V_i is the post-contingency voltage at a bus i

V_i^{sp} is the nominal voltage at a bus i

ΔV_i^{lim} is the maximum voltage change limit (normally 10 percent)

α is a factor that is usually chosen 1

w_{bi} is a weighting factor

Flow based index

The flow-based index ranks the contingencies based on the magnitude of the flow violations and the number of branches in the system where such violations occur [64]. The flow-based index is defined by:

$$PI_{MVA} = \sum_{i=1}^{nl} \frac{w_{li}}{2\alpha} \left(\frac{S_i}{S_i^{\lim}} \right)^{2\alpha} \tag{9.3}$$

where,

PI_{MVA} is the flow-based index

nl is the total number of monitored branches in the system

S_i is the post-contingency flow in branch i

S_i^{lim} is the short term emergency rating of branch i

α is a factor that is usually chosen 1

w_{li} is a weighting factor

The factor α used for ranking is usually assigned a value of 1 for both the voltage-based and the flow-based index [64]. Due to the particular choice of this factor the indices varies as a quadratic function of the voltage or flow violations.

The weighting factor w_{bi} and w_{li} in (9.2) and (9.3) respectively, are usually chosen by an operator or a planner to assign higher weights to the critical buses or the critical lines in the system. For example, if a particular line is important in a system and the overloading of this line cannot be tolerated, the planner can assign a higher weight w_{li} to that particular line. If a contingency leads to overloading of this important line, the corresponding contingency will have a higher value of the flow-based ranking index. Similarly, higher values of w_{bi} can be assigned to critical buses in the system, such that voltage violations at those

buses can be weighed more during the ranking process. After the indices are computed, the contingencies are then ranked based on the magnitude of the computed indices.

9.5 The *n*-1-1 contingency screening and the ranking process

The screening and the ranking methods described in the foregoing sections are combined for the complete *n*-1-1 contingency analysis process. Figure 9.12 provides a flow chart of the complete *n*-1-1 contingency analysis method.

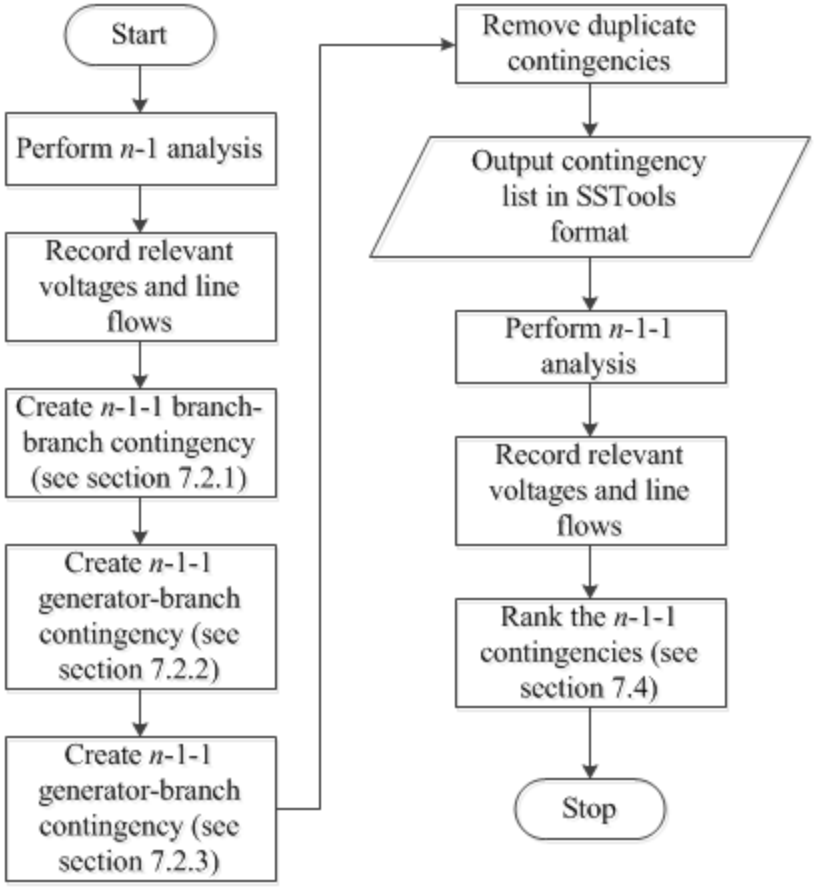

Figure 9.12 Flowchart of the *n*-1-1 contingency screening and ranking process

9.6 Summary

This chapter described the proposed contingency screening and ranking method for *n*-1-1 contingency analysis. The proposed method systematically screens the critical *n*-1-1 contingencies thus reducing the number of *n*-1-1 contingencies to be processed. Once an ac power-flow is performed for the screened *n*-1-1 contingencies, the contingencies can then be ranked by the voltage-based and the flow-based index. In addition to the detailed description of the screening and ranking methods, a flow chart for the complete *n*-1-1 contingency analysis process is provided in this chapter.

CHAPTER 10: *N*-1-1 CONTINGENCY ANALYSIS FOR SSA: APPLICATION TO A REAL SYSTEM

In chapter 9, a method for screening and ranking *n*-1-1 contingencies was proposed. In this chapter, the proposed method is used to screen critical *n*-1-1 contingencies and rank them for a real large power system. In the following sections, a brief description of the power system used for this study is provided. The various thresholds used in the screening and ranking process are defined and the results of the contingency analysis are presented here. Furthermore, the accuracy of the proposed screening method is tested by performing an exhaustive *n*-1-1 contingency analysis. The results of the comparative study are also presented in this chapter.

10.1 System description

The proposed contingency screening and ranking method was used to perform *n*-1-1contingency analysis for a selected utility within the WECC system. All voltage levels of 100 kV and above in the selected utility's service area was considered for the contingency analysis. A power flow file representing the entire WECC system, with detailed description of the selected utility's service area was used for the study. Table 10.1 lists the key features of the WECC system and the selected utility.

Table 10.1 Key features of the WECC system and the selected utility's service area

Description	WECC system	Selected utility (100 kV and above)
Buses	20605	291
Lines	17056	328
Transformers	7836	380
Generators	2737	197

10.2 *n*-1 contingency analysis using GE-PSLF SSTools

GE-PSLF was used to perform the *n*-1 contingency analysis. The SSTools module of GE-PSLF was used to generate the *n*-1 contingency list and subsequently perform the ac power flow analysis. The SSTools module generates a list of contingencies based on the user specified areas/zones and voltage levels within those areas/zones. The contingency list is exhaustive and consists of all credible contingencies in the specified region. Once a contingency list is generated, a monitoring file is prepared by the user. A monitoring file specifies the areas/zones and voltage levels within those area/zones, which shall be monitored to study the impact of the simulated outages. SSTools performs multiple ac power flow runs for all contingencies and reports the voltages and branch flows in the monitored portion of the system for further analysis.

10.3 *n*-1 contingency analysis results

The bus voltage and branch flow thresholds used for *n*-1 contingency analysis is listed in Table 10.2. If the bus voltage magnitudes or branch flows violate the thresholds listed in Table 10.2 for any *n*-1 contingency, the *n*-1 contingency is categorized as critical.

Table 10.3 lists the voltage levels that are monitored for contingency analysis. While performing ac power flow for contingency analysis, the following control actions were enabled:

1. The load tap changers were set to adjust taps to regulate voltages.
2. The phase shifters were set to adjust phase angles to control the flow.
3. The static VAr devices were set to regulate voltages based on their control types.
4. The area interchange was set to maintain the inter-area flows to the scheduled value.

Table 10.4 summarizes the *n*-1 contingency analysis results for the branch outages obtained from SSTools. For the generator outage contingencies, the system was re-dispatched according to a schedule provided by the utility. Table 10.6 summarizes the *n*-1contingency analysis results for the generation outages obtained from SSTools. From Table 10.5 and Table 10.6, it can be seen that 5 contingencies lead to voltage violations, 1 contingency lead to a flow violation and for 1 contingency the power flow failed to solve. The voltage and flow violations were observed in the system due to

1. Overvoltages at buses resulting from capacitive compensation from lightly loaded lines
2. Overvoltages at buses resulting from the capacitive compensation from fixed shunt devices
3. Existing undervoltage at buses in the base case

4. Overloading of parallel-connected transformer, when one of them is disconnected

The divergence of power flow can either be due to abnormal voltages in the system, or due to unwanted operation of voltage and power flow control devices like under load tap changers (ULTC), switchable reactor or capacitor banks and phase adjusters. Deadbands in discrete control devices can cause oscillations in the solution process without convergence. Therefore, it is important to analyze the cases where the power flow solution diverges or oscillates without reaching a solution. A method to analyze these cases is presented in a later section. In this particular case, the power flow solution diverges due to severely depressed voltage in a load pocket close to the disconnected branch.

Table 10.2 Bus voltage and branch flow threshold for *n*-1 contingency analysis

Voltage and flow threshold for *n*-1 contingency ranking	
Lower voltage threshold	0.95 pu
Upper voltage threshold	1.05 pu
Line flow threshold	Short term emergency rating (rating 2 in GE-PSLF)

Table 10.3 Voltage and generation level selected for monitoring bus voltages and branch flows and generator output

	Voltage and generation level monitored for contingency screening
Voltage	100kV - 500kV
Branch flows	100kV - 500kV
Generation	All generators with output more than 50 MW

Table 10.4 Summary of *n*-1 contingency analysis results for branch outages

***n*-1 branch contingencies (transformer and lines)**		
Number of *n*-1 contingencies (created by GE-PSLF)		403
Number of contingencies causing voltage violations	over-voltages (> 1.08 pu)	4
	under-voltages (< 0.95 pu)	1
Number of contingencies causing flow violations		1
Number of contingencies where power flow solution diverges		1
Number of contingencies where power flow solution oscillates and fails to converge		0

Table 10.5 Summary of n-1 contingency analysis results for generator outages

***n*-1 generation contingencies (SRP re-dispatch schedule)**		
Number of n-1 contingencies (created by GE-PSLF)		24
Number of contingencies causing voltage violations	over-voltages (> 1.08 pu)	0
	under-voltages (< 0.95 pu)	0
Number of contingencies causing flow violations		0
Number of contingencies where power flow solution diverges		
Number of contingencies where power flow solution oscillates and fails to converge		0

10.4 Parameters used in the *n*-1-1 contingency screening and ranking process

The screening process involves filtering candidate branches or generators for the second outage, based on the change in branch flow or reactive power output of a generator,

following the first outage. The screening criteria are unique for each type of *n*-1-1 contingency (branch-branch, generator-branch or generator-generator) and are described in later sections separately. The ranking process is same for all *n*-1-1 contingency types. The voltage thresholds, the flow thresholds and the weighting factors used for the ranking process are described in this section.

Table 10.6 lists the voltage and the flow thresholds used for the *n*-1-1 contingency analysis. If the bus voltages or the branch flows violate the thresholds listed in Table 10.6 for any *n*-1-1 contingency, the *n*-1-1 contingency is categorized as critical. Based on the thresholds given in Table 10.6, the weights w_{bi} and w_{li} of (9.2) and (9.3) are chosen. Table 10.7 lists the values of the weights w_{bi} and w_{li} used for ranking the *n*-1-1 contingencies. The weights are chosen in such a way that non-zero performance indices be assigned to only those *n*-1-1 contingencies, which cause violations in the system.

Table 10.6 Bus voltage and branch flow thresholds for *n*-1-1 contingency analysis

Voltage and flow thresholds for *n*-1-1 contingency ranking	
Lower voltage threshold	0.90 pu
Upper voltage threshold	1.08 pu
Line flow threshold	Short term emergency rating (rating 2 in PSLF)

Table 10.7 Choice of weights w_{bi} and w_{li} for n-1 contingency analysis

Weights for voltage based ranking	
Bus voltage limit	**Value of w_{bi}**
Between 0.9 pu and 1.08 pu	0
Greater than 1.08 pu or less than 0.9 pu	10
Weights for flow based ranking	
Branch flow limit	**Value of w_{li}**
Flow less than rating 2	0
Flow greater than rating 2	10

10.5 n-1-1 contingency analysis results

The n-1-1 contingency screening and ranking process described in sections 9.2, 9.4 and 9.5 was used to perform an n-1-1 contingency analysis for the selected utility. The branch MVA flows recorded during the n-1 contingency analysis were used to screen the candidate branches and generators for performing n-1-1 contingency analysis. The results of the n-1-1 contingency analysis are presented in the following subsections.

10.5.1 Branch-branch n-1-1 contingencies

The n-1-1 branch-branch contingencies were screened according to the steps described in section 9.2.1. The following two criteria were used to generate the screened n-1-1 contingency list:

1. All combinations of the first branch with any branch that has an *ACLODF* more than 5% due to outage of the first branch
2. All combinations of two branch outages, which causes the estimated flow on any branch to exceed 80% of its emergency rating

Table 10.8 summarizes the *n*-1-1 contingency screening results for the branch-branch outages. An ac power flow is performed for each screened *n*-1-1 contingency and the relevant voltages and flows are recorded for ranking the contingencies based on their severity. The SSTools module of GE-PSLF was used for processing the contingencies and recording the bus voltages and the branch flows in the monitored portion of the system.

Table 10.9 lists the three most severe *n*-1-1 contingencies, ranked based on their impact on the monitored system voltages. Table 10.10 lists the three most severe *n*-1-1 contingencies, ranked based on its impact on the monitored branch flows.

Table 10.8 Summary of the *n*-1-1 contingency screening results for the branch-branch outages

***n*-1-1 contingency branch-branch contingency screening**	
Number of *n*-1 contingencies (created by SSTools)	403
Number of *n*-1-1contingencies (screened)	**5549**
Number of *n*-1-1contingencies with voltage violations	3109
Number of *n*-1-1contingencies with flow violations	90
Number of screened *n*-1-1 contingencies where power flow solution diverges	17
Number of screened *n*-1-1 contingencies where power flow solution oscillates and fails to converge	0

Table 10.9 Three most severe contingencies ranked by the voltage-based index

Rank	*n*-1-1 Contingency	PI_V
1	1126-1145 and 1150-1133	990.8
2	1125-1175 and 1176-1114	599.1
3	1119-1145 and 1150-1133	588.9

Table 10.10 Three most severe contingencies ranked by the flow-based index

Rank	*n*-1-1 Contingency	PI_{MVA}
1	1315-1211 and 1198-1365	28.93
2	1314-1201 and 1217-1341	20.48
3	1119-1145 and 1150-1133	14.91

10.5.2 Generator-branch *n*-1-1 contingencies

The *n*-1-1 generator-branch contingencies were screened according to the steps described in section 9.2.2. The following two criteria were used to generate the screened *n*-1-1 contingency list to be used in SSTools.

1. The size of a generator has to be more than 50 MW to be considered for outage.
2. All combinations of a generator with any branch that has an increase in MVA flow more than 5% due to the first generator outage.

3. All combinations of two generators, which causes the estimated MVA flow on any branch to exceed 80% of its emergency rating

Table 10.11 summarizes the *n*-1-1 contingency analysis results for the generator-branch outages. A re-dispatch based on the generation re-dispatch schedule provided by the utility is performed after the first generator outage before the second branch outage. An ac power flow is performed for each screened *n*-1-1 contingency and the relevant voltages and flows are recorded. The SSTools module of GE-PSLF was used for processing the contingencies and recording the bus voltages and the branch flows in the monitored portion of the system.

From Table 10.11 it can be seen that five cases of *n*-1-1 generator-branch contingencies were reported to have voltage violations and one case had flow violation. However, these are the same violations reported during the *n*-1 branch contingency analysis. No new violations were observed due to the additional outage. Since no contingency was identified as critical, the contingency ranking process can be omitted for the *n*-1-1 generator-branch contingencies.

Table 10.11 Summary of the n-1-1 contingency screening results for the generator-branch outages

***n*-1-1 contingency generator-branch contingency screening**	
Number of *n*-1 contingencies (created by SSTools)	24
Number of *n*-1-1contingencies (screened)	474
Number of *n*-1-1contingencies with voltage violations	5*
Number of *n*-1-1contingencies with flow violations	1
Number of screened *n*-1-1 contingencies where power flow solution diverges	0
Number of screened *n*-1-1 contingencies where power flow solution oscillates and fails to converge	0

*Same as reported in the *n*-1 analysis (see Table 8.6). No new violations were reported during *n*-1-1 analysis.

10.5.3 Generator-generator n-1-1 contingencies

The *n*-1-1 generator-generator contingencies were screened according to the steps described in section 10.2.3. The following two criteria were used to generate the screened *n*-1-1 contingency list to be used in SSTools.

1. The size of a generator has to be more than 50 MW to be considered for outage.
2. All combinations of a generator with any generator that has a change in reactive power output of more than 5% due to the first generator outage
3. All combinations of a generator with any generator that is at its minimum or maximum reactive power limit

Table 10.12 shows the summary of the *n*-1-1 contingency analysis results for generator-generator outages. A re-dispatch based on the generation re-dispatch schedule provided by the utility is performed after the first generator outage before disconnecting the second generator. An inertial re-dispatch is performed after the second generator is disconnected. An ac power flow is performed for each screened *n*-1-1 contingency and the relevant voltages and flows are recorded. The SSTools module of GE-PSLF was used for processing the contingencies and recording the bus voltages and the branch flows in the monitored portion of the system.

From Table 10.12 it can be seen no voltage or flow violations were reported. Since no contingency was identified as critical, the contingency ranking process can be omitted for the *n*-1-1 generator-generator contingencies.

Table 10.12 Summary of the *n*-1-1 contingency screening results for the generator-generator outages

***n*-1-1 generation contingencies (generator and generator)**		
Number of *n*-1-1 contingencies (screened)		249
Number of contingencies causing voltage violations	over-voltages (> 1.08 pu)	0
	under-voltages (< 0.95 pu)	0
Number of contingencies causing flow violations		0
Number of screened *n*-1-1 contingencies where power flow solution diverges		0
Number of screened *n*-1-1 contingencies where power flow solution oscillates and fails to converge		0

10.6 Analysis of contingencies where power flow fails to solve

As discussed earlier, the contingency cases where an ac power flow fails to solve need to be analyzed further. Since a power flow solution cannot be obtained, the type of problem caused in the system by these contingencies cannot be determined with certainty. Therefore, a different approach needs to be undertaken to ascertain the type of problem that is caused due to these contingencies. Cases where an ac power flow fails to solve are not very commonly encountered in *n*-1 contingency analysis. This is evident from the *n*-1 contingency analysis results listed in Table 10.5 and Table 10.6. Out of the 403 possible *n*-1 contingencies, only 1 case leads to the divergence of the power flow solution. However, for *n*-1-1 contingencies, 17 cases were observed where the power flow solution diverges. This is because *n*-1-1 contingencies result in the loss of two system components, which is more severe compared to *n*-1 outages. These contingencies can be examined by performing a dynamic study, which simulates the opening of the second line. Such a time domain simulation can be performed as follows:

1. A power-flow is solved for the first outage. The power-flow solution is taken as the initial condition for the time domain simulation.
2. A time domain simulation is run and the second branch is opened at time instant t=1 sec.

As mentioned in section 10.3, in the *n*-1 contingency analysis results, the power flow failed to solve due to severely depressed voltages in a load area close to the disconnected branch. For the *n*-1-1 contingency cases, power flows failed to solve either due to depressed voltages in load areas or due to instability. Two *n*-1-1 contingencies cases lead

to instability, while the 15 remaining contingencies led to undervoltages at different load areas in the system. Two such representative cases from the *n*-1-1 contingency analysis results are discussed here.

Case a (instability): Outage of branches 1608-1701 and 1608-1509

A schematic one-line diagram of the area of interest is shown in Figure 10.1. 1905 MW active power is injected by the generation units at bus 1800. The disconnected branches 1608-1701 and 1608-1509 are marked with dotted cross. When these two branches are opened, the power injected at bus 1800 is exported through the path 1800-1823. The impedance of the path through the branch 1800-1823 is significantly high. The high impedance of the connecting path combined with the large power injection results in a low short circuit ratio at the bus 1800. Hence, opening the two lines causes the units connected at bus 1800 to go unstable. Figure 10.2 shows the relative rotor angles of selected generators in the region, when the branches are disconnected. From Figure 10.2, it can be seen that the rotor angles of the units connected at 1800 (CT1, CT2, CT3) units drift away after the lines are opened. Generators GT1 and GT2 in Figure 10.2 are two large generators in the concerned utility's service area. Angle instability was typically observed in the system, when the two main power exporting branches close to large generation units were disconnected.

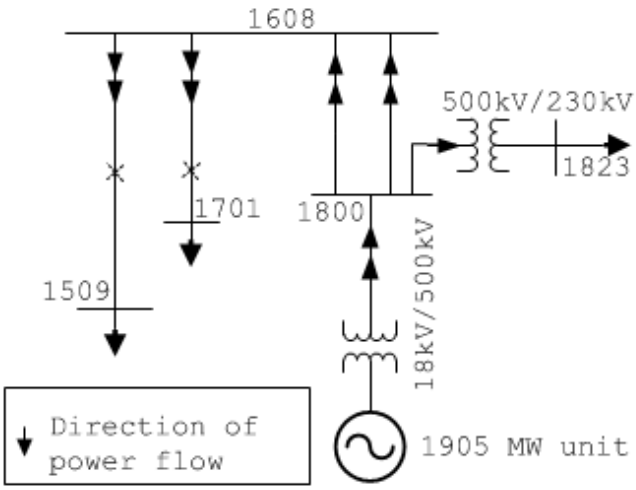

Figure 10.1 Schematic one-line diagram of the area near 1608-1701 and 1608-1509

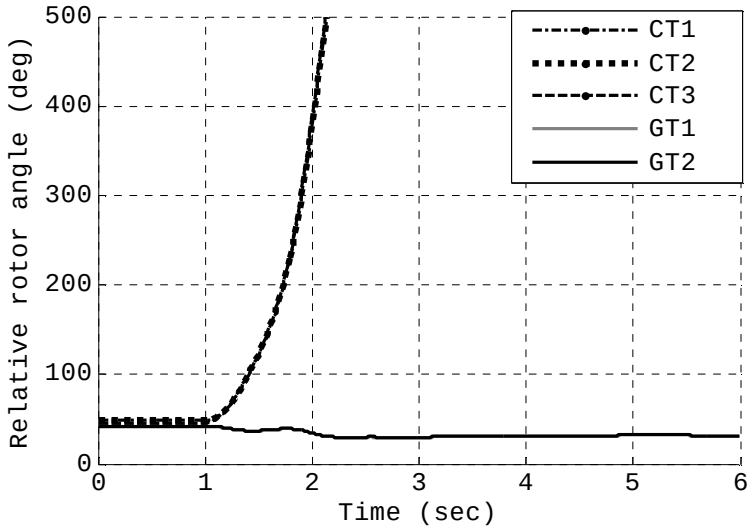

Figure 10.2 Relative rotor angle at selected generators in the region following the outage of branches 1608-1701 and 1608-1509

Case b (depressed voltages): Outage of branches 1159-1132 and 1217-1133

Figure 10.3 shows a schematic one-line diagram of the area of interest. The disconnected branches 1159-1232 and 1217-1133 are marked with cross. When these two lines are disconnected, the loads in the region are supplied through 1143-1218-1121-1122 (marked with dotted line), which has a considerably higher impedance. The large voltage drop on the higher impedance path and lack of reactive power resources in the region leads to depressed voltages at the load buses. Figure 10.4 shows the voltage at selected load buses in the region when the branches are disconnected. The power flow fails to solve for this case due of the abnormally low voltages in this area, resulting from the outage. However, angle instability was not observed at nearby generators. Figure 10.5 shows the relative rotor angle at selected generators (ST1, ST2, ST3) in the region when the branches are disconnected. Voltage problems were observed in the system, when power supply to affected load areas were re-routed through higher impedance paths, due to opening of two main supply branches.

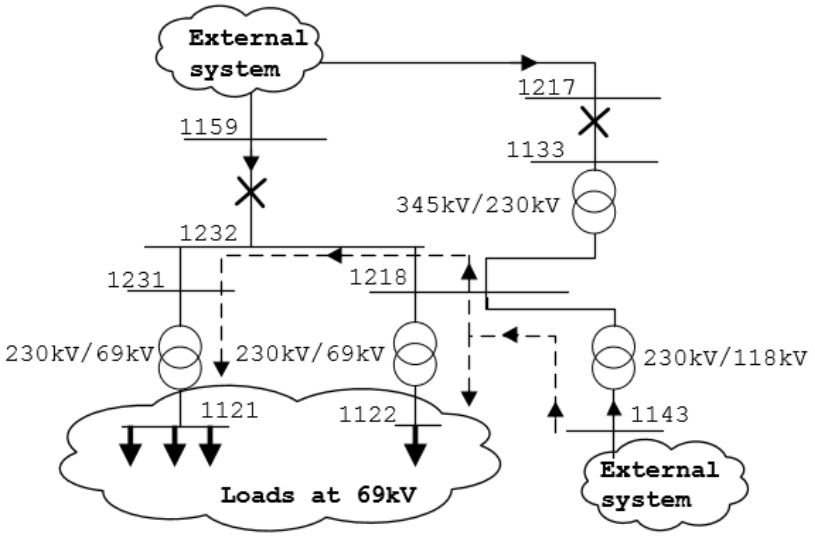

Figure 10.3 Schematic one-line diagram of the load area supplied by lines 1159-1232 and 1217-1133

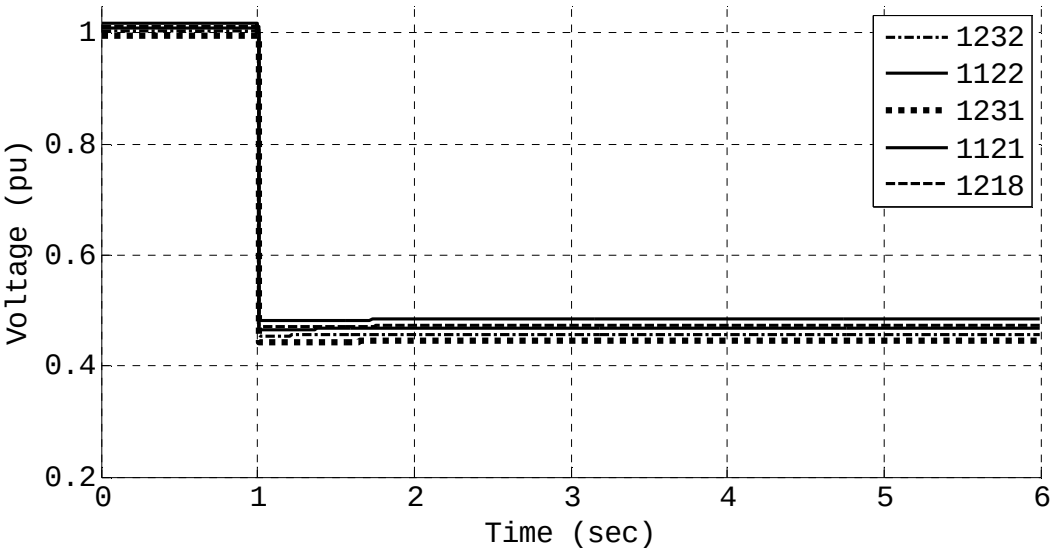

Figure 10.4 Voltage at selected buses in the region following the outage of branches 1159-1232 and 1217-1133

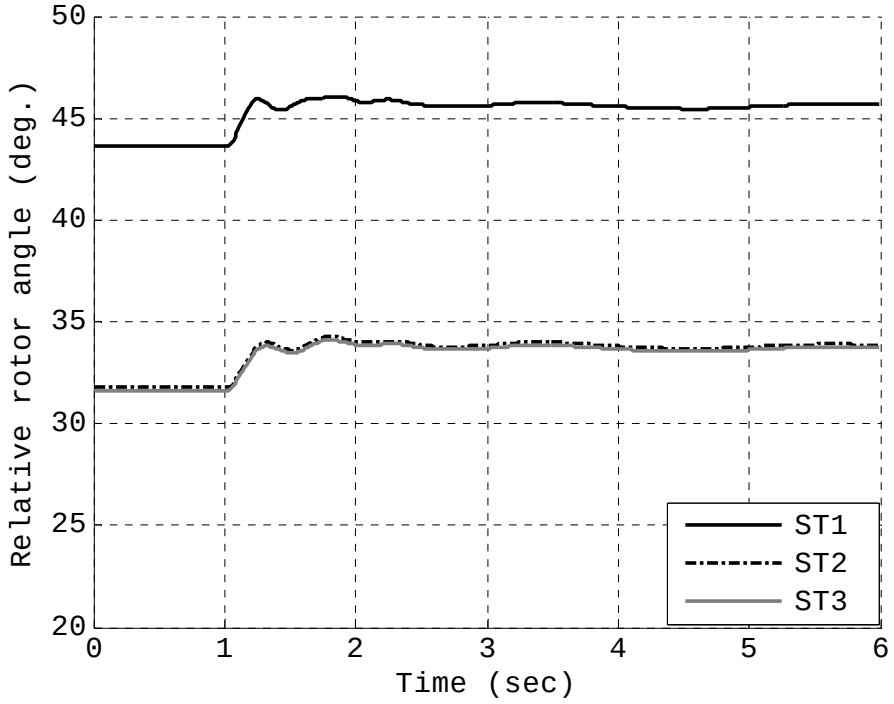

Figure 10.5 Relative rotor angle at selected generators in the region following the outage of branches 1159-1232 and 1217-1133

10.7 Comparison of results with exhaustive *n*-1-1 contingency analysis

Like any other screening method, it is important to check whether such a method successfully captures all the critical contingencies in a system. To check the efficiency of the proposed method, the results obtained in the preceding sections need to be compared against an exhaustive *n*-1-1 contingency analysis. The following subsections provide a comparison of the proposed method with an exhaustive *n*-1-1 contingency analysis performed for the system under study. The computational savings by adopting the proposed method are also illustrated.

10.7.1 Comparison of n-1-1 branch-branch contingency results

The SSTools double outage creator module was used to generate the exhaustive list of *n*-1-1 branch-branch contingencies. SSTools was then used to perform ac power flow analysis on the exhaustive list of contingencies. Table 10.13 provides a comparison of the results of the proposed screening method and the exhaustive analysis. From Table 10.13, it can be seen that both the exhaustive evaluation and the screening method yields the same number of contingencies leading to flow and voltage violations. The same branch-branch contingencies were identified as critical by both the methods. It should also be noted that the number of ac power flows to be performed is greatly reduced. The screening method reduces the number of cases to be evaluated by 93 percent.

Table 10.13 Comparison of the screening method with the exhaustive evaluation for the branch-branch contingencies

	Exhaustive evaluation	**Screening method results**
Number of possible *n*-1-1 contingencies	**81003**	
Number of *n*-1-1 (full power flow solution) cases to be analyzed	81003	5549
Voltage violations	3109	3109
Flow violations	90	90
Total flow or voltage violations	**3115**	**3115**
Total number of cases where power flow fails to solve	17	17

10.7.2 Comparison of *n*-1-1 generator-branch contingency results

The SSTools double outage creator module was used to generate the exhaustive list of *n*-1-1 generator-branch contingencies. SSTools was then used to perform ac power flow analysis on the exhaustive list of contingencies. The same re-dispatch schedule was used for both the screened analysis and the exhaustive analysis. Table 10.14 and provides a comparison of the results of the proposed screening method and the exhaustive analysis. From Table 10.14, it can be seen that both the exhaustive evaluation and the screening method yields the same number of contingencies leading to flow and voltage violations. The same generator-branch contingencies were identified as critical by both methods. The proposed screening method reduces the number of cases to be evaluated by 95 percent.

Table 10.14 Comparison of the screening method with the exhaustive evaluation for the generator-branch contingencies

	Exhaustive evaluation	**Screening method results**
Number of possible *n*-1-1 contingencies	**9672**	
Number of *n*-1-1 (full power flow solution) cases to be analyzed	9672	474
Voltage violations	5	5
Flow violations	1	1
Total flow or voltage violations	**6**	**6**
Total number of cases where power flow fails to solve	0	0

10.8 Comparison of *n*-1-1 generator-generator contingency results

The SSTools double outage creator module was used to generate the exhaustive list of n-1-1 generator-branch contingencies. SSTools was then used to perform ac power flow analysis on the exhaustive list of contingencies. The same re-dispatch schedule was used for both the screened analysis and the exhaustive analysis. Table 10.15 and provides a comparison of the results of the proposed screening method and the exhaustive analysis. From Table 10.15, it can be seen that the screening method reduces the number of cases to be evaluated by 13.5 percent. However, it should be noted that if the reactive power change threshold to screen the second candidate generator was increased from 5%, as mentioned in section 10.5.3, to 10% then the number of screened contingencies reduces to 175.

Table 10.15 Comparison of the screening method with the exhaustive evaluation for the generator-generator contingencies

	Exhaustive evaluation	**Screening method results**
Number of possible *n*-1-1 contingencies	**288**	
Number of *n*-1-1 (full power flow solution) cases to be analyzed	288	249
Voltage violations	0	0
Flow violations	0	0
Total flow or voltage violations	**0**	**0**
Total number of cases where power flow fails to solve	0	0

10.9 Summary

This chapter presented the *n*-1-1 contingency analysis results for a real large power system. The proposed *n*-1-1 contingency screening and ranking method was used to generate a reduced list of contingencies and rank them in order of their severity. The SSTools module of GE-PSLF was used to process the contingencies and record the relevant voltages and flows in the system. In addition, the contingency cases where the power flow fails to solve where discussed and a method to analyze such cases was presented here. In addition, the accuracy of the screening process was tested by comparing the screening results with an exhaustive *n*-1-1 contingency analysis. The comparison results show that the proposed screening method is able to capture all the critical contingencies in the system. The proposed contingency screening method greatly reduces the total number of ac power flows

that need to be performed. Therefore, the proposed technique enables significant savings in computational effort.

CHAPTER 11: PROPOSED N-1-1 CONTINGENCY SCREENING AND CLASSIFICATION FOR DSA

DSA for *n*-1-1 contingencies examines whether a system is able to maintain stability following a sequential outage of two network elements. The contingency events referred to in this chapter are three-phase faults on lines followed by removal of the faulted lines from service by appropriate protection devices. Faults are large disturbances on the system and have a significant impact on the transient stability.

11.1 Contingency screening and classification for DSA

DSA for *n*-1-1 contingencies is done in two steps. The first step is to simulate the initial contingency and check whether it is stable. If the system is stable and reaches an acceptable equilibrium after all automatic controls have acted, the second contingency is simulated. If the second contingency is stable and an acceptable steady state is reached, the *n*-1-1 contingency is labeled as secure. Otherwise, the *n*-1-1 contingency is labeled as insecure. *n*-1-1 contingency screening and classification for DSA will be simply referred to as *n*-1-1 contingency screening and classification for the remainder of the report.

As discussed earlier, one of the main challenges for *n*-1-1 contingency screening and classification is the large number of cases that need to be evaluated. As such, performing simplified fast calculations can become computationally prohibitive for realistic power systems. This part of the report focuses on the development of a fast and reliable method for screening and classifying *n*-1-1 contingencies. A two-stage approach is used to screen and classify the *n*-1-1 contingencies. In stage I, a subset of *n*-1-1 contingencies is screened for further classification. The screening process is based on the power flow results of the

n-1 analysis. In stage II, the screened contingencies are classified based on the kinetic energy gained due to the fault and the change in the magnitude of the Thévenin's impedance (Z_{th}) at the point of interconnection (POI) of the generators in the post-fault network. The proposed screening and classification method is implemented using MATLAB and GE-PSLF. The following sections provide detailed descriptions of stage I and stage II of the proposed method followed by a justification of the processes.

11.1.1 Stage I: Screening of *n*-1-1 contingencies

Stage I of the *n*-1-1 contingency screening and classification process deals with screening a subset of all possible *n*-1-1 contingencies, for further analysis. The screening process is based on the power flow results of the *n*-1 contingency analysis. The power flow solution after a contingency describes the post-disturbance equilibrium of the system, once all fast control actions have taken place. The impact of the second contingency on the system is dependent on this equilibrium point and hence the *n*-1 power flow solution is the starting point for the *n*-1-1 screening process. It should be noted that only stable *n*-1 contingencies are considered as the first contingencies in the screening process for *n*-1-1 analysis. This is a valid consideration as it is meaningless to analyze a successive contingency if the initial contingency is not stable. To generate the list of the screened *n*-1-1 contingencies involving branch-branch outages, the following steps are followed [87]:

1. Perform a full ac power-flow for all *n*-1 branch contingencies and record all the line MW flows.
2. For each branch outage, compute the percentages of MW flow in the outage branch that shows up in all other branches in the system. This percentage is

the similar to the line outage distribution factor (LODF) and will be referred to as *MWLODF* in the rest of this report. As an example, the *MWLODF* in a hypothetical line *A* for outage of line *B* is computed as follows:

$$MWLODF_{AB} = \left(\frac{MW_{n-1,AB} - MW_{base,A}}{MW_{base,B}} \right) 100 , \qquad (11.1)$$

where,

$MWLODF_{AB}$ is the percentage of MW flow on line *B* that shows up on line *A*.

$MW_{n\text{-}1,AB}$ is the MW flow on line *A* with line *B* disconnected.

$MW_{base,A}$ is the MW flow on line *A* in the base case (all lines in service).

$MW_{base,B}$ is the MW flow on line *B* in the base case (all lines in service).

3. All branches that have an *MWLODF* more than a set threshold for an *n*-1 contingency are screened as candidate branches for the second outage following that particular *n*-1 contingency.
4. The *n*-1-1 contingency list is updated to include all pairs of the *n*-1 outages and the corresponding screened second outages in step 3. Steps 2 to 4 are performed for all *n*-1 contingencies.
5. Finally, all duplicate *n*-1-1 contingencies are removed from the list and the pre-screened list of *n*-1-1 contingency I formed.

The screening method described here is similar to the screening method described in section 9.2.1 with the exception of using the *MWLODF* instead of the *ACLODF*. The screening process uses the change in MW flow as a screening parameter to select candidate branches for the second outage. Since dynamic security is of concern, change in the MW

flow is a suitable screening parameter as it influences the rotor angles of the generators in a system. A higher value of *MWLODF* indicates that the system has a radial structure in the region of interest and only a few branches compensate for the lost flow on the disconnected branch. This implies that the branch may be closer to a generation source or a load center where the network is close to radial. A fault on a line with a high *MWLODF* can be critical as the disturbance may be close to a generator or group of generators. Subsequent disconnection of the line to clear the fault can result in a weak post-disturbance network due to loss of a main transmission path. A lower value of the *MWLODF* indicates that the network is meshed and only a small fraction of the lost flow on the disconnected line shows up in the other lines. Power systems are typically meshed farther away from generation sources and load centers. Faults at such locations followed by the removal of the affected line neither causes a large disturbance nor weakens the transmission system significantly. It is worthwhile to mention that a higher value of the *MWLODF* does imply that a fault on the corresponding line will be more severe than on others. However, it is a good measure to identify critical lines, where faults could be possibly severe. The *MWLODF* serves as an index to screen critical lines rather than a measure of severity.

The screening process is conservative in the sense that not all screened cases are unstable. It should be noted that stability assessment is not an issue here. The screening and classification process aims to prioritize the analysis of cases, which are critical from a stability assessment viewpoint. The *n*-1-1 contingencies eliminated by the screening process are categorized as of least concern (LCR) for stability assessment. The screening process is expected to reduce the number of cases significantly, that need to be analyzed in stage II.

11.1.2 Stage II: Classification of screened *n*-1-1 contingencies

Stage II deals with classifying the screened *n*-1-1 contingencies obtained from stage I. The screened contingencies are classified based on two factors:

1. The total kinetic energy gained by the machines due to the applied fault
2. The maximum change in the magnitude of Z_{th} seen at the POI of a generator or a group of generators due to the removal of the faulted line from service

A short time domain simulation is conducted to compute the kinetic energy gained by the system at the end of the fault. Additionally, the change in the magnitude of Z_{th} as seen at the POIs of all generators/group of generators in the area of interest is computed after opening the faulted line. It is assumed that a fault applied on the system will be cleared in 5 cycles, which is a standard clearing time for modern circuit breakers rated for 100kV and above [90]. Based on the two measurements the contingencies are categorized as critical (CR), possibly critical (PCR) and non-critical (NCR). The following steps are followed to classify the screened contingencies:

1. Solve the power flow by removing the first line considered in *n*-1 contingency.
2. Perform a time domain simulation and apply a 5-cycle three-phase fault on the screened second line considered in the *n*-1-1 case. The time domain simulation is run only the till the fault is cleared.
3. Record the angular speed of selected generators at the end of the fault and compute the total kinetic energy gained by the system with respect to the

center of inertia (COI) [78] of the area of interest. The total kinetic energy gained during the fault is given by:

$$\omega_{coi} = \frac{\sum_{\text{all gens}} M_i \omega_i}{\sum_{\text{all gens}} M_i} \tag{11.2}$$

$$\Delta\omega_i = \omega_i - \omega_{coi} \tag{11.3}$$

$$KE = \sum_{\text{all gens}} \frac{1}{2} J_i (\Delta\omega_i)^2 \tag{11.4}$$

where,

ω_{coi} is the angular velocity of the center of inertia

ω_i is the angular velocity of the ith generator

M_i is the inertia constant of the ith generator

KE is the kinetic energy gained by the system

J_i is the moment of inertia of the ith generator

4. Remove the faulted line from service and compute the change in the magnitude of Z_{th} as seen at the POIs of all generators/group of generators in the region of interest.
5. Record the maximum change in the magnitude of Z_{th} and the corresponding bus number of the POI where it occurs. The maximum change in the magnitude of Z_{th} will be referred to as $|\Delta Z_{thmax}|$ in the rest of the report.

The stability of a power system during a fault depends on the kinetic energy gained by the system due to the fault and the robustness of the post-disturbance network [91]. This

can be understood by examining the equal area criterion for a one-machine infinite bus system. The idea has been extended to multi-machine systems as well [92]. During a fault, the ability of the network to export electrical power is severely restricted causing the machine to accelerate. Once the fault is cleared by opening the faulted line, the machine is able to export electrical power and it decelerates. The stability of the machine is dependent on its ability to decelerate in the post-disturbance condition and reach a steady state.

The kinetic energy gained by the system during a fault is computed by performing a short time domain simulation with a three-phase fault applied on the concerned branch. To estimate the ability of the system to decelerate, the change in the magnitude of Z_{th} seen into the system at the POI of the generator due to opening of the faulted line is computed. The buses, which are the POI of generating stations, are typically known to planners beforehand. The change in Z_{th} can be computed by using sparsity oriented compensation methods [93]. A review of the swing equation [91] indicates that a large change in the magnitude of Z_{th} results in a substantial reduction in the peak of the post-fault swing curve as compared to the pre-faulted condition. A reduction in the peak of the post-fault swing curve limits the ability of the generator to decelerate, thereby making it prone to instability. Hence, these two factors are chosen to categorize contingencies based on their impact on stability.

11.2 Categorization of *n*-1-1 contingencies

As mentioned in section 11.1.2, the screened contingencies are further grouped into three distinct categories. The three categories are CR, PCR, and NCR. Based on the kinetic

energy gained and the $|\Delta Z_{thmax}|$, each contingency is assigned one of these categories. Brief descriptions of the three different categories are as follows:

I. *Critical* (CR)

A Contingency is categorized as CR if both the kinetic energy and the $|\Delta Z_{thmax}|$ due to the contingency are high. A critical contingency implies that the fault is close to a generator and opening of the faulted line weakens the transmission system. Such cases are likely to have stability issues and warrant detailed time domain analysis

II. *Possibly critical* (PCR)

A Contingency that results in large kinetic energy and small $|\Delta Z_{thmax}|$ or small kinetic energy and large $|\Delta Z_{thmax}|$ is categorized as PCR. A large kinetic energy and small $|\Delta Z_{thmax}|$ implies that although the fault is close to generation units, the post disturbance network is strong. On the other hand, a large $|\Delta Z_{thmax}|$ and small kinetic energy indicates that although the post-fault network is weak, the fault is electrically distant from large generation units. Contingencies categorized as PCR may not be unstable under a given operating condition, but can become critical as the operating conditions change.

III. *Non critical* (NCR)

Contingencies that result in both small kinetic energy and small $|\Delta Z_{thmax}|$ are categorized as NCR. Detailed time domain analysis is not required for these contingencies.

Once the contingencies are categorized as CR, PCR and NCR, they can be displayed on a kinetic energy vs. $|\Delta Z_{thmax}|$ plot for ease of visualization. The visualization

approach is helpful as it enables a planner/operator to estimate the relative severity of the contingencies. Figure 11.1 shows the three regions on the kinetic energy vs. $|\Delta Z_{thmax}|$ plot. It should be noted that the boundaries of the three different regions are system dependent and hence, not defined explicitly. These boundaries can be defined ad hoc for a particular system and subsequently tuned over time to increase the efficiency of the classification process. The lack of an explicit definition of the boundaries does not negate the classification process, as this process does not judge whether a contingency is unstable. Rather, the classification process categorizes the contingencies based on their relative severity. A comprehensive stability assessment is performed via TDS, which is a more reliable method. The cases marked as CR and PCR should be assessed by detailed TDS. Cases marked as NCR and LCR can be assessed by early termination TDS [94], which is faster. The contingencies should be assessed in the order CR and PCR followed by NCR and LCR.

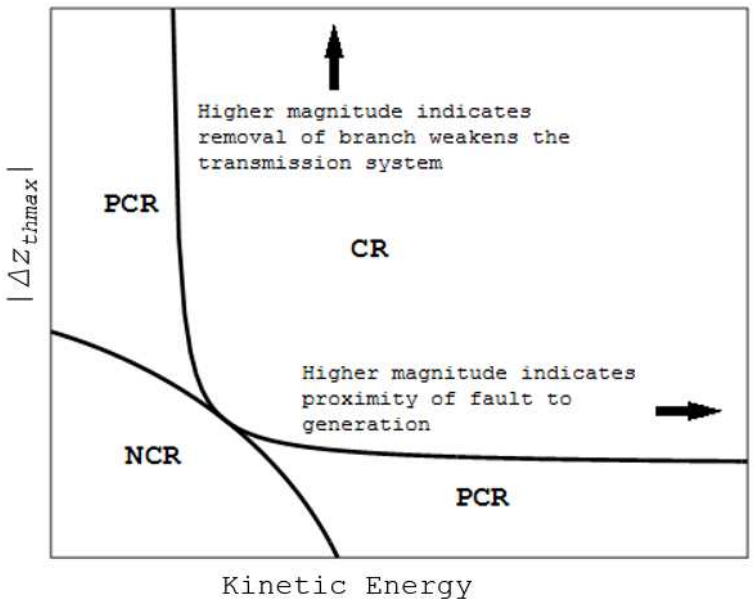

Figure 11.1 CR, PCR and NCR regions on the kinetic energy vs. $|\Delta Z_{thmax}|$

11.3 Summary

This chapter presented the proposed *n*-1-1 contingency screening and classification method for DSA. The proposed method works in two stages. In stage I, candidate *n*-1-1 contingencies are screened for the contingency classification process. In stage II, the screened *n*-1-1 contingencies from stage I are classified into four distinct groups CR, PCR, NCR and LCR. The contingencies categorized as CR and PCR are important from a transient stability viewpoint and warrant detailed analysis. The contingencies categorized as NCR and LCR are of the lowest priority for stability analysis. These contingencies do not need any detailed evaluation. Furthermore, a visualization approach is suggested which enables a better presentation of the contingency classification results. The proposed screening and classification method is expected to reduce the computational effort by reducing the number of cases that needs detailed evaluation.

CHAPTER 12: *N*-1-1 CONTINGENCY ANALYSIS FOR DSA: APPLICATION TO A REAL SYSTEM

In chapter 11, a method for screening and classifying *n*-1-1 contingencies was proposed. In this chapter, the proposed method is used to screen and classify *n*-1-1 contingencies for the selected utility in the WECC system. For DSA, the contingencies are screened and classified with respect to their impact on the system stability. In the following sections, the various thresholds used for the contingency screening process are presented. In addition, some examples are provided which highlight the main features of the proposed method.

12.1 Description of the case

Contingency screening and classification was performed for the same utility considered in chapter 10. In addition to using the power flow file, the dynamic data file containing the equipment dynamic models was used in this part of the work. The description of the WECC system and the selected utility's service area can be found in Table 10.1.

12.2 *n*-1 contingency screening and classification for the selected utility

Due to the lesser number of *n*-1 contingencies, the screening process of stage I can be omitted and the contingencies can be directly classified using the classification technique. Since the screening process is skipped, the list LCR for *n*-1 contingencies has no entries in it. Based on the dynamic characteristics, the contingencies are classified into three groups, CR, PCR and NCR. For the classification process, a 5-cycle three-phase fault

is considered as the disturbance on the system. It is assumed that the protection system clears the fault by removing the faulted line from service within 5-cycles [90].

MATLAB and GE-PSLF, was used to perform the *n*-1 contingency classification. The SSTools module of GE-PSLF was used to generate the *n*-1 contingency list. The GE-PSLF transient stability module [22] was used to perform the time domain simulations. MATLAB was used to analyze the output from PSLF and perform the remainder of the computations.

For the *n*-1 contingency classification study, the results are presented directly without detailed discussions. A comprehensive analysis of the method and results are presented later in the section dealing with *n*-1-1 contingency screening and classification. The *n*-1-1 contingencies provide a better insight into the screening and classification process and hence the detailed analysis is left for later. The following subsection presents the results of the *n*-1 contingency classification process.

12.2.1 *n*-1 contingency analysis results

SSTools generated a list of 403 branch-branch contingencies for the area/zones and voltage levels described in section 10.1. The contingencies were then classified as CR, PCR, and NCR as described in the section 11.2. 13 *n*-1 contingencies resulted in islanding of generation units. Islanding of generation units was detected by a large change in the $|\Delta Z_{thmax}|$ at the POI of these generation units. These 13 *n*-1 contingencies are excluded from further analysis. Figure 12.1 shows the location of the contingencies on a kinetic energy vs $|\Delta Z_{thmax}|$ plot. Contingencies that lead to islanding of generation units are not shown in Figure 12.1. The three different categories of contingencies are marked distinctly on the

plot. From Figure 12.1, it can be seen that none of the *n*-1 contingencies fall in the category CR. Detailed TDSs were performed for all the contingencies in the category PCR. All these contingencies were found to be stable.

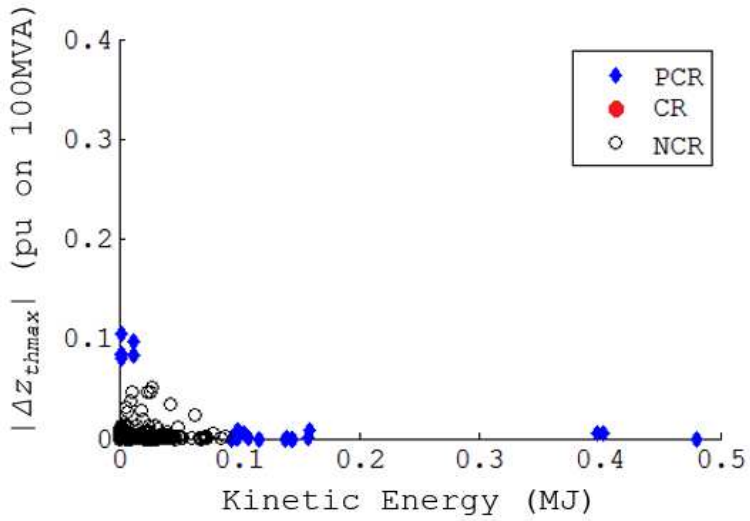

Figure 12.1 *n*-1 contingencies on a kinetic energy vs. $|\Delta Z_{thmax}|$ plot

12.3 *n*-1-1 contingency screening and classification for the selected utility

In *n*-1-1 contingency screening and classification, only stable *n*-1 contingencies are considered as first outages. The *n*-1 contingencies that are unstable or cause islanding of generation units are listed separately. In this particular study, for the system under consideration, all *n*-1 contingencies were stable and 13 *n*-1 contingencies lead to islanding of generation units. These 13 *n*-1 contingencies were excluded from the *n*-1-1 analysis.

The screening process described in stage I of the proposed method was used to screen candidate lines for simulating the second outage. The *MWLODF* threshold for screening candidate lines for the second outage was set to 40%. Lowering the *MWLODF* threshold did not result in screening of any additional unstable contingency. Hence, the set

threshold is sufficient for the screening process. As mentioned before, the *MWLODF* can be tuned over time for more efficient screening of contingencies. After the second set of candidate lines are screened, a list of the *n*-1-1 contingencies is created. The screened *n*-1-1 contingencies are then classified appropriately by the classification process described in section 11.2.

12.3.1 *n*-1-1 contingency analysis results

Table 12.1 lists the number of all possible *n*-1-1 contingencies and the number of screened contingencies. The screening process substantially reduces the number of cases to be classified. As indicated earlier, the screening process of stage I is conservative in nature. Not all screened contingencies are likely to have dynamic issues. However, the screening process eliminates all the *n*-1-1 contingencies that are least critical from a transient stability perspective [87].

Figure 12.2 shows the location of the screened *n*-1-1 contingencies on the kinetic energy vs. $|\Delta Z_{thmax}|$ plot. The different categories of contingencies are marked distinctly on the plot. Table 10.2 lists the number of *n*-1-1 contingencies in the four different categories. TDS were performed for the 204 screened *n*-1-1 contingencies. All the contingencies in the categories PCR and NCR were found to be stable. The 3 contingencies categorized as CR were found to cause instability. Table 12.3 presents the results of TDS for 8 selected contingencies in categories CR and PCR. The 8 selected contingencies (otg1-otg8) are marked in Figure 12.2. The 8 contingencies were chosen the cover the CR cases and the PCR cases, which resulted in high kinetic energy or high $|\Delta Z_{thmax}|$. The contingencies in the PCR region are stable at this operating condition. This is because in these cases either

the fault is far from large generation or the post-disturbance network is strong enough to provide adequate deceleration to the accelerating generators. Detailed TDS results for otg2, otg5 and otg7 are presented in Figure 12.3, Figure 12.4, and Figure 12.5 respectively. The relative rotor angles of the most affected generators due these contingencies are plotted. Generators G1to G7 are the generators, which are most affected by these contingencies. From Figure 12.3, it can be seen that contingency otg2, which is grouped as CR leads to instability. Contingencies otg5 and otg7, which are grouped as PCR, are stable.

Table 12.1 Metrics for the screening process in stage I

Total number of *n*-1 contingencies	**Total number of possible *n*-1-1 contingencies**	**Number of *n*-1-1 screened as candidate cases**
390	75855	204

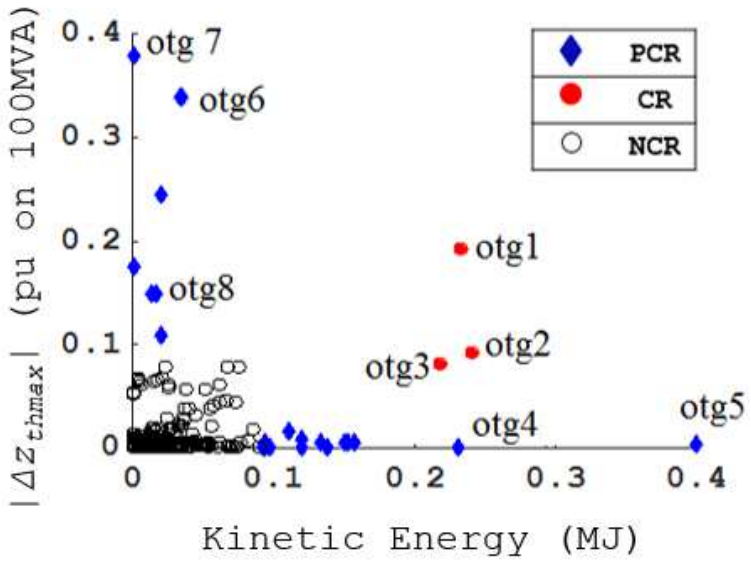

Figure 12.2 *n*-1-1 contingencies on a kinetic energy vs. $|\Delta Z_{thmax}|$

Table 12.2 Number of *n*-1-1 contingencies in different categories

Categories	CR	PCR	NCR	LCR
No. of contingencies	3	32	169	75651

Table 12.3. Stability status of selected contingencies after performing TDS

Contingency name	Type	Status (from TDS)
otg1	CR	Unstable
otg2	CR	Unstable
otg3	CR	Unstable
otg4	PCR	Stable
otg5	PCR	Stable
otg6	PCR	Stable
otg7	PCR	Stable
otg8	PCR	Stable

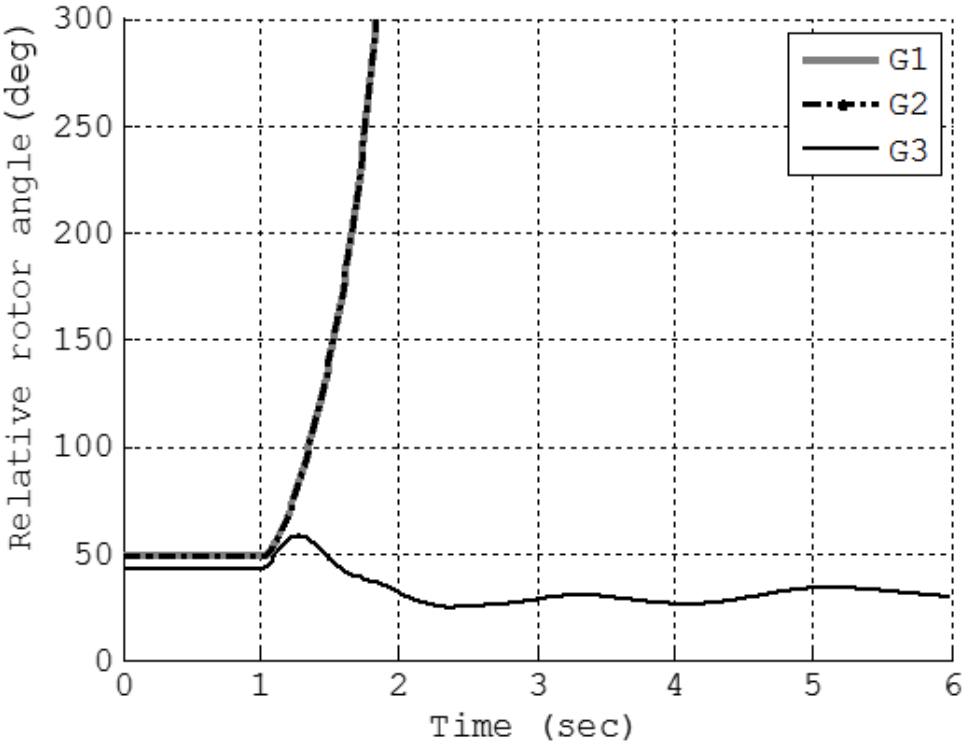

Figure 12.3 Relative rotor angles of generators G1, G2 and G3 for otg2

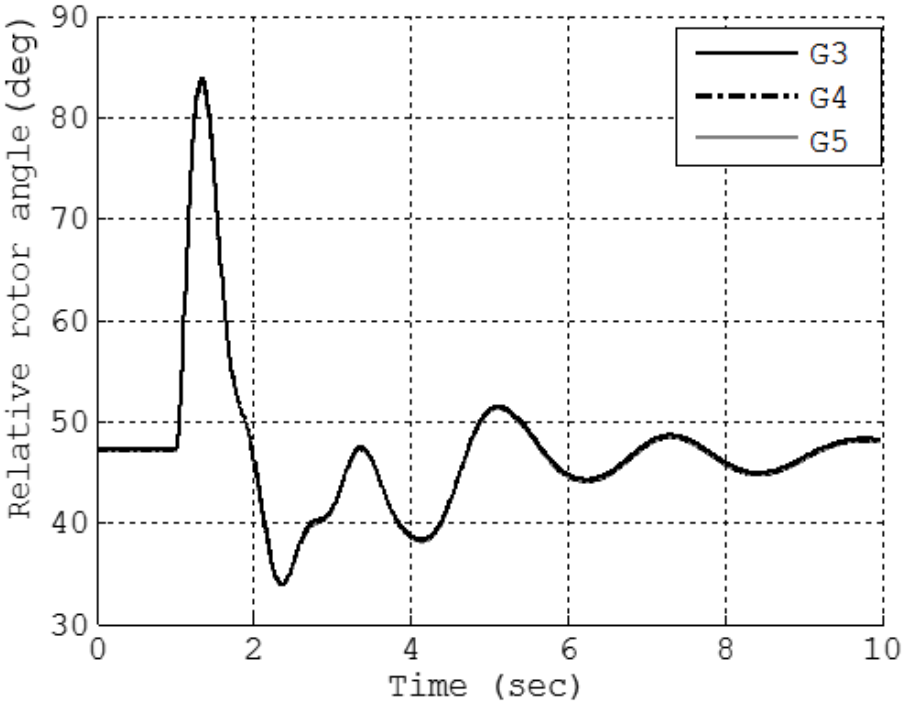

Figure 12.4 Relative rotor angles of generators G3, G4 and G5 for otg5

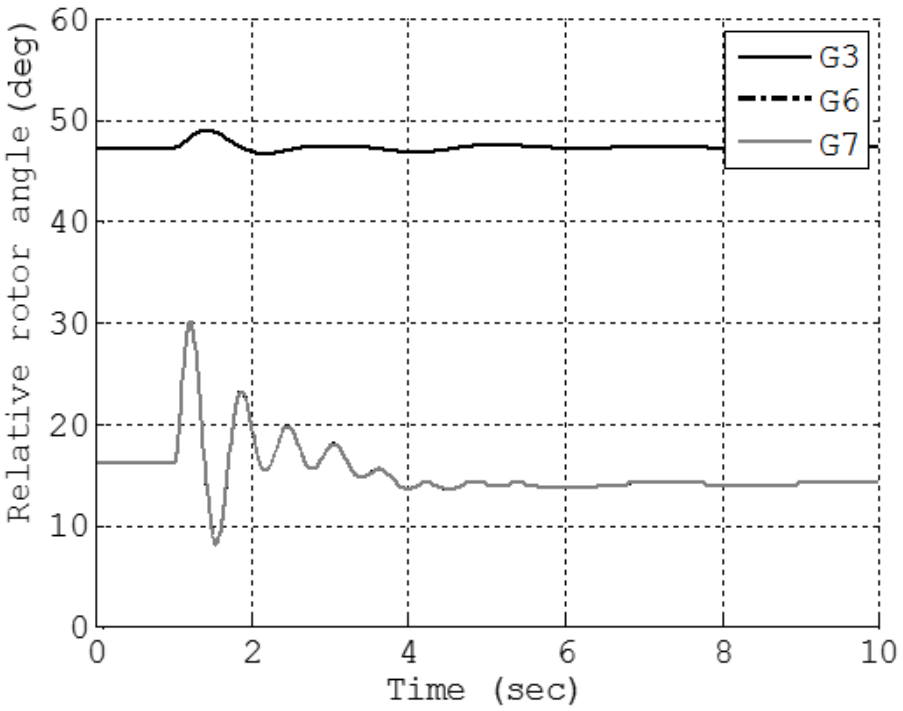

Figure 12.5 Relative rotor angles of generators G3, G6 and G7 for otg7

It is worthwhile to examine the contingencies categorized as PCR in further detail. As mentioned earlier, these contingencies could become critical due change in operating conditions. An example to illustrate such a case is as follows:

Case: otg8 - outage of the lines 1518–1519 and 1211-1212

Outage of line 1518–1519 is considered as the *n*-1 outage. A 5-cycle three-phase fault on line 1211-1212 and the ensuing outage is considered as the *n*-1-1 event. Figure 10.6 shows a schematic one-line diagram of the area of interest. From Figure 12.2, it can be seen that the contingency otg8 results in a large $|\Delta Z_{thmax}|$, though the kinetic energy gained is comparatively less. $|\Delta Z_{thmax}|$ for this contingency was recorded at bus 1212, which is the POI of 12 generators CTG1 to CTG 12, each rated at 44 MW. In the present scenario,

only 4 generators are switched on producing 140 MW. Since the machines are smaller and have low inertia, the total kinetic energy gained by the machines is not significantly high. Opening the considered lines (marked crosses in Figure 12.6) due to the sequential outages, results in a large $|\Delta Z_{thmax}|$. This is due to the high impedance of the path 1212-1518-1160 (marked with dotted line), through which the generation is connected to the rest of the system in the post-fault condition. As listed in Table 12.3, the contingency is stable for this operating scenario. Figure 12.7 shows the relative rotor angle of generator CTG1 connected at bus 1212 in the base case. The generators at bus 1212 oscillate together and hence the relative rotor angle of one of the generators is shown here. Generator G3 is a generator in the utility's service area, which is not affected by this contingency.

The total generation capacity at bus 1212 is 528 MW (12 units, 44 MW each). As such, the generation level may be increased under heavy load periods or due to the loss of generation at some other location in the system. Figure 12.8 shows the trace of the otg8 on the kinetic energy vs. $|\Delta Z_{thmax}|$ plot as the generation at 1212 is increased. Table 12.4 shows the different generation levels considered at bus 1212 for plotting Figure 10.8. From Figure 10.8 it can be seen that contingency otg8 approaches the CR region as the generation at bus 1212 is increased by connecting additional units. Figure 12.9 shows the relative rotor angles of CTG1 as the total generation connected at bus 1212 is increased. From Figure 12.9, it can be seen that the units at 1212 go unstable as the generation is increased to 510 MW. Hence as contingency otg8 moves into the CR region in Figure 12.7, it becomes unstable.

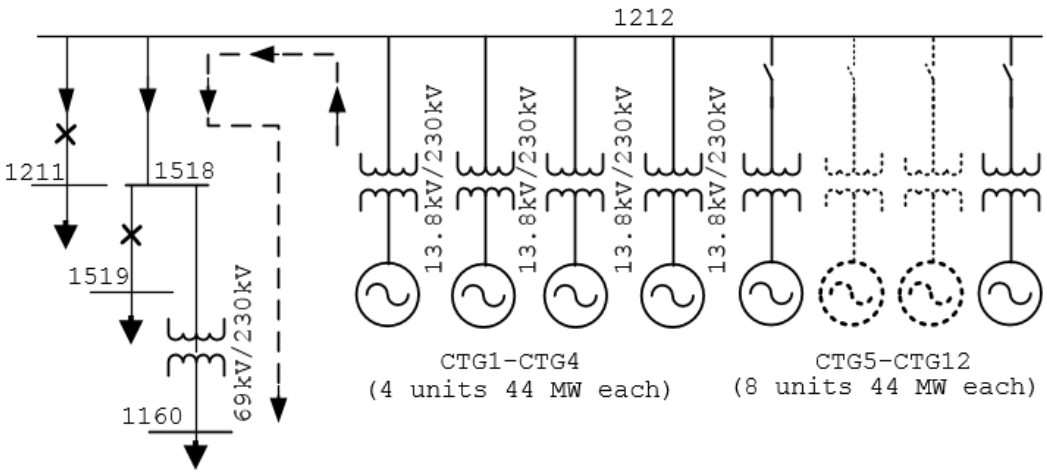

Figure 12.6 Schematic one-line diagram of region close to bus 1212

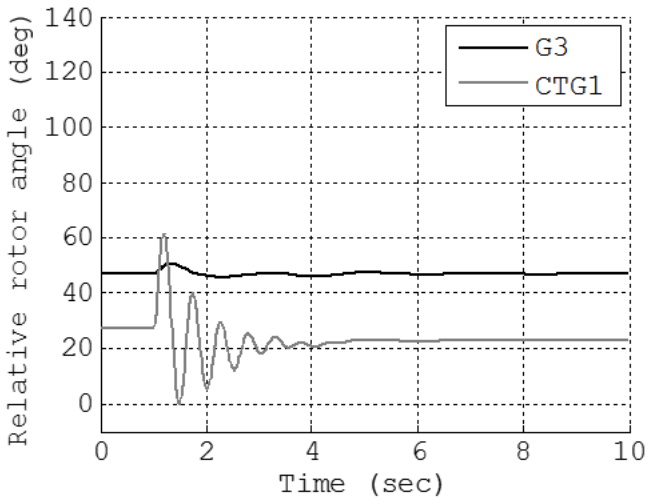

Figure 12.7 Relative rotor angles of generator CTG1 at bus 1212 and generator G1 in the base case

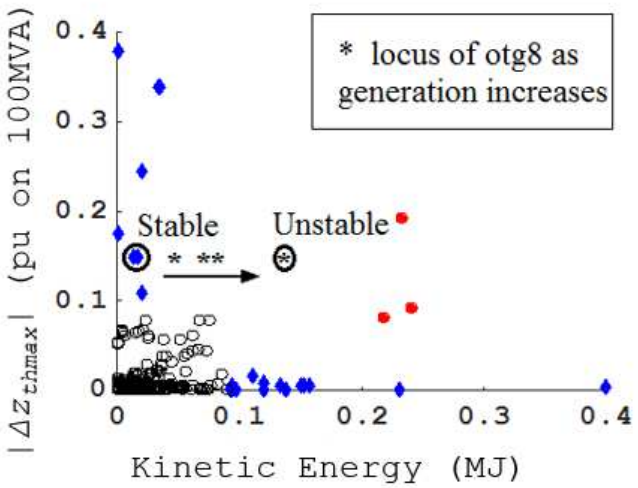

Figure 12.8 Trace of otg8 on the kinetic energy vs $|Z_{thmax}|$ plot

Table 12.4 Different generation levels at bus 1212

Units online at 1212	**Generation (MW)**
4 (base case)	140
8	290
10	335
10	360
12	510

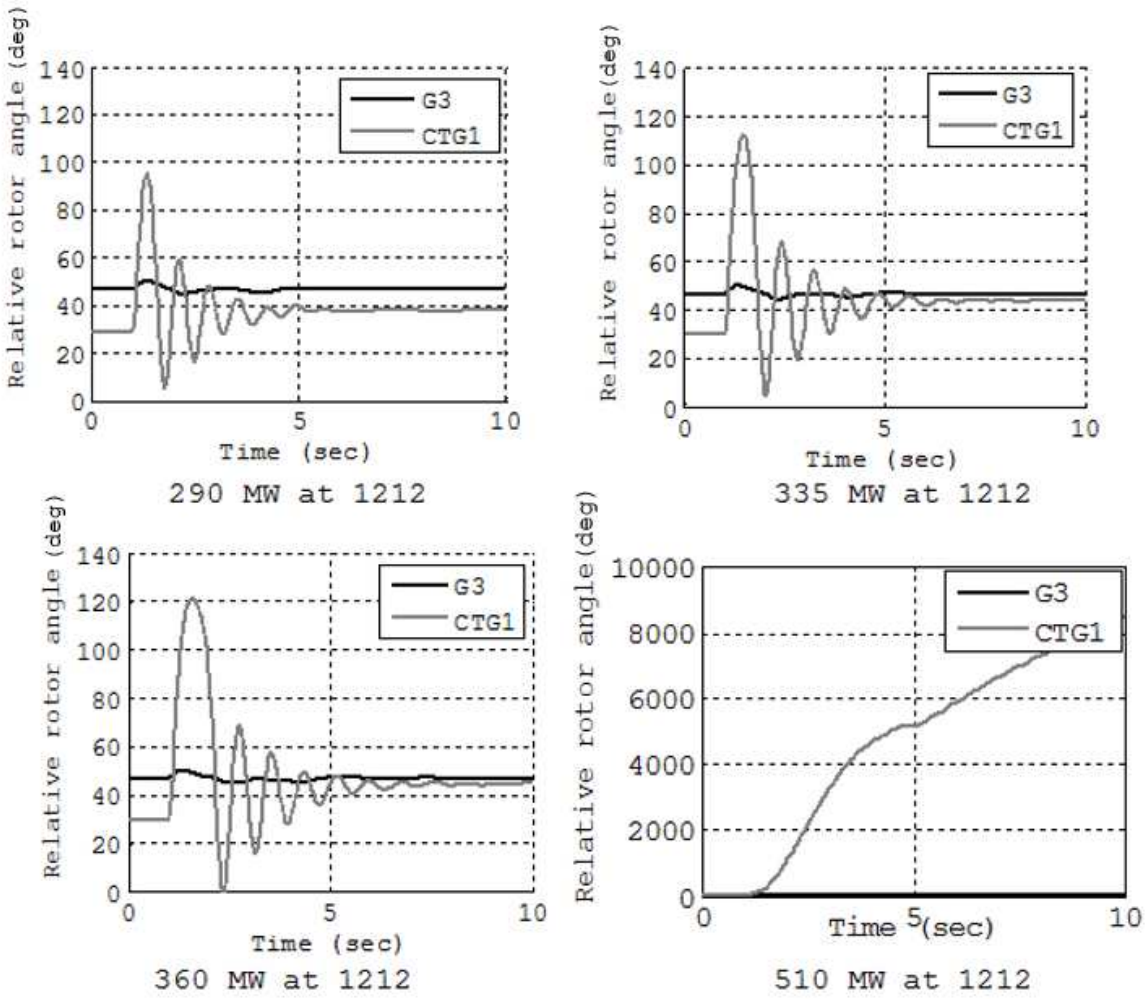

Figure 12.9 Relative rotor angles of generators at CTG1 and G3 for a different generation levels at 1212

12.4 Summary

This chapter presented the *n*-1-1 contingency screening and classification results for the selected utility in the WECC area. The contingency screening and classification method is applicable for branch-branch contingencies, which have significant impact on transient stability. The proposed method is used to generate a reduced list of *n*-1-1 contingencies and classify them based on their dynamic behavior. The screened contingencies are classified into four distinct groups CR, PCR, NCR and LCR based on their impact on the system. Furthermore, examples were provided to illustrate the different aspects of the screening and classification process. The important feature of the proposed method is that it reduces the computational burden significantly. The screening process reduces the number of contingencies that needs to be classified substantially. Further, the classification process identifies the cases that need detailed evaluation, without the need of any elaborate computation.

CHAPTER 13: CONCLUSIONS AND FUTURE WORK: *N*-1-1 CONTINGENCY ANALYSIS

13.1 Conclusions

Power system security assessment for *n*-1-1 contingencies is of paramount importance for the secure and reliable operation of power systems. The primary impediment in performing such assessments is the overwhelming number of cases that need to be analyzed. The work done here presents a systematic approach to *n*-1-1 power system security assessment for a realistic large power system. An *n*-1-1 contingency screening and ranking method was proposed for SSA and an *n*-1-1 contingency screening and classification method was proposed for DSA. The key merit of the proposed methods lies in the simplicity of their implementation and reliability in identifying the critical contingencies. The main conclusions of the study are as follows:

1. The proposed contingency screening and ranking method for SSA greatly reduces the number of contingencies to be evaluated for *n*-1-1 analysis. Since the number of ac power flow that needs to be performed is significantly less, the computational burden is alleviated.
2. A method to analyze the *n*-1-1 outages where power flow fails to solve was presented here. It is seen that such cases are important as the failure of power flow to solve can indicate abnormal voltages in portions of the system.

3. The proposed ranking of contingencies for SSA helps the operator/planner to identify contingencies, which have widespread or catastrophic impact on the system.
4. The proposed contingency screening and classification method for DSA performs a primary screening of contingencies and classifies the contingencies in 4 different groups. Detailed TDS is performed only for a small number of contingencies, which are categorized as CR or PCR. Since the screening and classification method relies on short TDS and *n*-1 contingency analysis results, it is computationally efficient.
5. The proposed visualization of contingencies on a kinetic energy versus $|Z_{th\text{-}max}|$ graph helps a planner/operator to identify the relative severity of the contingencies. Furthermore, it enables the planner/operator to determine whether the faults are close to generation or they lead to weakening of the transmission system or both.
6. The proposed methods were found to be accurate in the sense that these methods are able to identify all possible critical contingencies in the system. The methods were tested by exhaustive *n*-1-1 contingency analysis.

13.2 Future work

The proposed screening and ranking method for SSA and the screening and classification method for DSA were found to be effective on a realistic large-scale power system. These methods were used to identify contingencies that may jeopardize the steady state or transient behavior of the system in a fast and reliable manner. Fast contingency filters are

also extremely important building blocks of algorithms that address the security constrained optimal power flow (SCOPF) problem [96]. The applicability of these methods for such purposes needs to be studied. The application of the proposed methods can also be useful while studying corrective transmission switching [97], where it is important to identify whether switching a line may lead to dynamic issues in the system [97], [98]. The extension of the proposed techniques to aid transmission switching is an area that needs to be explored in future.

REFERENCES

[1] R. Podmore, J. C. Giri, M. P Gorenberg, J. P. Britton, N. M. Peterson, "An advanced dispatcher training simulator," *IEEE Trans. on Power Apparatus and Systems*, vol. PAS-101, no. 1, pp. 17-25, Jan. 1982

[2] IEEE PES Current Operational Problems Working Group, "Dispatcher training simulators lessons learned," *IEEE Trans. on Power Systems*, vol. 6, pp. 594-604, May 1991,

[3] T. J. Overbye, P. W. Sauer, C. M. Marzinzik, G. Gross, "A user-friendly simulation program for teaching power system operations," *IEEE Trans. on Power Systems*, vol. 10, no. 4, pp. 1725-1733, Nov. 1995.

[4] C. Concordia, *Synchronous Machines – Theory and Performance*, John Wiley and Sons, 1952.

[5] A. A. Fouad, P. M. Anderson, *Power System Control and Stability*, 2nd ed., IEEE Press, 2003.

[6] P. Kundur, *Power System Stability and Control*, Tata McGraw Hill, 1994.

[7] D. N. Kosterev, C. W. Taylor, W. A. Mittelstadt, "Model validation for the August 10, 1996 WSCC system outage," *IEEE Trans. on Power Systems*, vol. 14, no. 3, pp. 967–979, August 1999.

[8] IEEE Task Force on Load Representation for Dynamic Performance, "Load representation for dynamic performance analysis," *IEEE Trans. on Power Systems*, vol.8, no.2, pp.472-482, May 1993.

[9] IEEE Task Force on Load Representation for Dynamic Performance, "Standard models for power flow and dynamic performance simulation," *IEEE Trans. on Power Systems*, vol.10, no.3, pp.1302-1313, August 1995.

[10] L. Pereira, D. Kosterev, P. Mackin, D. Davies, J. Undrill, W. Zhu, "An interim dynamic induction motor model for stability studies in the WSCC," *IEEE Trans. on Power Systems*, vol. 17, no. 4, pp. 1108–1115, November 2002.

[11] Z. Y. Dong, A. Borghetti, K. Yamashita, A. Gaikwad, P. Pourbeik, J. V. Milanovic, "CIGRE WG C4.605 Recommendations on measurement based and component based load modelling practice", *CIGRE SC C4 2012 Colloquium*, Hakodate, Japan, October 2012.

[12] NERC Transmission system planning performance requirements, standard TPL-001-4 available online: http://www.nerc.com/files/TPL-001-4.pdf

[13] D. Kosterev, A. Meklin, "Load modeling in WECC," *Proc. of the IEEE Power Systems Conference and Exposition*, pp. 576-581, Atlanta, 2006.

[14] D. Kosterev, A. Meklin, J. Undrill, B. Lesieutre, W. Price, D. Chassin, R. Bravo, S. Yang, "Load modeling in power system studies: WECC progress update," *Proc. of the IEEE PES General Meeting*, pp. 1-8, Pittsburgh, July 2008.

[15] A. Maitra, A. Gaikwad, P. Pourbeik, D. Brooks, "Load model parameter derivation using an automated algorithm and measured data", *Proc. of the IEEE PES General Meeting*, Pittsburgh, July 2008.

[16] P. Pourbeik, "Approaches to Validation of power system models for system planning studies", *Proc. of the IEEE PES General Meeting*, Minneapolis, MN, July 2010.

[17] FERC/ NERC Staff, "Arizona-Southern California outages on September 8, 2011: Causes and Recommendation," Report published April 2012.

[18] NERC reliability concepts, accessed on Jan. 5, 2012, available online at: http://www.nerc.com/files/concepts_v1.0.2.pdf

[19] NERC, Transmission Planning (TPL) Standards, accessed on Jan. 5, 2012, available online at: http://www.nerc.com/files/TPL-002-0.pdf

[20] A. A. Fouad, F. Aboytes, V. F. Carvalho, 'Dynamic security assessment practices in North America," *IEEE Trans. Power Systems*, vol. 3, no. 3, pp 1310-1321, Aug. 1988.

[21] K. Morrison, L. Wang, P. Kundur, "Power system security assessment," *IEEE Power and Energy Magazine*, pp. 30-39, Oct. 2004.

[22] GE-PSLF 18.01 user manual, General Electric Intl. Ltd, Schenectady, USA, 2012

[23] Siemens PSS/E 34 program operation manual, Siemens Energy Inc. Energy Management Division, Schenectady, USA, 2015

[24] R. Tomovic, *Sensitivity Analysis of Dynamic Systems*, New York, McGraw Hill, 1963

[25] P. Frank, *Introduction to System Sensitivity Theory*. New York: Academic Press, 1978

[26] W. Feehery, J. Tolsma, P. Barton, "Efficient sensitivity analysis of large-scale differential-algebraic systems," *Appl. Number. Math*., v. 25, pp. 41 – 54, 1997.

[27] I. Hiskens and M. Pai, "Trajectory sensitivity analysis of hybrid systems," *IEEE Trans. Circuits Syst. I, Fundam. Theory Appl*., vol. 47, no. 2, pp. 204–220, Feb. 2000.

[28] I. Hiskens, "Nonlinear dynamic model evaluation from disturbance measurements," *IEEE Trans. on Power Systems*, vol. 60, no. 4, pp. 702-710, Nov. 2001.

[29] I. Hiskens, "Power system modeling for inverse problems," *IEEE Trans. Circuits Syst. I*, *Reg. Papers*, vol. 51, no. 3, pp. 539–551, Mar. 2004.

[30] I. Hiskens, J. Alseddiqui "Sensitivity, approximation, and uncertainty in power system dynamic simulation," *IEEE Trans. on Power Systems*, vol. 21, no. 4, pp. 1808-1820, Nov. 2006.

[31] M. J. Laufenberg, M.A. Pai, "A New approach to dynamic security assessment using trajectory sensitivities," *IEEE Trans. on Power Systems*, vol. 13, no. 3, pp. 953-958, Nov. 1998.

[32] I. A. Hiskens, "Iterative computation of marginally stable trajectories," *Int. J. Nonlinear and Robust Control*, vol. 14, pp. 911–924, 2004.

[33] G. Hou, V. Vittal, "Determination of transient stability constrained interface real power flow limit using trajectory sensitivity approach," *IEEE Trans. on Power Systems*, vol. 28, no. 3, pp. 2156-2163, Dec. 2012.

[34] I. Hiskens, "Systematic tuning of nonlinear power system controllers," *Proc. of the International Conference on Control Applications*, pp. 19-24, 2002.

[35] R. J. Leveque, *Finite Difference Methods for Ordinary and Partial Difference Equations*, SIAM, 2007.

[36] P. Davis, P. Rabinowich, *Methods of Numerical Integration*, 2nd ed., Academic Press 1984.

[37] G. Hou, "Trajectory sensitivity based power system dynamic security assessment," Ph.D. dissertation, Dept. Electrical Computer and Energy Eng., Arizona State University, Tempe, 2012.

[38] G. Hou and V. Vittal, "Cluster computing based trajectory-sensitivity analysis application to the WECC system," *IEEE Trans. Power Syst.*, vol. 27, no. 1, pp. 502–509, Feb. 2012

[39] F. Milano, "An open source power system analysis toolbox," *IEEE Trans. on Power Syst*., v. 20, No. 3, pp. 1199 – 1206, Aug. 2005

[40] MATLAB PSAT user manual available online: http://faraday1.ucd.ie/psat.html

[41] R. Bravo, J. Wen, D. Kosterev, B. Price, R. Yinger, "WECC Air Conditioner Motor Model Test Report," available online at: https://goo.gl/WXUdHB

[42] P. Mitra, V. Vittal, P. Pourbeik, A. Gaikwad, "Load sensitivity studies with non-smooth load behavior," *IEEE Trans. on Power systems*, accepted for publication on April 13, 2015.

[43] NERC Technical issues subcommittee and system protection and control subcommittee, "A technical reference paper fault induced delayed voltage recovery," accessed on Jan. 5, 2016, available online at: http://goo.gl/7dCmqj

[44] Y.C. Ho, X.R. Cao, *Perturbation analysis of discrete event dynamic systems*, Norwell, MA: Kluwer 1991.

[45] M.S. Branicky, V.S. Borkar, S.K. Mitter, "A unified framework for hybrid control: Model and optimal control theory," *IEEE Transactions on Automatic Control*, vol 43, pp 31 - 43, Jan. 1998.

[46] P. Jain, S. Bannerjee, "Border collision bifurcations in one dimensional maps," *International Journal of Bifurcation and Chaos*, vol 13, no 11, pp 3341-3351, 2003.

[47] D. Kirk, *Optimal Control Theory*, Prentice Hall, Englewood Cliffs, NJ, 1970.

[48] V. Donde, I. Hiskens, "Shooting methods for locating grazing phenomena in hybrid systems," *Int. J. Nonlinear and Robust Control,* vol. 16, no. 3, pp. 671–692, 2006.

[49] P. L. Dandeno, P. Kundur, A. T. Poray, M. E. Coultes, "Validation of turbogenerator stability models by comparison with power systems tests," *IEEE Transactions on Power Apparatus and Systems*, vol. 100, no. 4, pp. 1637-1645, 1981.

[50] I.M. Canay, "Determination of model parameters of machines from the reactance operators xd (js), xq(js) and modeling of alternating current machines having multiple rotor circuits," *IEEE Transactions on Energy Conversion*, vol. 8, no.5, pp. 272-279 and pp.280-296, 1993.

[51] L. Pereira, J. Undrill, D. Kosterev, D. Davies, S. Patterson, "A new thermal governor modeling approach in WECC,", *IEEE Trans. on Power Systems*, vol. 18, no. 2, pp. 819-829, 2003.

[52] EPRI, "Power Plant Model Validation Using On-Line Disturbance Monitoring," accessed on July 29, 2016, available online at: http://goo.gl/zh3u1d

[53] S. Son, S.H. Lee, D. Choi, K. Song, J. Park, Y. Kwon, K. Hur, J. W. Park, "Improvement of Composite Load Modeling Based on Parameter Sensitivity and Dependency Analyses," *IEEE Trans. on Power Systems*, vol. 29, no. 1, pp. 242-250, 2014

[54] J. Ma, D. Han, Ren-Mu He, Zhong-Yang Dong, D. J. Hill, "Reducing identified parameters of measurement-based composite load model," *IEEE Trans. on Power Sys*. Vol. 23, no. 1, pp. 76-83, Jan. 2008.

[55] J. Nocedal, S. Wright, *Numerical optimization*, 2nd ed., Springer Series in Operations Research, 2000.

[56] I. C. F. Ipsen, C. T. Kelley, S. R. Pope, "Rank-deficient nonlinear least squares problems and subset selection," *SIAM Journal on Numerical Analysis*, vol. 49, no. 3, pp. 1244-1266, 2011.

[57] "User's guide on a comprehensive resource for EMTDC," ver. 4.7,Manitoba HVDC Research Centre, Feb. 2010.

[58] Y. Liu, V. Vittal, J. Undrill, J. Eto, "Transient model of air-conditioner compressor single phase induction motor," *IEEE Trans. on Power Sys*. Vol. 28, no. 4, pp. 4528-4536, Nov. 2013.

[59] MATLAB® Optimization Toolbox R2015, Mathworks Inc. Natick, MA., 2015.

[60] TMinuit class reference documentation, accessed on June 25, 2016, available online at: https://goo.gl/hdJDwD.

[61] P. Kundur, J. Paserba, V. Ajjarapu, G. Andersson, A. Bose, C. Canizares, N. Hatziargyriou, D, Hill, A. Stankovic, C. Taylor, T. Van Cutsem, V. Vittal, "Definition and classification of power system stability, IEEE/CIGRE joint task force on stability terms and definitions report," *IEEE Trans. on Power Systems*, vol. 19, no. 3, pp.1387-1401, August 2004.

[62] J. Grainger, W. D. Stevenson, *Elements of power system analysis*, New York: McGraw Hill, 1994.

[63] Leonard L. Grisby, *Power Systems*, Boca Raton Fl. CRC Press, 2007.

[64] A. A. Fouad, F. Aboytes, V. F. Carvalho, 'Dynamic security assessment practices in North America," *IEEE Trans. Power Systems*, vol. 3, no. 3, pp 1310-1321, Aug. 1988.

[65] G. C. Ejebe, B. F. Wollenberg, " Automatic contingency selection," *IEEE Trans. on Power Apparatus and Systems*, pp. 97-109, vol. PAS-98, no. 1, January 1979.

[66] B. Stott and O. Alsac, "Fast Decoupled Load Flow," *IEEE Trans. on Power Apparatus and Systems*, vol. 93, pp. 859-869, May 1974

[67] N.M. Peterson, W.F. Tinney and D.W. Bree, "Iterative linear ac power flow solution for fast approximate outage studies," *IEEE Trans. on Power Apparatus and Systems*, vol. 91, pp. 2048, Oct. 1972

[68] T. A. Mikolonnas, B. F. Wollenberg, " An advanced contingency selection algorithm," *IEEE Trans. on Power Apparatus and Systems*, vol. 100, no.2, pp. 608-617, April 1981

[69] G. D. Irisarri, A. M. Sasson, "An automatic contingency selection method for on-line security analysis," *IEEE Trans. on Power Apparatus and Systems*, vol. 100, no.4, pp.1838-1844, April 1981

[70] S. Vemuri, R. E. Usher, "On-line automatic contingency selection algorithms," *IEEE Trans. on Power Apparatus and Systems*, vol. 102, no.2, pp. 346-354, Feb. 1983

[71] A. P. S. Meliopoulos, C. Cheng, " A New Contingency Ranking Method," *Proc. of Energy and Information Technologies in the Southeast*, pp. 837-842, vol. 2, April 1989.

[72] J. Zaborszky, Keh-Wen Whang, K. Prasad, "Fast contingency evaluation using concentric relaxation," *IEEE Trans. on Power Apparatus and Systems*, vol. 99, no. 1, pp. 28-36, Jan. 1980.

[73] V. Brandwajn, "Efficient bounding method for linear contingency analysis," *IEEE Trans. on Power Systems*, vol. 3, no. 1, pp.38-43, Feb 1988

[74] G. C. Ejebe, H. P. Van Meeteren, & B. F. Wollenberg, "Fast contingency screening and evaluation for voltage security analysis," *IEEE Trans. on Power Systems*, vol. 3, no. 4, pp. 1582-1590, 1988.

[75] V. Brandwajn, M.G. Lauby, "Complete bounding method for AC contingency screening," *IEEE Trans on Power Systems*, vol. 4, no. 2, pp. 724-729, May 1989.

[76] S.M. Chan, V. Brandwajn, "Partial Matrix Refactorization," , *IEEE Power Engineering Review*, vol. 6, no. 2, pp.44-45, Feb. 1986.

[77] M. A. Pai, K. D. Demaree, P. W. Sauer, "Transient energy margins and sensitivity models for dynamic security assessment," *Proc. of American Control Conference*, 1983

[78] M. A. El-Kady, C. K. Tang, V. F. Carvalho, A. A. Fouad, V. Vittal, "Dynamic security assessment utilizing the transient energy function method," *IEEE Trans. on Power Systems*, vol. 3, no. 1, pp. 284-291, 1986

[79] H. D. Chiang, J. S. Thorp, "The closest unstable equilibrium point method for power system dynamic security assessment," *IEEE Trans. on Circuits and Systems*, vol. 36, no. 9, pp. 1187-1200, 1989

[80] W. Li, A. Bose, "A Coherency Based Rescheduling Method for Dynamic Security." Proceeding of the 20th International Conference on Power Industry Computer Applications, Columns, Ohio, 1997

[81] G. C. Ejebe, G. D. Irisarri, "A Sparse Formulation and implementation of the transient Energy Function Method for Dynamic Security Analysis." *Electrical Power & Energy Systems*, Vol 18 No. 1 February 1996

[82] V. Chadlavada, V. Vittal, G. C. Ejebe, G.D. Irisarri, J. Tong, G. Pieper, M. McMullen, "An on-line contingency filtering scheme for dynamic security assessment,", *IEEE Trans. on Power Systems*, vol. 12, no. 1, pp. 153-161, 1997

[83] Y. Mansour, E. Vaahedi, A. Y. Chang, B. R. Corns, M.W. Garret, K. Demaree, T. Athay, K. Cheung, "B. C. Hydro's on-line transient stability assessment (TSA) model development, analysis, and post-processing," *IEEE Trans. on Power Systems*, vol. 10, no. 1, pp. 241-253, 1995

[84] V. Brandwajn, A. B. R. Kumar, A. Ipakchi, A. Bose, S. D. Kuo, "Severity indices for contingency screening in dynamic security assessment," *IEEE Trans. on Power Systems*, vol. 12, no. 3, pp. 1136-1142, 1997

[85] C. Fu, A. Bose, "Contingency ranking based on severity indices in dynamic security analysis," *IEEE Trans. on Power Systems*, vol. 14, no. 3, pp. 980-985, 1999.

[86] G. Irisarri, D. Levner, and A. Sasson, "Automatic contingency selection for on-line security analysis—real-time tests," *IEEE Trans. Power App. Syst*., vol. PAS-98, no. 5, pp. 1552–1559, Sep. 1979.

[87] P. Mitra, V. Vittal, B. Keel, J. Mistry, " A systematic approach to *n*-1-1 power system security assessment," *IEEE Journal of Power and Energy Systems*, accepted for publication on April 11, 2015

[88] C.M. Davis, T. Overbye, "Multiple element contingency screening," *IEEE Trans. on Power Systems*, vol. 26, no. 3, pp. 1294-1301, 2011.

[89] SSTools Contingency Screening and Ranking for N-1-1 manual, General Electric Intl. Ltd, Schenectady, USA, 2012

[90] SSTools Thermal and Voltage Analysis manual, General Electric Intl. Ltd, Schenectady, USA, 2012

[91] *IEEE Standard for AC High-Voltage Circuit Breakers Rated on a Symmetrical Current Basis - Preferred Ratings and Related Required Capabilities for Voltages above 1000 V*, IEEE standard C37.06-2009, Nov, 2009

[92] A.A. Fouad, V. Vittal, *Power System Transient Stability Analysis Using the Transient Energy Function Method*, New Jersey, Prentice-Hall inc., 1992.

[93] D. Ernst, D. Ruiz-Vega, M. Pavella, P. Hirsch, D. Sobajic, "A unified approach to transient stability contingency filtering, ranking and assessment," *Proc. of Power Engineering Society Summer Meeting*, Vancouver, BC, 2001.

[94] O. Alsac, B. Stott, W. F. Tinney, "Sparsity-oriented compensation methods for modified network solutions," *IEEE Trans. on Power Apparatus and Systems*, vol 102, no. 5, pp. 1050-1060, Nov 1983

[95] V. Kolluri, S. Mandal, M. Y. Vaiman, M. M. Vaiman, S. Lee, and P. Hirsch, "Fast fault screening approach to assessing transient stability in entergy's power system," *Proc. IEEE/PES General Meeting*, Tampa, FL, Jun. 24-27, 2007, 2007

[96] Capitanescu, F., Martinez Ramos, J. L., Panciatici, P., Kirschen, D., Marano Marcolini, A., Platbrood, L., Wehenkel, L., "State-ofthe-art, challenges, and future trends in security constrained optimal power flow," *Electric Power Systems Research*, 81(8), 1731-1741.

[97] K.W. Hedman, S.S. Oren, R. P. O'Neil, "A review of transmission switching and network topology optimization," *Proc. of IEEE PES General Meeting 2011*, pp. 1-7, July 2011.

[98] M. S. Ardakani, X. Li, P. Balasubramanian, K. W. Hedman, M. A. Khorshand, "Real-time contingency analysis with transmission switching on real power system data," *IEEE Trans. on Power Systems*, vol. 31, no. 3, pp. 2501-2502, 2015

APPENDIX A

WECC MODEL DESCRIPTION AND LOAD DATA

Table A1. System characteristics of the WECC system

Buses	Lines	Transformer	Generator	Load
15437	13178	5727	2059	6695

Table A2. Load composition based on region

Region	**Motor A**	**Motor B**	**Motor C**	**Motor D**
NWC_RES	0.07	0.07	0.02	0.16
NWC_COM	0.19	0.09	0.03	0.03
NWC_MIX	0.14	0.08	0.03	0.08
NWC_RAG	0.11	0.08	0.39	0.05
NWV_RES	0.10	0.10	0.03	0.21
NWV_COM	0.21	0.10	0.03	0.04
NWV_MIX	0.17	0.10	0.03	0.09
NWV_RAG	0.12	0.09	0.41	0.05
NWI_RES	0.10	0.12	0.02	0.31
NWI_COM	0.27	0.10	0.03	0.06
NWI_MIX	0.19	0.10	0.03	0.16
NWI_RAG	0.13	0.09	0.40	0.09
RMN_RES	0.07	0.08	0.02	0.18
RMN_COM	0.19	0.10	0.03	0.04
RMN_MIX	0.14	0.09	0.02	0.10
RMN_RAG	0.11	0.08	0.36	0.06
NCC_RES	0.08	0.08	0.03	0.18
NCC_COM	0.20	0.09	0.03	0.04
NCC_MIX	0.15	0.08	0.03	0.09
NCC_RAG	0.12	0.08	0.40	0.05
NCV_RES	0.12	0.13	0.03	0.34
NCV_COM	0.29	0.10	0.04	0.07
NCV_MIX	0.21	0.10	0.03	0.16
NCV_RAG	0.13	0.09	0.41	0.09
NCI_RES	0.10	0.11	0.03	0.23
NCI_COM	0.22	0.10	0.03	0.04
NCI_MIX	0.17	0.10	0.03	0.10
NCI_RAG	0.13	0.09	0.42	0.06

Region	Motor A	Motor B	Motor C	Motor D
SCC_RES	0.08	0.08	0.03	0.16
SCC_COM	0.18	0.10	0.03	0.03
SCC_MIX	0.14	0.09	0.03	0.08
SCC_RAG	0.12	0.08	0.38	0.05
SCV_RES	0.11	0.12	0.03	0.27
SCV_COM	0.22	0.10	0.04	0.04
SCV_MIX	0.17	0.10	0.03	0.12
SCV_RAG	0.13	0.09	0.41	0.07
SCI_RES	0.12	0.09	0.04	0.11
SCI_COM	0.21	0.10	0.04	0.02
SCI_MIX	0.18	0.09	0.04	0.04
SCI_RAG	0.13	0.08	0.43	0.03
DSW_RES	0.07	0.16	0.02	0.43
DSW_COM	0.21	0.11	0.04	0.10
DSW_MIX	0.15	0.12	0.03	0.23
DSW_RAG	0.12	0.10	0.38	0.14
HID_RES	0.09	0.12	0.03	0.26
HID_COM	0.19	0.10	0.04	0.04
HID_MIX	0.15	0.10	0.04	0.11
HID_RAG	0.12	0.09	0.41	0.07

P.S The above mentioned data comes from the load composition excel sheet provide by EPRI and is only for research purposes

Table A3. Description of load model parameters and default values

Motor A, B and C				
S. No	**Variable**	**Description**	**Unit**	**Value**
1	-	Bus number	int	
2	*Sn*	Power rating	MVA	
3	*Vn*	Voltage rating	kV	
4	*fn*	Frequency rating	Hz	60
5	-	Model order	int	5
6	*Sup*	Startup control	{0.1}	
7	*rS*	Stator resistance	p.u	0.013 (Motor A), 0.031 (Motor B and C)
8	*xS*	Stator reactance	p.u	0.067 (Motor A), 0.1 (Motor B and C)
9	*rR1*	1st cage rotor resistance	p.u	0.009 (Motor A), 0.018 (Motor B and C)
10	*xR1*	1st cage rotor reactance	p.u	0.17 (Motor A), 0.18 (Motor B and C)
11	*rR2*	2nd cage rotor resistance	p.u	0
12	*xR2*	2nd cage rotor reactance	p.u	0
13	*xm*	Magnetization reactance	p.u	3.8 (Motor A), 3.2 (Motor B and C)
14	*Hm*	Inertia constant	p.u	1.5 (Motor A), 0.7 (Motor B and C)
15	*a*	Tm coefficient	p.u	0 (Motor A), 0.23 (Motor B and C)
16	*b*	Tm coefficient	p.u	0 (Motor A), 0.12 (Motor B and C)
17	*c*	Tm coefficient	p.u	1 (Motor A), 0.12 (Motor B and C)
18	*tup*	Startup time	t	
19	-	Allow working as brake	{0.1}	
20	*u*	Connection status	{0.1}	
21	*Kp*	Active power component	%	
22	*ST*	A fast trip motor?	{0,1}	
23	*Vt*	Voltage threshold to trip ST motor	p.u	
24	*Ttd*	Time delay to trip ST motor	s	

Motor D				
S. No	**Variable**	**Description**	**Unit**	**Unit**
1	V_{brk}	Compressor breakdown voltage	pu	0.86
2	V_{stall}	Stall voltage	pu	0.7
3	T_{stall}	Time to stall	sec	0.033
3	R_{stall}	Stall resistance of the induction machine	pu	0.124
4	X_{stall}	Stall reactance of the induction machine	pu	0.114
5	*Kp1*	Active power coefficient in state 1 in p.u P/p.u V		0
6	*Np1*	Active power exponent in state 1		1
7	*Kq1*	Reactive power coefficient in state 1 in p.u Q/p.u V		6
8	*Nq1*	Reactive power exponent in state 1		2
9	*Kp2*	Active power coefficient in state 2 in p.u P/p.u V		12
10	*Np2*	Active power exponent in state 2		3.2
11	*Kq2*	Reactive power coefficient in state 2 in p.u Q/p.u V		11
12	*Nq2*	Reactive power exponent in state 2		2.5
13	K_{pf}	Active power frequency sensitivity in p.u P/p.u f		1
14	K_{qf}	Reactive power frequency sensitivity in p.u Q/p.u f		-3.3